UNIVERSITÉ D'OTTAWA
ÉCOLE DES ETUDES SUPERIEURES ET DE LA RECHERCHE

UNIVERSITY OF OTTAWA
SCHOOL OF GRADUATE STUDIES AND RESEARCH

PERMISSION DE REPRODUIRE ET DE DISTRIBUER LA THÈSE - *PERMISSION TO REPRODUCE AND DISTRIBUTE THE THESIS*

NOM DE L'AUTEUR* - *NAME OF AUTHOR*

SARAVANOS, Constantine

ADRESSE POSTALE - *MAILING ADDRESS*

965 Crown Court,

Highland Village, Texas, U.S.A. 66721

GRADE - *DEGREE*

Ph.D. (Electrical Engineering)

ANNÉE D'OBTENTION - *YEAR GRANTED*

1996

TITRE DE LA THÈSE - *TITLE OF THESIS*

OPERATIONAL WINDOW OF SINGLE MODE OPTICAL FIBERS

L'AUTEUR PERMET, PAR LA PRESENTE, LA CONSULTATION ET LE PRÊT DE CETTE THÈSE EN CONFORMITÉ AVEC LES RÈGLEMENTS ÉTABLIS PAR LE BIBLIOTHÉCAIRE EN CHEF DE L'UNIVERSITE D'OTTAWA. L'AUTEUR AUTORISE AUSSI L'UNIVERSITÉ D'OTTAWA, SES SUCCESSEURS ET CESSIONNAIRES, À REPRODUIRE CET EXEMPLAIRE PAR PHOTOGRAPHIE OU PHOTOCOPIE POUR FINS DE PRÊT OU DE VENTE AU PRIX COÛTANT AUX BIBLIOTHÈQUES OU AUX CHERCHEURS QUI EN FERONT LA DEMANDE.

LES DROITS DE PUBLICATION PAR TOUT AUTRE MOYEN ET POUR VENTE AU PUBLIC DEMEURERONT LA PROPRIÉTÉ DE L'AUTEUR DE LA THESE SOUS RÉSERVE DES RÈGLEMENTS DE L'UNIVERSITÉ D'OTTAWA EN MATIÈRE DE PUBLICATION DE THÈSES.

THE AUTHOR HEREBY PERMITS THE CONSULTATION AND THE LENDING OF THIS THESIS PURSUANT TO THE REGULATIONS ESTABLISHED BY THE CHIEF LIBRARIAN OF THE UNIVERSITY OF OTTAWA. THE AUTHOR ALSO AUTHORIZES THE UNIVERSITY OF OTTAWA, ITS SUCCESSORS AND ASSIGNEES, TO MAKE REPRODUCTIONS OF THIS COPY BY PHOTOGRAPHIC MEANS OR BY PHOTOCOPYING AND TO LEND OR SELL SUCH REPRODUCTIONS AT COST TO LIBRARIES AND TO SCHOLARS REQUESTING THEM.

THE RIGHT TO PUBLISH THE THESIS BY OTHER MEANS AND TO SELL IT TO THE PUBLIC IS RESERVED TO THE AUTHOR, SUBJECT TO THE REGULATIONS OF THE UNIVERSITY OF OTTAWA GOVERNING THE PUBLICATION OF THESES.

March 28, 1996
DATE

×
(AUTEUR) SIGNATURE *(AUTHOR)*

* NB LE MASCULIN COMPREND EGALEMENT LE FEMININ

FS10-A525 86/12

UNIVERSITÉ D'OTTAWA UNIVERSITY OF OTTAWA

ÉCOLE DES ÉTUDES SUPÉRIEURES ET DE LA RECHERCHE

SCHOOL OF GRADUATE STUDIES AND RESEARCH

Constantine SARAVANOS

AUTEUR DE LA THÈSE-*AUTHOR OF THESIS*

Ph.D. (Electrical Engineering)

GRADE-*DEGREE*

Electrical Engineering

FACULTÉ, ÉCOLE, DÉPARTEMENT-*FACULTY, SCHOOL, DEPARTMENT*

TITRE DE LA THÈSE-*TITLE OF THE THESIS*

OPERATIONAL WINDOW OF SINGLE-MODE OPTICAL FIBERS

Dr. George Costache

DIRECTEUR DE LA THÈSE-*THESIS SUPERVISOR*

EXAMINATEURS DE LA THÈSE-*THESIS EXAMINERS*

R. Harrison

B. Syrett

I. Najadi

L. Roy

Dr. Joseph De Koninck

(LE DOYEN DE L'ÉCOLE DES ÉTUDES SUPÉRIEURES ET DE LA RECHERCHE) SIGNATURE (*DEAN OF THE SCHOOL OF GRADUATE STUDIES AND RESEARCH*)

ARCS

Operational Window of Single-Mode Optical Fibers

Constantine Saravanos

Dissertation submitted to the
School of Graduate Studies and Research
in partial fulfillment of the requirements for the degree of
DOCTOR OF PHILOSOPHY

Ottawa-Carleton Institute for Electrical Engineering
Department of Electrical Engineering
Faculty of Engineering
University of Ottawa

April 7, 1996

ABSTRACT

The purpose of this Ph.D. thesis is to define the design window of single-mode dispersion-unshifted fibers. This window, defined in the mode field diameter (MFD) and cutoff wavelength (λ_C) plot, is determined by the fiber properties with regards to the chromatic dispersion, the bend loss sensitivity at 1550 nm and the modal noise penalty imposed on high speed operating systems.

This has been achieved by developing numerical models used to analyze the properties of optical fibers. These models were used to calculate the propagation characteristics of optical fibers and from them their physical properties, such as the dispersion and bending loss of the fundamental mode. Similar programs, used in the calculations of the LP_{11} mode attenuation and bend performance, determined the fiber's modal noise sensitivity and from it the upper limit of cutoff wavelength.

ACKNOWLEDGMENTS

I want to express my gratitude to my advisor Dr. George Costache for all the support and motivation that he gave me even after I was transferred from Ottawa. I also wish to express my appreciation to Dr. Richard Lowe for the guidance that he gave me to develop my scientific skills. Furthermore, I am grateful to my examining committee for all their helpful comments.

I am also obliged to Northern Telecom, my company for 13 years and the place where I learned everything that I know about Fiber Optics. A special thanks also goes to Siecor, my current company. My management in both corporation encouraged me to continue with this work and helped me achieve this difficult goals. I am proud to be a member of these two organizations.

Finally, I am grateful to my family for the continued assistance and encouragement that they provided me over the years.

MAJOR CONTRIBUTIONS

Even though the majority of this work is new, its major scientific can be summarized by the following points:

- An accurate numerical model was developed and used to determine not only the chromatic dispersion as a function of the mode field diameter and the cutoff wavelength, but several other parameters such as dependencies of the chromatic dispersion slope and the dispersion characteristics of a unique dispersion-shifted fiber. A vast amount of experimental results were used to validate the model.

- The bend loss characteristics of the optical fibers was determined theoretically, and a fit based on the MFD/λ_c was developed. This optimized fit was used to define the bend loss in the design diagram.

- A lot of effort was devoted to the study of the modal noise properties. Most of this area is not well understood and is of great interest to the technical community. Explanations, backed with experimental and theoretical calculations, were given on the differences of the matched and depressed-cladding performance. Conservative, yet practical, limits were suggested upon which the upper limit of cutoff wavelength was determined. The bend and length dependence of cutoff wavelength was used to widen this limit further, by imposing controlled bends in the fiber layout.

By using this work, the performance of fiber optics systems using current fiber types can improve significantly. This study can also be used to design future fibers and refine the operation of fiber optics systems even further.

TABLE OF CONTENTS

1.	**INTRODUCTION**	**1**
2.	**THESIS ORGANIZATION**	**7**
3.	**FIBER DESIGN STRUCTURE**	**8**
4.	**NUMERICAL INVESTIGATION**	**14**
	4.1 Introduction	14
	4.2 Scalar Wave Equation — Derivation from Maxwell's Equations	15
	4.3 Numerical Solution of the Scalar Wave Equation by the Finite Element Method (FEM)	23
	4.4 Numerical Solution of the Scalar Wave Equation by the Finite Difference Technique	31
5.	**CHROMATIC DISPERSION PROPERTIES OF OPTICAL FIBERS**	**37**
	5.1 Introduction	37
	5.2 Chromatic Dispersion Calculations for Dispersion-Unshifted Fibers	44
	5.3 Chromatic Dispersion of a Dispersion Shifted Fiber	49
6.	**BENDING AND MICROBENDING LOSSES OF OPTICAL FIBERS**	**54**
	6.1 Introduction	54
	6.2 Bending loss of Matched-Cladding Fibers	62
	4.3 Bending loss of Depressed-Cladding Fibers	68
7.0	**MODAL NOISE OF SINGLE-MODE FIBER OPTICS SYSTEMS**	**72**
	7.1 Introduction	72

7.2 Phenomenological Explanation 74

7.3 Modal Noise Theory 79

7.4 Theoretical Investigation of the LP_{11} Mode Attenuation 84

7.4.1 Matched-Cladding Fibers 84

7.4.2 Depressed-Cladding Fibers 90

7.5 Experimental Investigation 93

7.5.1 Measurement Apparatus 93

7.5.2 LP_{11} Mode Attenuation Measurements 97

7.6 Correlation between the Length Dependence and the LP_{11} Mode Attenuation 101

7.7 Curvature Dependence of Cutoff Wavelength 104

7.7.1 Minimum Bend Diameter - Limitations due to bends 104

7.7.2 Minimum Bend Diameter - Limitations due to fiber stress 104

7.7.3 Bend Dependence of Cutoff - Theoretical Calculations 108

7.7.4 Bend Dependence of Cutoff - Experimental Results 116

7.8 Modal Noise Calculation 120

7.8.1 Noise-to-Signal Ratio 120

7.8.2 Excitation Efficiency of the LP_{11} Mode 122

7.8.3 Experimental Verification of Modal Noise 125

7.8.4 Setting the Modal Noise Limits on Fiber Optics Systems 131

7.9 Determining the Lower Cutoff Wavelength Limit 134

7.9.1 The Case of Unbent Fiber 134

LIST OF FIGURES

3.1:	Four types of polarization maintaining fibers. (a) Geometrically induced birefringence. (b) Bow-type fiber. (c) Panda fiber. (d) Elliptical cladding fiber. The dark areas symbolize refractive index reduction and tension-induced birefringence.	**9**
3.2:	Two-dimensional refractive index profile of a matched-cladding single-mode fiber	**9**
3.3:	Two-dimensional profile of dispersion-modified fibers. (a) Triangular profile dispersion-shifted fiber. (b) Multiple core dispersion-flattened fiber.	**10**
3.4:	Three different types of matched-cladding fibers. (a) The most common fiber type with GeO_2 doped core and pure silica cladding. (b) A matched-cladding fiber with F-doped cladding. (c) A pure-silica core matched-cladding fiber.	**11**
3.5:	One (a) and two-dimensional (b) refractive index profile of the depressed-cladding single-mode fibers. For this popular fiber type, the inner/outer cladding boundary is fundamental to the propagation characteristics of the optical fiber.	**12**
4.1:	Normalized profile of a dispersion-shifted fiber manufactured by the MCVD process. The profile is triangular and has a central dip due to GeO depletion	**30**
4.2:	Normalized propagation constant as a function of the normalized frequency for the above fiber profile.	**30**
4.3:	Normalized propagation constant as a function of normalized frequency for a step-index profile fiber.	**35**

4.4: Differences between calculated and literature[74] results of the normalized propagation constant. 36

5.1: (a) Sellmeier form of the time delay equation, common to all dispersion-unshifted fibers. (b) Wavelength derivative to the Sellmeier equation, which corresponds to the fiber's chromatic dispersion. 42

5.2: Group delay and chromatic dispersion of dispersion-unshifted, dispersion-shifted and dispersion-flattened fibers. The refractive index profile of each fiber type is shown in the same diagram[18]. 43

5.3: Comparison between calculated and measured values of zero-dispersion wavelength for dispersion-unshifted fiber. 45

5.4: Design diagram of a step-index matched-cladding dispersion-unshifted fiber. 46

5.5: Dependence of dispersion slope on the zero dispersion wavelength. 47

5.6: Experimentally determined dependence of the dispersion slope on the zero dispersion wavelength. The lower and upper limits are based on calculated values by using the most commonly adopted upper and lower cutoff wavelength values of 1330 and 1200 nm respectively. 48

5.7: Refractive index profile of the dispersion-shifted fiber under study. 50

5.8: Zero dispersion wavelength as a function of cutoff wavelength for fibers with their numerical apertures varying from 0.16 to 0.22. These parameters were calculated for an *a/b* value of 0.375. 51

5.9: Zero dispersion wavelength as a function of cutoff wavelength for fibers with varying a/b values and NA of 0.2. 52

5.10: Dispersion slope as a function of cutoff wavelength for fibers with varying *a/b* value and NA of 0.2. **53**

6.1: Refractive index profile of a matched-cladding single-mode fiber, and its equivalent index when the fiber is bent. The shaded area above the effective refractive index indicates the region where the mode is radiated. **55**

6.2: (a) By decreasing the bend radius of the fiber, the loss due to radiation increases as shown by the shaded area. (b) The effect of wavelength on the bending loss of single-mode fibers. As the wavelength increases, the fiber's effective index decreases, resulting to higher radiation losses. **57**

6.3: Bend loss effect on depressed-cladding single-mode fibers. Depending on the bend radius and the wavelength of operation, radiation may occur in the outer cladding, inner/outer cladding boundary, or inner cladding. **59**

6.4: Tension and compression applied to the fiber during bending. **60**

6.5: Fiber microbends and their transformation to equivalent refractive indices. **61**

6.6: Bending loss of a step-index matched-cladding fiber as a function of the mode field diameter and the cutoff wavelength for 100 bends of 2.5 cm radius. **62**

6.7: Bend loss of the fundamental mode of a matched-cladding fiber as a function of the MFD $/\lambda_{CO}$ for the same bend configuration. **64**

6.8: Bend loss of the fundamental mode of a matched-cladding fiber as a function of the "index correction factor" $(\text{MFD})^{0.8}/\lambda_{co}$. **65**

6.9: Design diagram of a matched-cladding single-mode fiber with the defined bend loss limit. **66**

6.10: Bend loss as a function of $(MFD)^{0.8}/\lambda_{co}$ for the fundamental mode of a matched-cladding fiber. The bend configuration is one loop of 1.25 cm radius. **67**

6.11: Bend loss of a depressed-cladding fiber as a function of the MFD/λ_C **69**

6.12: Design diagram of a depressed-cladding single-mode fiber. **71**

6.13: Worst-case bend loss comparison for matched- and depressed-cladding fibers. **71**

7.1: Generation of modal interference for two closely spaced connection joints. **75**

7.2: a. Optical intensity output of a multi-longitudinal mode laser. The intensity fluctuates due to the Fabry-Perot effect of the laser structure. b. Mode partitioning noise in this laser type results to intensity fluctuations in specific modes, and therefore to modal noise. **76**

7.3: a. Spectral output of single longitudinal mode laser. Most of the power is present in the first mode. b. As the power hops from one mode to the other, significant fluctuation in output wavelength occurs. This phenomenon, called mode hopping, results to modal noise generation. **77**

7.4: Modal interference pattern of a single-mode fiber. The parameters used in these calculations: $\alpha_{splice} = 0.5$ dB, $\lambda_c = 1250$ nm, L = 50 cm. **81**

7.5: Splice loss as a function of wavelength for three different fiber stub spacings: 5, 50 and 100 cm. **81**

7.6: Modal noise sensitivity as a function of the fiber stub length. The three curves are generated for a fiber stub with the LP_{11} mode cutoff wavelength of 1240 nm and system operating wavelengths of 1230, 1240 and 1260 nm. **83**

7.7: Attenuation of the LP_{11} mode for matched-cladding fiber with infinitely extended cladding **85**

7.8: The actual structure of a matched-cladding single-mode optical fiber. The actual dimensions are: Core = 8.5 μm, Cladding = 125 μm, Coating = 250 μm. **85**

7.9: The actual refractive index profile of a matched-cladding single-mode fiber. **86**

7.10: LP_{11} mode attenuation for one meter length of a matched-cladding fiber with finite cladding dimensions as a function of the difference between the normalized frequencies at cutoff wavelength and at the operating wavelength. **89**

7.11: Refractive Index profile of depressed-cladding fiber. **90**

7.12: LP_{11} mode attenuation as a function of the V value for inner cladding to core ratios of 5, 6, and 7. The inner cladding depression is 20%. **92**

7.13: Measurement apparatus of the LP_{11} mode attenuation. **93**

7.14: Light launching system of the measurement apparatus shown in figure 5.13. **94**

7.15: Changes of the cutoff wavelength measurement depending on whether the fiber is over-or undefiled. **95**

7.16: Measurement of the LP_{11} mode attenuation **98**

7.17: LP_{11} mode attenuation as a function of wavelength for matched- and depressed-cladding fibers. **99**

7.18: Length dependence of cutoff wavelength for three different matched- and depressed-cladding fibers. **100**

7.19: Calculated and experimental results of the LP_{11} attenuation for depressed-cladding fiber **102**

7.20: Calculated and experimental results of the LP_{11} attenuation for matched-cladding fiber **103**

7.21: Stresses applied on a bent optical fiber. **104**

7.22: Toroidal coordinate system used in the bend analysis of optical waveguides. **109**

7.23: The effect of bend on the loss of the LP_{01} and LP_{11} mode. **109**

7.24: Bend loss of matched-cladding fiber as a function of the V-value for MFD **111**

7.25: Calculated values of bend dependence of cutoff wavelength for fibers with MFDs of 8, 8.5, 9, 9.5, and 10 microns. **112**

7.26: Curvature dependence of cutoff for bend radii of 2.5 and 14 cm. The lines shown are linear fit to the calculated points. **114**

7.27: The effect of the Mode Field Diameter on the bend loss of the LP_{11} mode. $(\beta_{11})_l$ is the propagation constant of the large MFD, while $(\beta_{11})_S$ is the one for small MFD. **115**

7.28: Measured bend dependence of cutoff wavelength for four different types of single-mode fibers. **116**

7.29: Correlation between bend dependence of cutoff and theoretical calculations. The theory is in good agreement with the experiment. **119**

7.30: Experimental setup to evaluate the excitation coefficient of the LP_{11} mode. **123**

7.31: Measurement apparatus of modal noise penalty. **126**

7.32: Measured bit-error-rate (BER) as a function of received power for splice losses ranging from 0 to 4 dB. **127**

7.33: Measured and calculated modal noise penalty as a function of splice loss for a constant BER of 10^{-9}. **128**

7.34: Measured and calculated modal noise penalty as a function of cutoff wavelength for a BER of 10^{-9}. **130**

7.35: Estimated cutoff wavelength as a function of length for matched and depressed-cladding fibers. **136**

7.36 Maximum cutoff wavelength of unbent single-mode fibers as a function of modal noise penalty for splice losses of 0.5, 1, and 2 dB. The three different plots correspond to fiber lengths of 0.5meters (a), 1 meter (b) and 10 meters (c) **137**

7.37: Upper limit of cutoff wavelength for matched- and depressed-cladding fibers at 10 meters length and 0.05, 0.1 and 0.5 dB modal noise penalty. No bend is applied. **138**

7.38: Maximum allowable cutoff wavelength as a function of splice loss for **138**

modal noise penalties of 0.1, 0.5, and 1 dB. The fiber length is 1 meter.

7.39: Same as figure 5.37 but with a fiber length of 0.5 meters. **139**

7.40: Maximum allowable cutoff wavelength as a function of the bend diameter of optical fiber. The fiber length for this fiber is 0.5 meters. **141**

7.41: Maximum allowable cutoff wavelength as a function of the bend diameter for 0.5, 1 and 2 meters fiber lengths. The modal noise penalty is 0.5 dB and the loss at each splice point is 2 dB. **142**

7.42 Maximum cutoff wavelength as a function of splice loss for bent (solid) and unbent (dashed), matched- and depressed-cladding single-mode fibers. The three different plots correspond to fiber lengths of 0.5meters (a), 1 meter (b) and 10 meters (c) **144**

7.43: Maximum cutoff wavelength as a function of splice loss for 0.5, 1 and 10 meters of fiber length and no applied bend. **145**

7.44: Upper limit of cutoff wavelength for minimum fiber length of 0.5, 1 and 10 meters. An 8 cm bend is applied in all configurations. **145**

7.45: Design diagram of matched-cladding fiber **147**

7.46: Design diagram of a depressed-cladding fiber **147**

LIST OF TABLES

I.	Previously measured parameters A_i and λ_i for pure silica, 1% GeO_2 dopes and 1% F doped.	**39**
II.	Polynomial fit to curvature dependence of cutoff. The slope of the curve is shown at two different radii of 2.5 and 14 cm.	**102**
III.	Experimental determination of parameters C and S for two depressed- and one matched-cladding fibers.	**117**
IV.	Worst-case values used to determine modal noise limits.	**133**

LIST OF SYMBOLS

MFD	Mode field diameter
λ_C	Cutoff wavelength of the LP_{11} mode
LED	Light emitting diode
LD	Laser diode
NA	Numerical aperture
a	Core radius
Δn^-	Refractive index difference between SiO_2 and depressed-cladding
Δn^+	Refractive index difference between SiO_2 and core
b	Inner cladding radius
$\vec{E}$	Electric field vector
$\vec{H}$	Magnetic field vector
ω	Angular frequency
μ	Magnetic permeability
ε	Electric permittivity
μ_0	Magnetic permeability in free space
ε_0	Magnetic permittivity in free space
$n(r)$	Refractive index of material
λ	Wavelength of light
k	Wavenumber
ν	Azimuthal wavenumber
β	Propagation constant
ρ	Radial distance
ϕ	Angular deviation
z	Axial distance
n_{cl}	Refractive index of cladding
n_C	Refractive index of core
Δ	Relative index difference

$LP_{m,n}$	Linearly polarized modes
$N(r)$	Index function
V	Normalized frequency
B	Normalized propagation constant
υ	Solution to the wave equation (finite element method)
$\alpha_i(r)$, $\alpha_j(r)$	Interpolation function
l_{ij}	Distance between points i and j
$K_m(x)$	Modified Bessel function of the second order
n_{dir}	Total number of points
γ	Propagation constant in the cladding
MCVD	Modified chemical vapour deposition
h	Length of each finite difference segment
s	Segment number
S	Total number of segments
τ	Group delay
c	Speed of light
D	Chromatic dispersion
λ_0	Zero dispersion wavelength
S_0	Slope at zero dispersion wavelength
Vc	Normalized frequency at cutoff wavelength
NA	Numerical aperture
$n_b(r)$	Equivalent refractive index
R	Radius of curvature
n_{eff}	Effective refractive index
n_{0c}	Refractive index of outer cladding
$\Phi(\Omega)$	Spectrum of microbends
η	Transmission efficiency at a splice point
$\Delta\beta$	Propagation constant difference between the LP_{01} and LP_{11} modes
α_{11}	Attenuation of LP_{11} mode

Δn	Index difference between core and cladding
X	Experimental constant determined by the length-dependence of cutoff constant
α_{splice}	Splice loss
n_j	Refractive index of cladding
$J_m(x)$	Bessel Function of the first kind
$I_m(x)$	Modified Bessel function of the first kind
$H_m^{(2)}(x)$	Hankel function of the second kind
$H_m^{(1)}(x)$	Hankel function of the second kind
χ	Propagation parameter in the core
γ	Propagation parameter in the cladding
ρ	Propagation parameter in the coating
σ	Propagation parameter in inner cladding (for dispersion-shifted fibers)
P_r	Radiated power
P_z	Transmitted power
C	Length dependence of cutoff constant
σ_{max}	Maximum stress
E	Young's modulus
ε	Strain
t	Coating thickness
S	Curvature dependence of cutoff
w	Mode field radius
σ_m	Noise to signal ratio
T	Power transmission
k	Mode partition noise
A	Excitation efficiency of the LP_{11} mode
ΔP	Modal noise penalty
P_{11}	Power in the LP_{11} mode

P_{01}	Power in the LP_{01} mode
ΣP	Power in all the other modes
P_r	Received power
λ_s	System (operating) wavelength
BER	Bit-error-rate
TIA	Telecommunications industry association
FOTP	Fiber optics test procedure

1. INTRODUCTION

During the last decade, optical communications have moved from the research laboratories into the field. While numerous fiber types have been fabricated in the laboratories, only very few have been deployed in the field. The fibers that are used widely in field installations are separated into multimode fibers, i.e., fibers supporting several hundreds of modes at the wavelength of operation, and single-mode fibers, i.e., fibers that operate at wavelengths where only one mode is guided.

Even though the first low loss optical fibers fabricated in the research labs were single-mode [1], the fibers employed initially in the field were multimode. Difficulties experienced in coupling light into the small core of single-mode fibers and splicing and interconnection between fibers prevented them from being used widely in the field at that time. To the contrary, multimode fibers offered the distinct advantage of ease of splicing, connectorization and launching efficiency from light emitting diodes (LED), and laser diodes (LD) to the fiber, due to their large core size and the Numerical Aperture (NA). The refractive index profile of telecommunication-quality multimode fiber is nearly parabolic in shape, so that group velocity differences between the modes are minimized, increasing the fiber bandwidth by reducing the effect of the intermodal dispersion. In the late 1970's and early 1980's research efforts were placed to determine the propagation properties of this fiber type. These studies were responsible for the optimization of the loss and bandwidth of this fiber. At that time a second window of operation was introduced at 1300 nm, where both the material dispersion properties of the glass and the fiber loss are minimized. The prediction of the propagation characteristics of this fiber type was based on geometrical optics, or the Wentzel, Kramer, Brillouin (WKB) method, a simplified approximation to the Maxwell's differential equations[2]. Even though we were able to understand the fiber's optical transmission characteristics, several fiber parameters were over- or underestimated, such as the bandwidth[3]. During that time, no numerical techniques were successfully applied to optimize the design of this fiber type.

The WKB approximation declines substantially in accuracy as the number of modes decreases. For the case of single-mode fibers, the WKB approximation is not valid. Since its introduction, the refractive index of the conventional single-mode fiber has been approximated by a step index profile. Due to the simplicity of its structure, the step index equivalent single-mode fiber can be analyzed by using Maxwell's equations, especially if some simple approximations are made. The step index equivalence gave meaningful results regarding the propagation properties of the fiber. It also contributed to the understanding of the optical properties of this fiber type, and to the development of the concept of linearly polarized modes, LP_{nm}[4]. However, some propagation properties of single-mode fibers could not be calculated. Significant deviations of the actual index profile from the step index approximation are caused by the fabrication process. These variations are characteristic of the process used, and can be repeatable for fibers manufactured by the same process. The fiber's chromatic dispersion is a propagation property most sensitive to the exact shape of the fiber profile[5]. In addition, the fiber waveguide properties are altered due to geometrical deformation of the fiber's axis, which is caused by the cabling process of the optical fiber, and by the field installation of the fiber optic cables[6]. For these reasons, a numerical model is necessary in order to predict accurately these propagation properties of conventional optical fiber waveguides.

Recently, new fiber types have been designed with altered waveguide characteristics caused by adjusting the refractive index profile of the fiber[18]. These efforts have resulted in the development of the dispersion-shifted and dispersion-flattened fiber types. By fabricating fibers using these designs, it is possible to match the wavelength of the optimum dispersion to the minimum attenuation. This has resulted in optical transmission systems with increased repeater spacing in the optical cable link. The propagation properties of these fiber types can be analyzed only by numerical techniques. This is due to the complexity of the refractive index profile of the fiber, where an exact solution of the Maxwell's equation becomes impossible. Up to date numerical models have been extremely valuable tools in the prediction of the propagation parameters of single-mode fibers, and in the development of new fiber designs.

In order to determine the applicability of a numerical model even further, a review of the waveguide characteristics of optical fibers is necessary. These characteristics can be separated into those that contribute to the increase in the waveguide loss, and those that alter the dispersion properties. As will be seen later, these parameters can be determined for any refractive index profile, by solving Maxwell's equations.

The parameters that contribute to the loss of an optical waveguide are of great importance to the fiber designer. Due to recent improvements in process control, losses as low as 0.15 dB/km have been achieved for single-mode optical fibers in the wavelength region of 1550 nm[7]. Recently, sources at this wavelength have become available, increasing the utilization of this window of operation. By employing fibers with such low losses, repeater spans as long as 200 km have been demonstrated at different laboratories, making fiber optics telecommunications particularly attractive to transoceanic transmission[8]. For this type of fiber design, extrinsic loss increases, caused by waveguide phenomena, cannot be tolerated. These waveguide induced losses are separated into the following two categories:

(a) Losses caused by the waveguide structure due to leakage of the fundamental mode in the depressed-cladding fiber design caused by the location of the inner/outer cladding interface. For improperly designed fibers, this can be the dominant loss mechanism, especially in the longer wavelength range of 1550 nm. These losses have been eliminated by reducing the depressed level of the inner cladding.

(b) Attenuation of the fundamental mode due to the deformation of the fiber axis. This occurs either during the cabling process, where the fiber can be deformed by microbends that may cause a significant loss increase at low temperatures, or during the cable installation, where thousands of bends of relatively large radius of curvature over 1 km length can impose a severe fiber loss, causing system failure. These effects can be reduced by selecting the proper fiber and cable designs, by careful control of the fiber layout conditions during the splicing and connectorization process and by the proper selection of the design window.

The chromatic dispersion properties of the optical waveguide can become the limiting factor to the maximum link length, especially for those fiber types where the zero dispersion wavelength coincides with the fiber's minimum loss. If these fiber parameters are not optimized, the performance capabilities of the system can be affected significantly. It was previously thought that the dispersion effect was significant if used in combination with large spectral width sources. These include the multi-longitudinal mode lasers or light emitting diodes (LED's). It was believed that these effects could be reduced with the use of very narrow spectral width sources, such as single-longitudinal mode lasers. It has been recently discovered, however, that even in this case secondary dispersion effects can degrade the system performance characteristics. These effects are present in high bit rate applications[9] and increase the modal noise sensitivity of the system.

In addition to the above parameters, others are also of extreme importance to the fiber designer. A very significant parameter is the fiber's Mode Field Diameter (MFD), which influences the fiber's ease of connectorization and splicing. The joint loss of optical fibers was reduced by limiting the variability of the MFD to ± 0.5 μm around a nominal value. As we will discuss later, this nominal value varies with the fiber type.

Most of these parameters can be predicted numerically from the solution of the scalar wave equation. By solving the eigenvalue problem, the propagation constant of the fundamental and higher order modes is found as a function of the wavelength. The eigenfunctions of this differential equation predict the fiber's mode field diameter, and therefore its splicing and cabling performance. It is, therefore, obvious that such a unified numerical model is an extremely useful tool to the fiber designer. A complete analysis of new fiber types can be developed, and their optical performance can be accurately predicted, decreasing the development cost and time significantly.

In the past, several numerical models were developed to accurately predict the fiber properties from the solution of the scalar wave equation[10,11,12]. The two most important methods being used today are the finite differences and the finite element techniques. This is especially true for the case of dispersion-unshifted fibers, i.e., fibers whose chromatic dispersion is altered only slightly by waveguide effects[13]. For other parameters, such as the bending and microbending fiber loss, the agreement between theory and experiment is poor[14]. The same is true in the case of the dispersion-shifted fiber, whose chromatic dispersion is altered greatly due to waveguide effects. The differences between experimental and calculated results are caused by measurement errors [15] and by the inaccuracies of the model.

The purpose of this work is to develop numerical models and use them to define the design window of single-mode dispersion unshifted optical fibers. Numerical methods were used before to predict some propagation properties of optical fibers. These models were not used to define the allowable window of operation based on accurate and meaningful measurements. The properties of chromatic dispersion, bend loss and modal noise were used individually. No work has been published to connect these important properties together and develop a well-defined design window of operation. In this work numerical models will be developed to predict accurately the dispersion properties of the optical waveguide. Based on a physical explanation of the observed differences between the experimental results and the numerical calculations, accurate predictions of the bending performance of optical fibers will be made.

The most significant goal of this work, though, is to uncover limitations of currently used deployment techniques and recommend methods for improvements. This includes the dispersion properties and bend loss limits. By performing accurate calculations, it is shown that the design window can be increased and the optical performance of the fiber can improve significantly. A complete analysis on the modal noise generation of optical fibers will increase the upper limit of the cutoff wavelength and will improve the layout configuration of the optical fibers. This will result in a reduction of the amount of the required fiber in distribution frames and splice organizers, and will increase the density of fibers in central telecommunications offices where extra space comes at a great premium.

2. THESIS ORGANIZATION

After the introduction, which was presented in the first section, an overview of the optical fiber designs is presented in Section 3. In this section, the design of single-mode optical fibers used for this work is defined.

Section 4 presents a numerical investigation of the propagation characteristics of optical fibers. The section starts with the derivation of the scalar wave equation from Maxwell's equations. The one-dimensional scalar wave equation is solved numerically using finite elements and finite differences methods. These methods are used to find the relationship of the propagation constant as a function of the normalized frequency which in turn is utilized to calculate the chromatic dispersion properties of optical fibers. These properties are found in Section 5 and are used to define the window of operation of single-mode fibers. The same section also describes the chromatic dispersion properties of a unique dispersion-shifted fiber.

In Section 6, the bend loss of the fundamental mode of single-mode optical fibers is shown. An empirical equation was developed and used to define the bend loss limit on the MFD-Cutoff Wavelength diagram.

Section 7, the longest section of this work, establishes the cutoff wavelength limit based on the modal noise of single-mode fibers. After a phenomenological and theoretical explanation of modal noise and the evaluation of the attenuation and bend loss properties of the LP_{11} mode, the section establishes the upper limit of cutoff wavelength for a 0.5 meters fiber with and without the formation of a bend on the fiber configuration. This parameter completes the design window of single-mode fibers.

Section 8 presents a summary of the test methods used to obtain the experimental results, while the conclusions are given in Section 9. Finally, Section 10 suggests research that can be used to enhance the understanding of the single-mode fibers even further.

3. FIBER DESIGN STRUCTURE

In order to be able to understand the propagation characteristics of an optical waveguide, it is necessary to examine the fiber structures to be analyzed. It is simple enough to separate the fiber structures into two categories: structures with and structures without angular symmetry. The first category includes all the fibers that are currently used in the telecommunications industry. Single mode fibers with such structure support two orthogonally polarized degenerate modes (i.e., modes with the same propagation constant).

The second category includes polarization maintaining fibers used in fiber sensor technology, and will be used in future coherent telecommunications systems. In these fibers the polarization degeneracy of the two orthogonal modes is removed using geometrical or stress-induced asymmetries. A fiber profile with geometrical asymmetry is shown in Figure 3.1(a). Figures 3.1(b) to 3.1(d) present the fiber profile of stress-induced birefringence. The purpose of this study is to evaluate the properties of fibers with angular symmetry, and the analysis of birefringent fibers is outside the scope of this work

It is of great importance to understand the different fiber types in terms of their profile's shape. An important parameter is the refractive index profile of the fiber that refers to the variation of the refractive index as a function of the radial distance from the fiber center. The part of the fiber profile where the refractive index is higher than that of the rest of the fiber, is called the "**core**" of the fiber. The outer part of the fiber, with refractive index lower than that of the core, is called the "**cladding**" area of the fiber. The refractive index in this region is usually the same or lower than the refractive index of pure silica. According to the Telecommunications Industries Association (TIA) specifications, standard single-mode fibers are separated into three different categories:

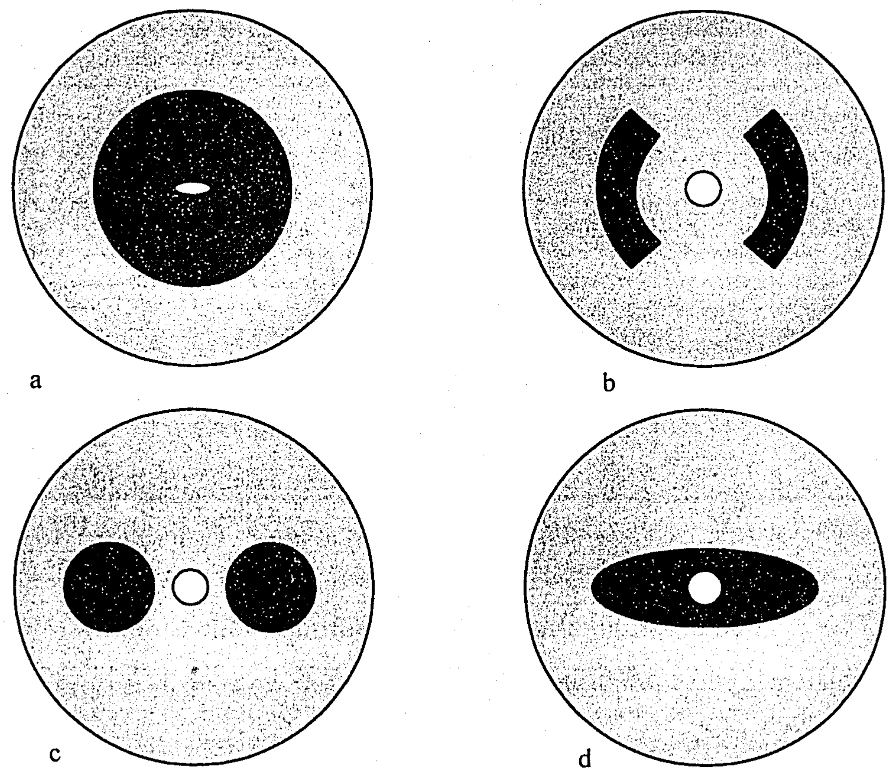

Figure 3.1: Four types of polarization maintaining fibers. (a) Geometrically induced birefringence. (b) Bow-type fiber. (c) Panda fiber. (d) Elliptical cladding fiber. The dark areas symbolize the refractive index reduction and tension-induced birefringence.

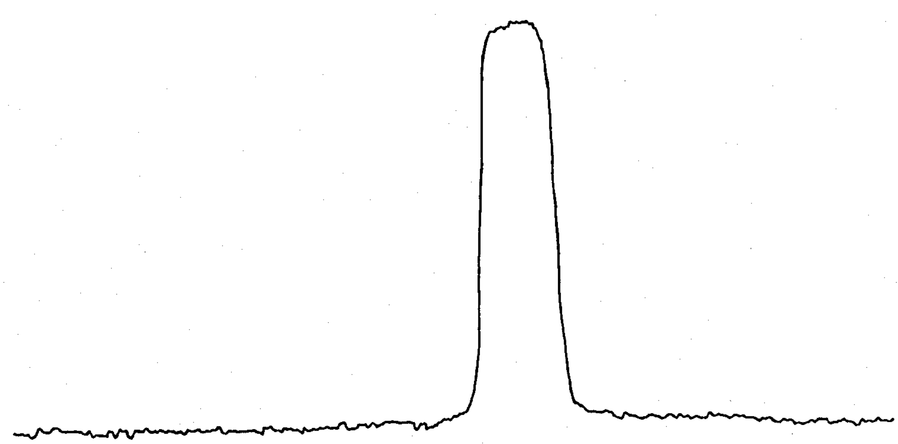

Figure 3.2: One-dimensional refractive index profile of a matched cladding single-mode fiber measured by the refracted-near-field technique

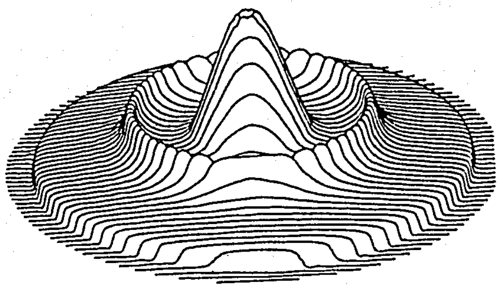

(a)

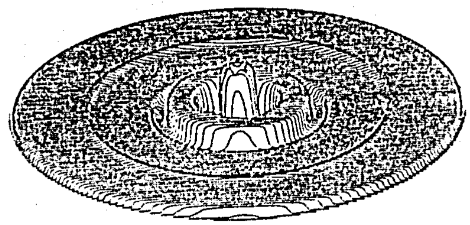

(b)

Figure 3.3: Two-dimensional profile of dispersion-modified fibers. (a) Triangular profile dispersion-shifted fiber. (b) Multiple core dispersion-flattened fiber.

Class IVa, or **dispersion unshifted fibers**, where the dispersion properties of the fiber deviate only slightly from the characteristics of the materials that compose the fiber[16,17,18]. A typical one-dimensional refractive index profile of this fiber type manufactured by the outside-vapour-phase deposition method is shown in Figure 3.2.

Class IVb, or **dispersion-shifted fibers**, where the wavelength of zero dispersion coincides with the wavelength of minimum loss, which for single-mode silica-based fibers is located around 1550 nm[19,20,21]. Figure 3.3a shows a two-dimensional profile of a dispersion-shifted fiber.

Class IVc, or **dispersion-flattened fibers**, where the fiber's chromatic dispersion crosses the zero axis at two different wavelengths. These fibers are practically dispersion-free, since the amount of dispersion between these two wavelengths is very small[22,23]. In Figure 3.3b, a two-dimensional profile of a dispersion-flattened fiber is shown.

From all these designs, class IVa fibers are deployed in more than 90% of the currently used telecommunications systems with the remaining being of the class IVb type. Even though both class IVa and IVb will be analyzed in terms of their dispersion characteristics, this work will concentrate on the propagation properties of dispersion unshifted fibers. Depending on their refractive index profile, these fiber types are separated into two different categories:

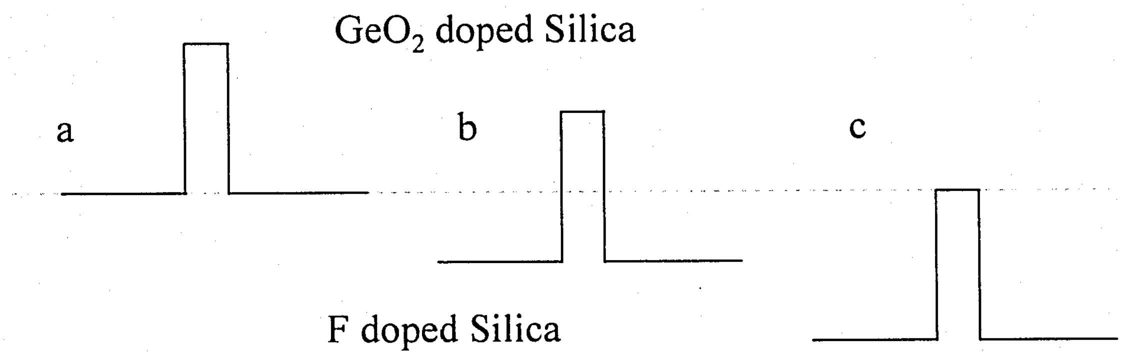

Figure 3.4: Three different types of matched-cladding fibers. (a) The most common fiber type with GeO_2 doped core and pure silica cladding. (b) A matched-cladding fiber with F-doped cladding. (c) A pure-silica core matched-cladding fiber.

The first fiber type, known as the **"matched-cladding"** fiber[24,25], is characterized by a cladding refractive index that is constant over the whole cladding region. In currently available commercial fibers, this fiber type is fabricated by a pure silica cladding, and a germanium oxide (GeO_2) doped core. Most recently, "matched-cladding" fiber types have been formed by a fluorine-doped cladding and a pure silica core, or with a heavily fluorine-doped cladding and a slightly fluorine-doped core. Due to design problems, very few of these fibers are currently in use. For all these fiber types the waveguide effects remain the same and only the material effects change. These fibers are completely characterized by their core size and the refractive index difference between the core and the cladding. The propagation properties of these fibers are the simplest ones to analyze.

A schematic diagram of the three different matched-cladding fiber types is presented in Figure 3.4.

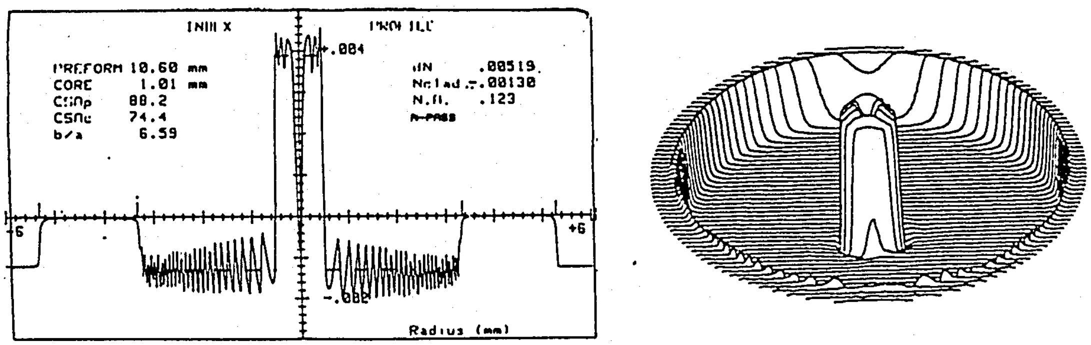

(a) (b)

Figure 3.5: One (a) and two-dimensional (b) refractive index profile of the depressed-cladding single-mode fibers. For this popular fiber type, the inner/outer cladding boundary is fundamental to the propagation characteristics of the optical fiber.

The second fiber type is referred to as a **"depressed-cladding"** fiber[26,27], and the fiber's cladding is separated in two areas: the inner and the outer cladding. The "inner" cladding surrounds the core area, and is of lower refractive index than the "outer" cladding, which completes the fiber structure. For this fiber type, the "outer" cladding is always composed of pure silica, while the "inner" cladding is made of fluorine-doped silica, and the core of germania doped silica. In order to characterize properly this fiber structure, the following parameters should be known:

(a) The core radius, a.

(b) The refractive index difference between the core and inner cladding, Δn.

(c) The inner cladding depression, $\Delta n^{-}/\Delta n^{+}$.

(d) The inner cladding to core ratio, b/a.

An one-dimensional index profile of a depressed-cladding single-mode fiber, as fabricated by the Modified Chemical Vapour Deposition (MCVD) process, is shown in Figure 3.5 (a). The two-dimensional profile of the same fiber is shown in Figure 3.5 (b).

4. NUMERICAL INVESTIGATION

4.1 Introduction

In order to develop models that define the boundaries of the operating window of single mode optical fibers, we have to understand the physical meaning of their propagation properties, and be able to determine these parameters quantitatively. This is especially true for the determination of the chromatic dispersion properties of optical fibers, the wavelength at which only one mode propagates (cutoff wavelength), the field distribution at the end face of the fiber and the bend losses of the first and second order modes. These parameters can be calculated if the propagation constant is determined as a function of the wavelength of the electromagnetic field and the dimensions of the waveguide. These calculations are obtained from Maxwell's equations. As in most actual problems, however, an exact solution of Maxwell's equations is impossible to achieved. For that reason, scientists try to simplify the differential equations as much as possible, and use numerical techniques to determine their.

In the following sections the one-dimensional scalar wave equation is derived from Maxwell's equations by assuming cylindrical symmetry. This equation is simplified further and by solving it its eigenvalues are dctermined. The numerical solution is achieved by using two numerical techniques: the finite element (FEM) and finite difference (FDM) methods. These methods were used to evaluate the propagation characteristics of a step-index fiber. Since it is possible to obtain an exact solution of the propagation properties for this fiber type, this analytical solution is compared to the numerical one calculated by the FEM and the FDM method. This comparison indicates that the FDM method, as was formulated here, produces more accurate results. For that reason, this method was used to evaluate the numerical properties of the optical fiber with arbitrary refractive index profile.

4.2 Scalar Wave Equation — Derivation from Maxwell's Equation

It is well known that Maxwell's equations in source-free media, as is the case of monochromatic light propagation in optical waveguides, take the form:

$$\vec{\nabla} \times \vec{E} = -i\omega\mu\vec{H} \tag{4.1}$$

$$\vec{\nabla} \times \vec{H} = i\omega\varepsilon\vec{E} \tag{4.2}$$

In the above equations $\vec{E}$ and $\vec{H}$ are the electric and magnetic fields, respectively, while μ and ε are the material's permeability and permittivity respectively. For the case of optical waveguides, the medium's permeability takes the value of free space, μ_0, while the permittivity is given by the relationship:

$$\varepsilon = \varepsilon_0 n^2(r) \tag{4.3}$$

where ε_0 denotes the free-space permittivity, r the position and $n(r)$ the refractive index of the material.

By combining the two Maxwell's equations, the following equation is obtained:

$$\vec{\nabla} \times \vec{\nabla} \times \vec{H} = \omega^2 \vec{\nabla} \times (\varepsilon\mu\vec{H})$$

Since,

$$\vec{\nabla} \times \vec{\nabla} \times \vec{H} = \vec{\nabla}(\vec{\nabla} \cdot \vec{H}) - \nabla^2 \vec{H}$$

and by assuming that the permeability is constant throughout the space and equal to μ_o, then

$$\vec{\nabla} \cdot \vec{H} = \vec{\nabla} \cdot (\vec{B} / \mu_o)$$
$$= 0$$

Therefore,

$$\vec{\nabla} \times \vec{\nabla} \times \vec{H} = -\nabla^2 \vec{H}$$

The wave equation in the optical waveguide finally becomes:

$$\nabla^2 \vec{H} + \frac{1}{\varepsilon} \vec{\nabla} \varepsilon \times (\vec{\nabla} \times \vec{H}) + k^2 \vec{H} = 0 \tag{4.4}$$

with

$$k = \omega \sqrt{\mu \varepsilon}$$
$$= \frac{2\pi n}{\lambda} \tag{4.5}$$

being the wavenumber at the operating wavelength.

Finally, the wave equation becomes:

$$\nabla^2 \vec{H} + \vec{\nabla} g \times (\vec{\nabla} \times \vec{H}) + k^2 \vec{H} = 0 \tag{4.6}$$

where

$$g = \ln(k^2) \qquad (4.7)$$

Up to this point no assumptions have been made regarding the weakly guiding approximation of the optical fiber. For most cases we can assume that the gradient term of the differential equation can be neglected, since no drastic change of the refractive index of the material occurs [29]. In that case the differential equation is simplified greatly to take the form:

$$\nabla^2 \vec{H} + k^2 \vec{H} = 0 \qquad (4.8)$$

Several more assumptions can be made with regards to the media and the geometry of the waveguide. For common fiber types these are:

(a) The majority of the fibers used in telecommunications applications are circularly symmetric. For most practical cases they are perfectly straight and uniform along their length. Therefore, a cylindrical coordinate system can be applied, and can greatly simplify the three-dimensional differential equation described earlier. A cylindrical coordinate system is defined, *(ρ, ϕ, z)* where the z axis coincides with the fiber axis.

(b) The fibers that will be evaluated in this work have a refractive index that is homogenous along the entire fiber length and isotropic along all directions. These assumptions simplify the model even further, and reduce the uncertainty of polarization effects on the fibers.

Using cylindrical coordinates the magnetic field is written as:

$$\vec{H}(\rho,\phi,z) = \vec{H}(\rho,0,0)\exp[i(\omega t - v\phi - \beta z)] \qquad (4.9)$$

where ν is the azimuthal wavenumber

β is the propagation constant.

In cylindrical coordinates the Laplacian takes the form:

$$\nabla^2 \vec{H} = \frac{1}{\rho}\frac{\partial}{\partial\rho}\left[\rho\frac{\partial\vec{H}}{\partial\rho}\right] + \frac{1}{\rho^2}\frac{\partial^2\vec{H}}{\partial\phi^2} + \frac{\partial^2\vec{H}}{\partial z^2} \tag{4.10}$$

and the wave equation finally becomes:

$$\frac{1}{\rho}\frac{d}{d\rho}\left[\rho\frac{d\vec{H}}{d\rho}\right] + \left[\frac{\nu^2}{\rho^2} - \beta^2 - \mu_0\varepsilon\omega^2\right]\vec{H} = 0 \tag{4.11}$$

By using the wavenumber concept,

$$\begin{aligned} k^2(\rho) &= \mu_0\varepsilon\omega^2 \\ &= n^2(\rho)\frac{2\pi}{\lambda} \end{aligned}$$

the above equation becomes:

$$\frac{1}{\rho}\frac{d}{d\rho}\left[\rho\frac{d\vec{H}}{d\rho}\right] + \left[\frac{\nu^2}{\rho^2} - \beta^2 - k^2(\rho)\right]\vec{H} = 0 \tag{4.12}$$

In this section we are concerned about the "weakly guided mode" approximation, which was first introduced by Gloge [3] for the analysis of cylindrical dielectric waveguides. It is well known that the propagation constant of the optical fiber is bounded by the following inequality:

$$n_{cl}\,k < \beta < n_c\,k \tag{4.13}$$

where n_c is the maximum refractive index in the core

n_{cl} is the refractive index of the cladding

For optical fiber we can also assume that the relative refractive index change, Δ, between the core and cladding is much lower than one, or:

$$\Delta = \frac{n_c^2 - n_{cl}^2}{2n_c^2} \approx \frac{n_c - n_{cl}}{n_c} << 1 \tag{4.14}$$

and, therefore, we can assume that the propagation constant can be approximated as a constant and

$$\beta \approx n_{cl} k \tag{4.15}$$

This expression is valid whenever the exact value of β is not important.

The solution of the scalar wave equation, as derived by using the previous approximation, gives rise to the linearly polarized, LP, modes[6]. In order to understand the origin of these modes, it is important to look at the exact solution of the step-index approximation of the scalar wave equation, which generates the HE and EH modes of the cylindrical waveguide. It has been previously shown that the $HE_{m+1,1}$ and the $EH_{m-1,1}$ are almost degenerate modes. This means that these modes have the same propagation constant, and by combining them their superposition field is linearly polarized. That is how the Linearly Polarized (LP) mode concept was generated. As mentioned earlier, for these fiber types it is possible that the two modes are not completely degenerate, and it is possible to propagate in the fiber with different propagation constants, causing the superposition field between the two of them to change periodically along the fiber length. The length periodicity is an important parameter for the characterization of polarization maintaining fibers, or even for normal fibers, when their polarization dispersion properties are analyzed, and is called the "beat length" of the fiber[32].

A universal solution can be found to the scalar wave equation if a normalization is applied[33]. This normalization is expressed in terms of the fiber's core radius, the refractive index difference and the operating wavelength, and can be very useful in determining the propagation properties independently of these parameters.

In order to normalize the scalar wave equation, though, it is necessary to know the fiber's index function, which represents the shape of the fiber's refractive index. This function is given by the following equation:

$$n^2(r) = n_c^2\left[1 - 2\Delta N(r)\right] \tag{4.16}$$

where Δ is the refractive index difference and N(r) the index function. This function represents the change of the refractive index with the radial position from the center of the fiber, and takes the following form at the extreme values:

$$\begin{aligned} N(r) &= 1 \quad \text{for} \quad r > 1 \text{ (in the cladding)} \\ &= 0 \quad \text{for} \quad r < 1 \text{ (in the core)} \end{aligned} \tag{4.17}$$

There are two additional parameters that can be normalized: One is related to the wavelength of operation, and is called the normalized frequency. The other is related to the propagation constant, and is called the normalized propagation constant. These two parameters are expressed by the following relations:

$$V = \frac{2\pi}{\lambda} a n_c \sqrt{2\Delta} \qquad \text{(normalized frequency)} \tag{4.18}$$

$$B^2 = \frac{n_c^2 - k^2\beta}{2\Delta n_c} \quad \text{(normalized propagation constant)} \tag{4.19}$$

By using the normalized radius $(r = \rho/a)$ as a variable, together with the above normalized parameters, the scalar wave equation takes the form:

$$\frac{d^2H}{dr^2} + \frac{1}{r}\frac{dH}{dr} + q^2(r)H(r) = 0 \tag{4.20}$$

where the parameter $q^2(r)$ is expressed in terms of the normalized frequency, V, the normalized propagation constant, B, and the index function of the fiber, N(r):

$$q^2(r) = V^2 [B^2 - N(r)] \tag{4.21}$$

It is, therefore, obvious that the propagation characteristics of a fiber structure can be determined if the index function, or the shape of its refractive index, is known. The solution is found if the same boundary conditions as described above are applied to the fiber.

The solution of the scalar wave equation represents the solution to the guided modes that propagate in the fiber. It is known that modes other than the guided modes also propagate in the fiber structure. These modes, called the radiation modes, are very important in characterizing the fiber's loss characteristics, such as the bending and microbending loss, and can be expressed with an equation similar to the scalar wave equation[34]:

$$\frac{d^2H}{dr^2} + \frac{1}{r}\frac{dH}{dr} + \left[-k^2 n_0^2(r) - \beta_r^2 - \frac{1}{r^2} \right] H = 0 \tag{4.22}$$

In contrast to the guided modes, the propagation constant β_{r} of the radiation modes is continuous and has to obey the inequality:

$$\beta_r = (\beta_0 - \Delta\beta) < kn_{cl} \tag{4.23}$$

By integrating the previous equation, the following integrodifferential equation can be generated:

$$r\frac{dH}{dr} + \int \left[k^2 n_0^2(r) - \beta_r^2 - \frac{1}{r^2}\right] H(r) r dr = 0 \tag{4.24}$$

The aim is to solve the above equation for any fiber type. This can be done by using numerical techniques for an arbitrary index profile, and determining the normalized coupling coefficient between the guided and the radiation modes. The loss due to microbending can easily be determined by knowing the coupling coefficient[35,36].

4.3 Numerical Solution of the Scalar Wave Equation by the Finite Element Method (FEM)

The Finite Elements Method has been used previously to solve the scalar wave equation. The most successful technique to date is based on the Galerkin method of moments[10]. This method has shown the capability for determining the propagation characteristics of step index fibers, even though the analysis of the propagation properties of other fiber designs has not been performed. The technique has not been used to determine the bending and microbending properties of the fiber.

In this work an accurate method of solving the scalar wave equation is proposed using the Finite Element Method (FEM). This method is developed in terms of a variational principle for the scalar wave equation[37,38]. This leads to the derivation of the functional of the equation, whose minimization results in a matrix of equations of standard eigenvalue form. Below, a formulation of the problem is given.

As shown in the previous section, the three-dimensional scalar wave equation is:

$$\nabla^2 \vec{H} + k^2(r)\vec{H} = 0 \tag{4.10}$$

By assuming that u is the solution of equation (4.10), the functional takes the following form:

$$F = \int\left(\vec{\nabla} u\right)^2 dxdy - \int k^2(r)udxdy \tag{4.25}$$

The integration is performed over the region enclosing the field.

As explained earlier, cylindrical symmetry was assumed in the fiber structure. Therefore, the problem reduces to one dimension, simplifying the solution even further. In that case the differential equation takes the form of the scalar wave equation described earlier. The functional can also be written in terms of the cylindrical coordinates in one dimension, as:

$$F = \int \left(\bar{\nabla} u\right)^2 r dr - \int q^2(r) u^2 r dr \tag{4.26}$$

The term $q^2(r)$ is given by the relationship presented in the previous section:

$$q^2(r) = V^2\left[B^2 - N(r)\right] \tag{4.21}$$

By substituting $q^2(r)$ in the functional, and by discretizing the region where the functional is applied, the following form is obtained:

$$\begin{aligned} F &= \Sigma \int \left(\bar{\nabla} u\right)^2 r dr - \Sigma \int q^2(r) u^2 r dr \\ &= \Sigma \int \left(\bar{\nabla} u\right)^2 r dr - V^2 B^2 \Sigma \int u^2 r dr + V^2 \Sigma \int N(r) u^2 r dr \\ &= \Sigma \left\{ \int \left[\left(\bar{\nabla} u\right)^2 + V^2 N(r) u^2 \right] r dr - V^2 B^2 \int u^2 r dr \right\} \end{aligned} \tag{4.27}$$

The above equation can be expressed in a matrix form. For an optical fiber with a known refractive index profile, the unknown parameters in the above system of equations are:

(a) The field values u_i at the discretization points. These are the eigenfunctions of the above system of equations.

(b) The normalized propagation constant, B, for a particular normalized frequency, V, or the eigenvalue of the same system of equations.

In a first order linear approximation the solution $u(r)$ of the differential equation is given by a piecewise linear function:

$$u(r) = c_0 + c_1 r \tag{4.28}$$

For two points i and j separated by a distance l_{ij}, the above solution can be written as:

$$u(r) = \alpha_i(r)u_i + \alpha_j(r)u_j \tag{4.29}$$

where u_i and u_j are the solutions at points i and j. The terms $\alpha_i(r)$ and $\alpha_j(r)$ are the interpolation functions and are calculated to be:

$$\alpha_i(r) = \frac{r - r_i}{l_{ij}} \tag{4.30}$$

$$\alpha_j(r) = \frac{r_j - r}{l_{ij}} \tag{4.31}$$

The solution of the differential equation can be found by minimizing the functional with respect to u. This is accomplished by differentiating the functional with respect to u, and setting the derivative equal to zero. A simple method of calculating the derivative of the functional is by differentiating the terms that contain u.

$$u^2 = \alpha_i^2 u_i^2 + \alpha_j^2 u_j^2 + 2\alpha_i \alpha_j u_i u_j$$

The above form is differentiated with respect to u_i and u_j:

$$\frac{\partial u^2}{\partial u_i} = 2\alpha_i^2 u_i + 2\alpha_i \alpha_j u_j \tag{4.32}$$

$$\frac{\partial u^2}{\partial uj} = 2\alpha_j^2 u_j + 2\alpha_i \alpha_j u_i \tag{4.33}$$

If cylindrical coordinates are assumed, $\bar{\nabla} u$ is calculated as:

$$\bar{\nabla} u = \frac{\partial u}{\partial \rho}\hat{\rho} + \frac{1}{\rho}\frac{\partial u}{\partial \phi}\hat{\phi} + \frac{\partial u}{\partial z}\hat{z}$$

For the case of optical fibers with refractive index symmetry around their cylindrical axis, the above equation reduces to:

$$\bar{\nabla} u = \frac{\partial u}{\partial \rho}\hat{\rho}$$

or,

$$\bar{\nabla} u = \frac{u_j - u_i}{l_{ij}} \tag{4.34}$$

and finally,

$$\frac{\partial}{\partial u_i}(\bar{\nabla} u) = \frac{u_j}{l_{ij}} \tag{4.35}$$

$$\frac{\partial}{\partial u_j}(\bar{\nabla} u) = -\frac{u_i}{l_{ij}} \tag{4.36}$$

simplifying the form of the functional even further.

By substituting equations (4.32), (4.33), (4.35) and (4.36) into equation (4.27), the following matrix equation is found:

$$S - V^2 B^2 T = 0 \tag{4.37}$$

where

$$S_{ij} = \sum\left[\int \vec{\nabla}\alpha_i(r)\cdot\vec{\nabla}\alpha_j(r)rdr - V^2\int N(r)\alpha_i(r)\alpha_j(r)rdr\right] \tag{4.38}$$

and

$$T_{ij} = \sum \int \alpha_i(r)\alpha_j(r)rdr \tag{4.39}$$

By performing the integration between the points i and j, the above elements of the matrix are found. The solution of the system of equations will resolve the problem's eigenvalues, together with the eigenfunctions. The normalized propagation constant is calculated from the calculated eigenvalues, while the distribution of the field is determined from the eigenfunctions.

The above numerical problem can be solved if the boundary conditions are known. These include the boundary conditions for the fiber center, and for a point away from the center. The boundary conditions at the fiber center depend on the mode whose propagation characteristics will be calculated. In the cladding, however, two types of boundary conditions can be applied.

(a) The field far away from the fiber core becomes zero. This requires that the field at large distances from the fiber core is known.

(b) It is assumed once again that the cladding extends indefinitely, and the field in this region behaves as a modified Bessel function[39]. This function is the exact solution of the differential equation in the cladding region of optical fibers.

$$f(r) = A K_m(\gamma r) \tag{4.40}$$

where K_m is the modified Bessel function of second kind of the mth order, where m denotes the azimuthal mode number, used in the scalar wave equation. In the above equation A is an unknown constant, proportional to the field amplitude. Finally, γ is the propagation constant in the cladding, and is related to the propagation constant β according to the equation

$$\gamma = \sqrt{\beta^2 - k_{cl}^2} \tag{4.41}$$

with k_{cl} being the cladding wavenumber

$$k_{cl} = n_{cl}\, k$$

A program that presents the finite element solution of the wave equation is shown in Appendix 1. In this FORTRAN program the normalized propagation constant is calculated as a function of the normalized frequency. The input variables needed by the program are the normalized index, N, and the normalized position, r. The total number of points, n_{optl}, is the summation of the values in the core and the values in the cladding.

In this program, the number of points in the core is 25 and in the cladding is 3. We have also chosen the data points to be distributed unequally in the core and cladding. The refractive index data in the core are taken at equal normalized intervals of 0.04, while that in the cladding at 1, 2, and 12.5. Of course, the normalized index in the cladding is 1, while in the maximum point of the refractive index is zero. The total number of elements is given by the total number of points minus the number of Dirichlet points, n_{dir}.

For each value of V, the interpolation functions are calculated first. Afterwards, the gradients of the interpolation functions are calculated, and the values are used to determine the elements of the matrices S and T. The values of B are calculated from the solution of the eigenvalue equation. From this solution 27 eigenvalues are calculated. These correspond to the solutions of the 27 first modes. The accuracy of the modes decreases as the mode number increases. This software is used to calculate the normalized propagation constant of the LP_{01} mode only. The first boundary condition was used for the solution of this problem, by assuming that the field far away from the core becomes zero. The value assumed being far away from the core is for an r of 12.5. Because of this assumption, the accuracy of the wave equation's numerical solution will not be as high. The assumption of the second boundary condition, where the field in the cladding behaves as a modified Bessel function, will give more acceptable results. This boundary condition has been applied to the finite differences method of the wave equation's numerical solution.

The normalized propagation constants of two different refractive index profiles were calculated using the above finite element program: the step index profile and the profile of an actual dispersion-shifted fiber. The step index profile was used to determine the validity and therefore the usefulness of the model, since the theoretical values of this profile type are very well known. It was found that the calculated propagation constants of the step index differ significantly from the theoretical ones. The difference is attributed to the inappropriate boundary conditions used. The proper boundary condition would produce a more accurate number, and the software can be applied to determine the propagation parameters of the optical fiber, such the chromatic dispersion. These differences yielded chromatic dispersion variations that were biased by several nm. The same model was used to determine the propagation characteristics and subsequently the chromatic dispersion of the dispersion-shifted fiber whose index function is shown in Figures 4.1. Figure 4.2 presents the calculated normalized propagation constant as a function of the normalized theory. The calculated zero dispersion wavelength (see Section 3) was compared to the measured and a disagreement of more than 50 nm was found.

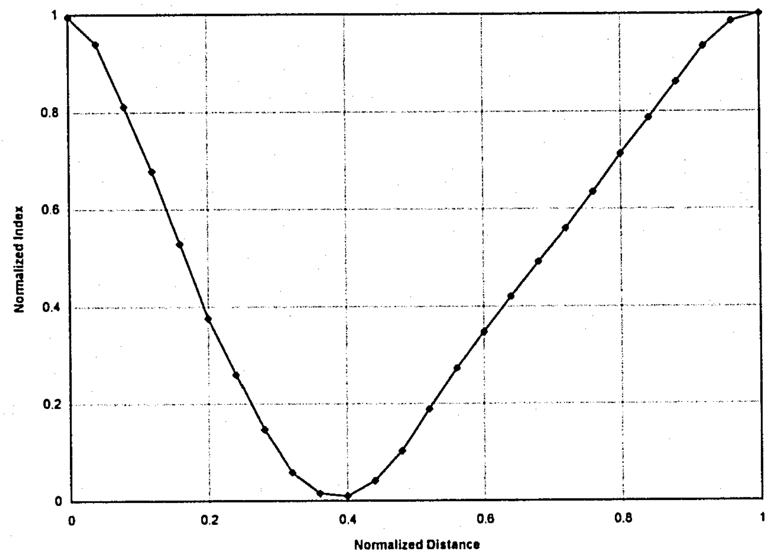

Figure 4.1: Normalized profile of a dispersion shifted fiber manufactured by the MCVD process. The profile is triangular and has a central dip due to GeO depletion.

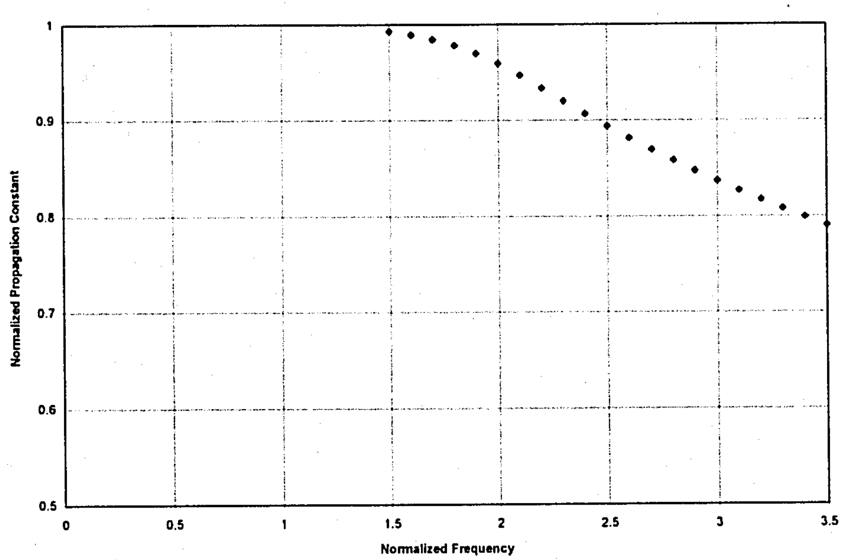

Figure 4.2: Normalized propagation constant as a function of the normalized frequency for the above fiber profile.

4.4 Numerical Solution of the Scalar Wave Equation by the Finite Difference Technique

A one-dimensional finite-difference model can also be developed to determine the eigenvalues and eigenfunctions of the scalar wave equation. This is accomplished by dividing the core region into *2L* segments, each of length *h*. The first and second derivative of the field are given by the equations:

$$H'_s = \frac{H_{s+1} - H_{s-1}}{2h} \tag{4.42}$$

$$H''_s = \frac{H_{s+1} - 2H_s + H_{s-1}}{h^2} \tag{4.43}$$

and therefore the scalar wave equation (4.20) becomes:

$$\frac{H_{s+1} - 2H_s + H_{s-1}}{h^2} + \frac{1}{h(s-1)} \frac{H_{s+1} - H_{s-1}}{2h} + V^2(B^2 - N_1)H_s = 0 \tag{4.44}$$

for $1 \leq s \leq S$

where S is the total number of points.

The boundary conditions can be inserted for every mode that has to be calculated. For the LP_{01} propagation mode, the following boundary conditions apply:

$H(0) = 1$

$H'(0) = 0$

alternatively, the above conditions can be expressed in finite differences as

$$H_1 = 1 \tag{4.45}$$

$$H_1' = \frac{H_2 - H_1}{2h} = 0 \tag{4.46}$$

Another boundary condition can be developed from the scalar wave equation, by approximating the limit as the distance from the fiber center approaches zero:

$$\lim_{r\to 0} \frac{d^2 H}{dr^2} + \lim_{r\to 0}\left[\frac{1}{r}\frac{dH}{dr}\right] + \lim_{r\to 0} q^2(r)H(r) = 0$$

Therefore, the following value is obtained at the limit:

$$\begin{aligned}\lim_{r\to 0} \frac{d^2 H}{dr^2} &= -q^2 H(0)/2 \\ &= [N(0) - B^2]V^2/2\end{aligned} \tag{4.47}$$

The final boundary condition can be applied at the core-cladding interface, where the electric field and its first derivative have to be continuous. In this case, it can be assumed with very good accuracy, that the field in the cladding can take the form of the modified Bessel function of the second kind, as it occurs in the usual step index approximation[40]:

$$H(r) = AK_0[V\sqrt{1-B^2}\,r] \tag{4.48}$$

At r = 1 (i.e. in the core/ cladding interface), the equation in the boundary becomes

$$\frac{dH/dr}{H} = V(1-B^2)\frac{K_0'[V\sqrt{1-B^2}]}{K_0[V\sqrt{1-B^2}]} \tag{4.49}$$

From equations (4.40) and (4.41) the second field point, H_2, can be calculated:

$$H' = \frac{H_2 - H_0}{2h} = 0$$

Therefore,

$$H_2 = H_0 \tag{4.50}$$

At the same time, from finite differences the second derivative is found to be

$$H'' = \frac{H_2 - 2H_1 + H_0}{h^2} = \frac{(N_1 - B^2)V^2}{2}$$

Therefore,

$$H_2 = H_1 + V^2 h^2 \frac{N_1 - B^2}{4} \tag{4.51}$$

If the index of refraction in digitized form is known, together with the parameters V, h, and B, the first two components of the field can be calculated. Subsequently, the field of the whole fiber structure can be calculated. This is accomplished by using the following equation, as derived from the scalar wave equation, after digitizing using finite difference principles:

$$H_{s+1} = \frac{2(s-1)[2 - h^2 V^2 (B^2 - N_s)]H_s - (2s-3)H_{s-1}}{2s-1} \tag{4.52}$$

The above equation is valid for

$2 \leq s \leq S\text{-}1$

The question remains as to how to select the proper B value. This can be accomplished by satisfying the boundary condition at the core/cladding interface, where the field and its derivative just inside the core are both equal to the one just into the cladding. By satisfying equation (4.49) this relationship can be guaranteed, and therefore the proper solution of the equation can be found.

After the eigenvalues of the scalar wave equation have been found, the following propagation properties of the optical fiber waveguide can be calculated:

(a) chromatic dispersion effects in optical fiber

(b) leakage loss of the fundamental and second order modes

(c) effects of bending on the fiber propagation characteristics (Bending loss)

(d) loss due to microbends in optical fibers (Low temperature cabling effects)

(e) loss characteristics of the second order (LP_{11}) mode for determination of the minimum fiber length, bend configuration and cutoff wavelength (Modal Noise).

This numerical model was used to determine the chromatic dispersion effects of several types of optical fibers. A detailed amount of work has been performed to date and the leakage loss phenomenon has been eliminated by following some standard design principles. The remaining parameters can be obtained by using a step-profile approximation and avoiding the use of the numerical model. This logical approximation has been used to obtain the bend loss properties of the fundamental mode and the loss characteristics of the second order mode.

The software used to determine the propagation parameters of the optical fiber is given in Appendix 2.

The required parameter for the calculation of the normalized propagation constant is the normalized index profile of the fiber. This profile can be of step or parabolic index shape or it can be an actual profile of a fabricated fiber. The profiles are generated by the software after their type is specified.

The parameter B is calculated by matching the fields in the core/cladding boundary. The field in the core is calculated using equations (4.50), (4.51) and (4.52). The field in the cladding is calculated by using equation (4.48). In the same program the Bessel functions of the second kind are also calculated. By using an iterative method at $r = 1$, the proper B value that is required to get the fields matched is determined.

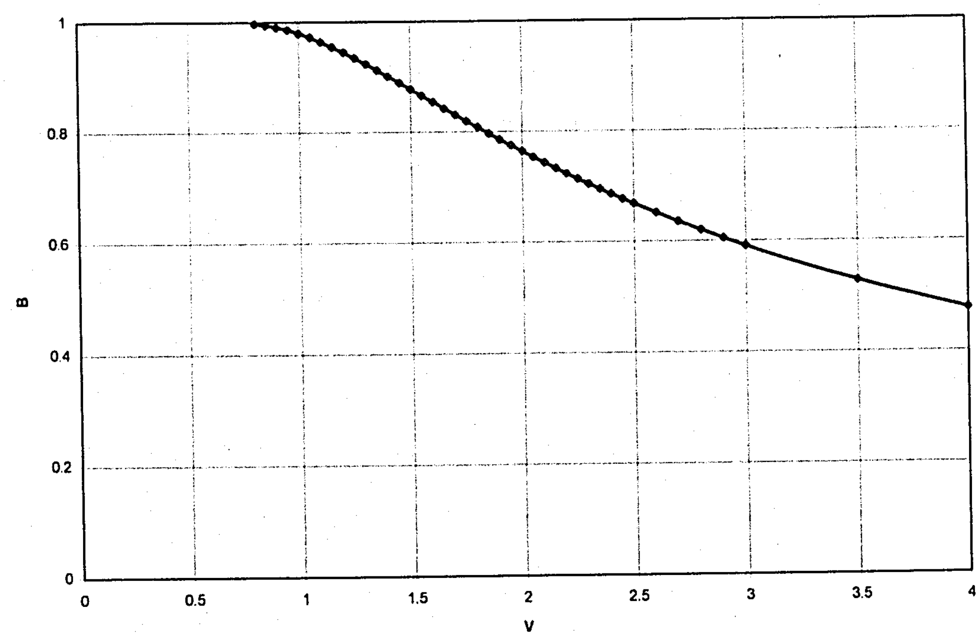

Figure 4.3: Normalized propagation constant as a function of normalized frequency for a step-index profile fiber.

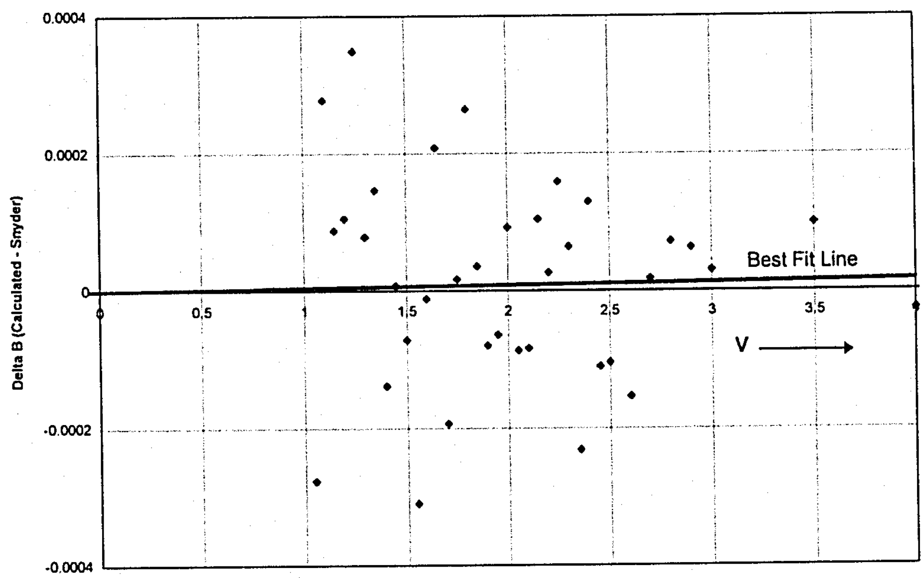

Figure 4.4: Differences between calculated and literature[74] results of the normalized propagation constant.

As was the case with the finite element methods, an actual comparison between theory and literature results was performed for the case of the step index fiber. The calculated normalized propagation constant is given in Figure 4.3 for V values ranging from 0.85 to 4. Figure 4.4 demonstrates the difference between the calculated values and results obtained from the literature[74]. This figure demonstrates that the model has identical accuracy to the literature results, calculated using the theoretical values. The best fit line through the data is close to the V-axis of the plot. The spread in the data is due to the rounding of the literature values. This spread increases at lower V values where a greater precision is required to calculate the propagation constant. A systematic calculation error would result in biased, rather than completely unbiased errors. Due to the greater accuracy of this model, the rest of the calculations were obtained using the finite difference rather than the finite element program.

5.0 CHROMATIC DISPERSION PROPERTIES OF OPTICAL FIBERS

5.1 Introduction

In this section the dispersion properties of an optical waveguide will be determined for an arbitrary refractive index profile. These dispersion effects will be calculated by taking into consideration both the material and waveguide properties of the fiber. Even though, up to now, several workers have attempted to calculate the fiber's dispersion properties, these attempts have been unsuccessful for complicated (e.g. dispersion-shifted) fiber designs, where the waveguide properties have been altered significantly on purpose. The models that currently exist can only predict dispersion trends .

In these calculations, the material effects occur due to the change of the refractive index with the wavelength. The refractive index of the fiber increases with the concentration of GeO_2, which is used as a dopant in the core, and decreases with the concentration of F, which is used as a dopant in the cladding for the depressed cladding fiber design[41,42]. The evaluation of the refractive index as a function of wavelength for doped silica has been previously determined experimentally by several researchers[43,44,45], and these values will be used here to assist in the calculation of dispersion. These values are given in a form of a three-term Sellmeier equation [46].

Below, the chromatic dispersion of the fiber is analyzed using the definition of the group delay. It is well known that the group delay can be determined from the following relationship:

$$\begin{aligned}\tau &= L\frac{d\beta}{d\omega} \\ &= L\,\frac{\lambda^2}{2\pi c}\,\frac{d\beta}{d\lambda}\end{aligned} \tag{5.1}$$

In the above equations L is the fiber length. The propagation constant, β, of the fiber is calculated as a function of the fiber normalized propagation characteristics that were defined in equation (2.19):

$$\beta^2 = \frac{2\pi}{\lambda} n_c^2 - \frac{V^2 B^2}{a^2} \tag{5.2}$$

The differentiation of β with respect to k will lead to the time delay equation shown above. By using the proper mathematical manipulation, the following equation can be derived:

$$\tau = \frac{L}{c} \frac{\left[n_c^2 - n_c \frac{dn_c}{d\lambda} \right] - R\left[(n_c^2 - n_{cl}^2) - \lambda \left[n_c \frac{dn_c}{d\lambda} - n_{cl} \frac{dn_{cl}}{d\lambda} \right] \right]}{\sqrt{n_c^2 - B^2 (n_c^2 - n_{cl}^2)}} \tag{5.3}$$

In the above equation, n_c is the refractive index of the core, n_{cl} is the refractive index of the cladding, and R is given by the relationship:

$$R = \frac{d(V^2 B^2)}{dV^2} \tag{5.4}$$

The chromatic dispersion, D, can be calculated from the derivative of the time delay equation.

$$D = \frac{1}{L} \frac{d\tau}{d\lambda} \tag{5.5}$$

The time delay is calculated numerically from equation (5.3). In this equation the parameters that need to be known are the refractive indices of the core and the cladding, n_c and n_{cl}, their dependence on the operating wavelength, λ, the normalized propagation constant, B, and the parameter R. The calculation of the parameter B has been discussed in the previous section. The rest of the parameters are calculated as follows:

The refractive index and its dependence on the wavelength of operation depends on the chemical composition of the fiber structure. Previous researchers have calculated the refractive index of silica doped with GeO_2 and F at different levels of dopant concentration. It was determined that these data fit into a Sellmeier-type equation that has the form:

$$n(\lambda) = \sum_{i=1}^{3} A_i \frac{\lambda^2}{\lambda^2 - \lambda_i^2} \tag{5.6}$$

The parameters A_i and λ_i depend on the composition of the glass. These values were determined experimentally and they are given in Table I for pure SiO_2, 1% GeO_2 doping and 1% F doping.

Table I: Previously measured parameters A_i and λ_i for pure silica, 1% GeO_2 doped and 1% F doped [45].

	SiO_2	**1% GeO_2, 99% SiO_2**	**1% F, 99% SiO_2**
A_1	0.6960879652	0.698304741	0.6889520717
A_2	0.4078604866	0.410080268	0.4020508503
A_3	0.8975816327	0.897385476	0.8765030972
λ_1	0.070890217	0.069786567	0.06566476307
λ_2	0.113859382	0.115574370	0.11789379080
λ_3	9.896161007	9.896161041	9.84285326400

The concentration of GeO_2 is found from the refractive index of the core and the cladding. The parameters A_j and λ_j are extrapolated to their appropriate value depending on the doping composition of the glass. For that purpose, an iterative method is used to determine the dopant concentration from the numerical aperture of the fiber, which corresponds to the refractive index difference between the core and the cladding.

The parameter R is calculated in the main program by using the Rayleigh-Ritz quotient[93]. This quotient is given by the following equation:

$$R = \frac{d(V^2B^2)}{dV^2} = \frac{\langle NH^2 \rangle}{\langle H^2 \rangle}$$

where

$$\langle NH^2 \rangle = \int_{-\infty}^{\infty} NH^2 r dr$$

$$\langle H^2 \rangle = \int_{-\infty}^{\infty} H^2 r dr$$

and N being the index function and H the field.

For a typical fiber, the time delay data fits a three-term Sellmeier equation [46]. This equation has the form:

$$\tau = \tau_0 + \frac{S_0}{4}(\lambda^2 - \frac{\lambda_0^4}{\lambda^2}) \tag{5.8}$$

In the above equation the parameter λ_0 is the zero dispersion wavelength, while S_0 is the dispersion slope. The chromatic dispersion on the fiber is calculated by differentiating the time delay with respect to the wavelength. From the differentiated data, the parameters λ_0 and S_0 can be explained:

- λ_0 is the wavelength at which the fiber dispersion is zero

- S_0 is the slope of the dispersion curve at the zero dispersion wavelength.

The equation that characterizes the fiber's dispersion properties has the following form:

$$D = \frac{S_0}{4}\left[\lambda - \frac{\lambda_0^4}{\lambda^3}\right] \tag{5.9}$$

An example of the time delay equation and the chromatic dispersion dependence on wavelength is shown in Figure 5.1.

Recently, an interest has been shown in fibers operating at unconventional wavelengths. Over the past several years, great interest has concentrated on the operation of conventional dispersion-unshifted class IVa single-mode fiber in the short wavelength region, where low-cost laser sources with the accompanying electronics are currently available, and at long wavelengths, where the fiber attenuation is minimized. For these applications, the dispersion characteristics of the fibers have to be determined at these wavelengths, where significant deviations from the Sellmeier equation may be observed [47]. Fiber applications at short wavelengths are not attainable now, but several links with standard fiber operate at long wavelengths. For that reason, the determination of the dispersion slope is of great importance. Slope errors can amplify chromatic dispersion errors at 1550 nm. In the following section, we calculate the dispersion slope as a function of the fiber parameters for standard fiber types.

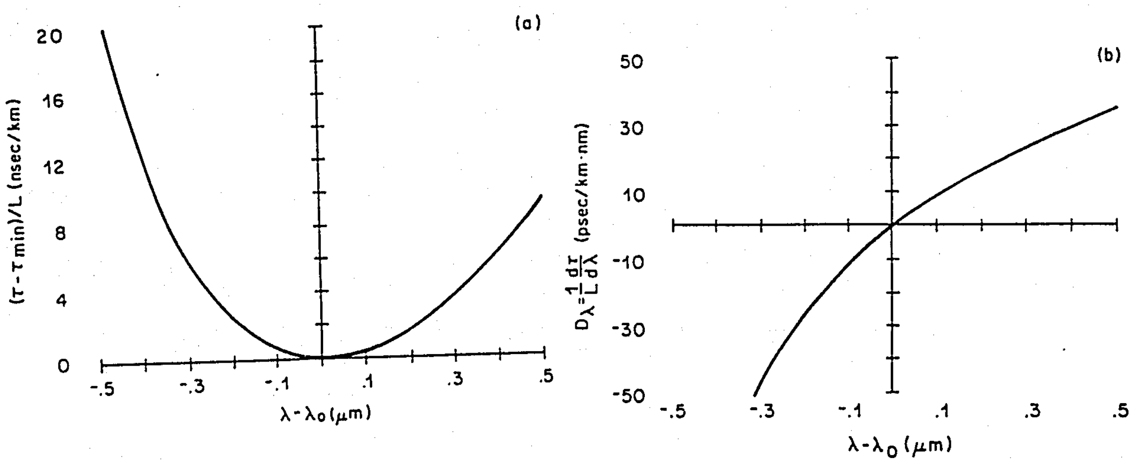

Figure 5.1: (a) Sellmeier form of the time delay equation, common to all dispersion-unshifted fibers. (b) Wavelength derivative of the Sellmeier equation, which corresponds to the fiber's chromatic dispersion.

One of the most significant technical challenges during the last decade has been the alteration of the fiber's chromatic dispersion by adjusting its profile. As described above, two additional fiber types have been developed by using the above approach:

(a) The dispersion-shifted fiber (Figure 1.3a), with its dispersion characteristics shown in Figure 5.2.

(b) the dispersion-flattened fiber. Its profile was shown in Figure 1.3b, and its dispersion characteristics in Figure 5.2. Such a fiber has low dispersion over a wide wavelength range.

While the model developed in this work is meant to concentrate on dispersion-unshifted fibers, it has also been applied to a special type of dispersion-shifted fiber that presents significant advantages over the ones shown in the Figure below.

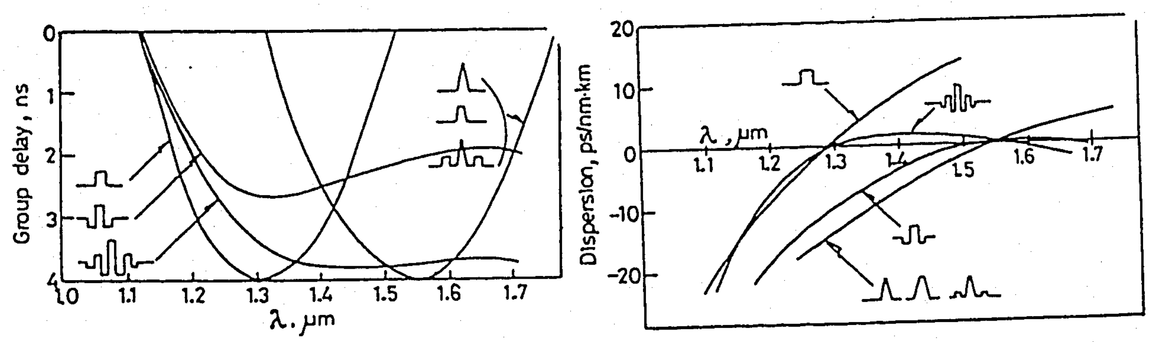

Figure 5.2: Group delay and chromatic dispersion of dispersion-unshifted, dispersion-shifted and dispersion-flattened fibers. The refractive index profile of each fiber type is shown in the same diagram [18].

5.2 Chromatic Dispersion Calculations for Dispersion Unshifted Fibers

The chromatic dispersion calculations are given in Appendix 3, together with the calculations of the propagation characteristics of optical fibers. As mentioned earlier, the refractive indices as a function of the wavelength are determined from the GeO_2 concentration of the core and the F concentration of the cladding using Sellmeier's equations. The dopant concentrations and the fiber core are determined by defining any two of the following parameters: The numerical aperture, the core size, the cutoff wavelength and the mode field diameter. These parameters are interrelated by the following equations [92]:

$$\frac{MFD}{a} = 0.65 + 0.434\left(\frac{\lambda}{\lambda_c}\right)^{3/2} + 0.0149\left(\frac{\lambda}{\lambda_c}\right)^{6}$$

$$V_c = \frac{2\pi}{\lambda_c} aNA$$

where λ is the operating wavelength and λ_c the fiber cutoff wavelength.

The parameter R is also calculated in the corresponding section. Finally, the group delay and the chromatic dispersion are determined from all the above parameters.

The model was tested by comparing theoretical and experimental results. The experimental values were measured by using the Nd-YAG laser method described in Section 7.4. This comparison is shown in Figure 5.3.

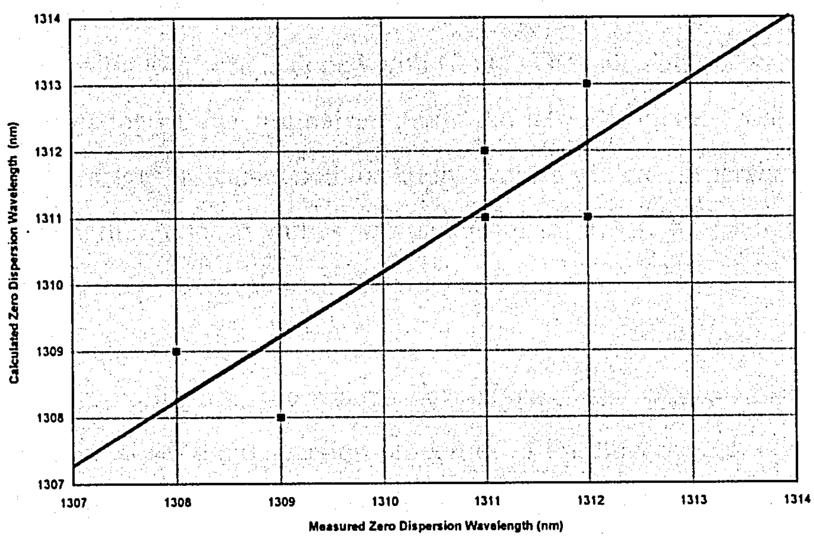

Figure 5.3: Comparison between calculated and measured values of zero-dispersion wavelength for dispersion-unshifted fiber.

The measurements were performed on fibers of varying length. The mode field diameters and cutoff wavelengths were measured in both lengths. In some cases severe deviations occurred from one end to the other due to variations in the fiber fabrication process. The fiber parameters were averaged from one end to the other by assuming that their variation was linear. As seen from this figure, the worst case deviation between the measured and the calculated values is approximately 1 nm. We also observe no bias results and the slope of the line is one. Considering the measurement inaccuracies, being of the order of one nm, and the parameter variation along the fiber length, the agreement is better than expected. The deviations between calculated and experimental results are due to measurement discrepancies and not to inaccuracies of the model.

During the fabrication of optical fibers, parameters such as the mode field diameter and the cutoff wavelength are always measured in standard qualification testing. It would be of great interest to calculate rather than measure the chromatic dispersion of each fabricated fiber from the routinely measured parameters of MFD and cutoff wavelength.

In order to generalize the model, a step index fiber was assumed. The cladding is made of pure silica, while the core is doped with GeO_2. The calculations were completed by a simple modification of the original program. An iterative method was used, where the mode field diameter was calculated for known values of zero dispersion wavelength and cutoff wavelength. A set of values was generated for cutoff wavelength intervals of 10 nm and zero dispersion wavelength intervals of 5 nm.

As seen from the diagram, the shaded box indicates the area of allowable MFD and cutoff operation where the dispersion properties of the fiber remain within the specified limits. The dispersion limits are set between 1300 and 1320 nm, while the MFD limits are set between 9 and 10 μm. The cutoff wavelength limit is below 1330 nm. The purpose of this limit will be discussed in the section of modal noise. The only line missing from the diagram is the bend loss limitation. This limit will be set in the bend loss section.

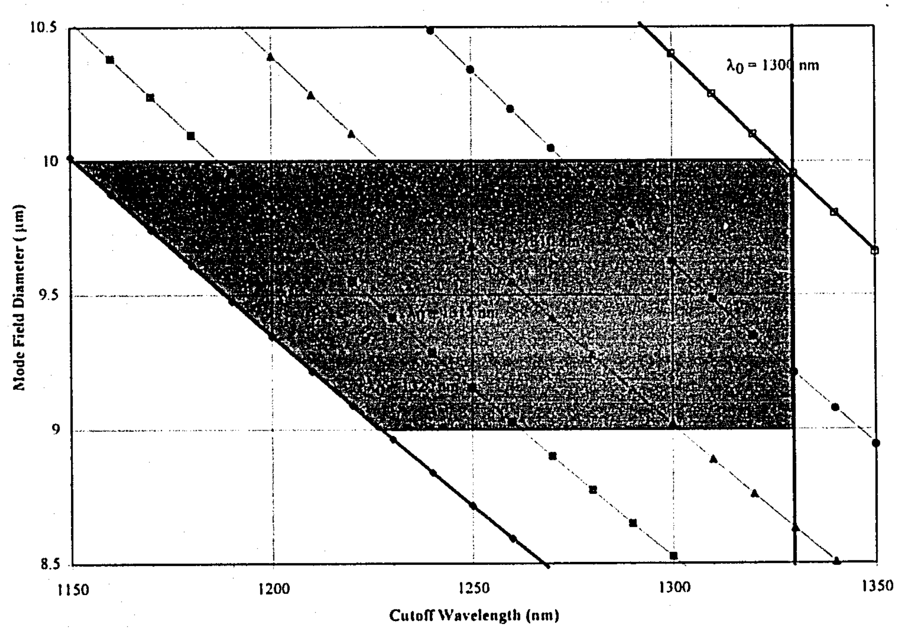

Figure 5.4: Design diagram of a step-index matched-cladding dispersion-unshifted fiber.

The model was also applied to predict the dispersion slope from the zero dispersion wavelength value. It was observed experimentally that in general the dispersion slope decreases as the zero dispersion wavelength increases. This dependence was calculated by using the earlier model. The dispersion slope and zero dispersion wavelength were calculated for fibers with different MFDs and cutoff wavelengths. The calculated dispersion slope was plotted as a function of the zero dispersion wavelength while the cutoff wavelength was kept constant. A linear relationship between the dispersion slope and the zero dispersion wavelength was obtained. By changing the cutoff wavelength another linear relationship is generated. These results are shown in Figure 5.5, for several cutoff wavelengths.

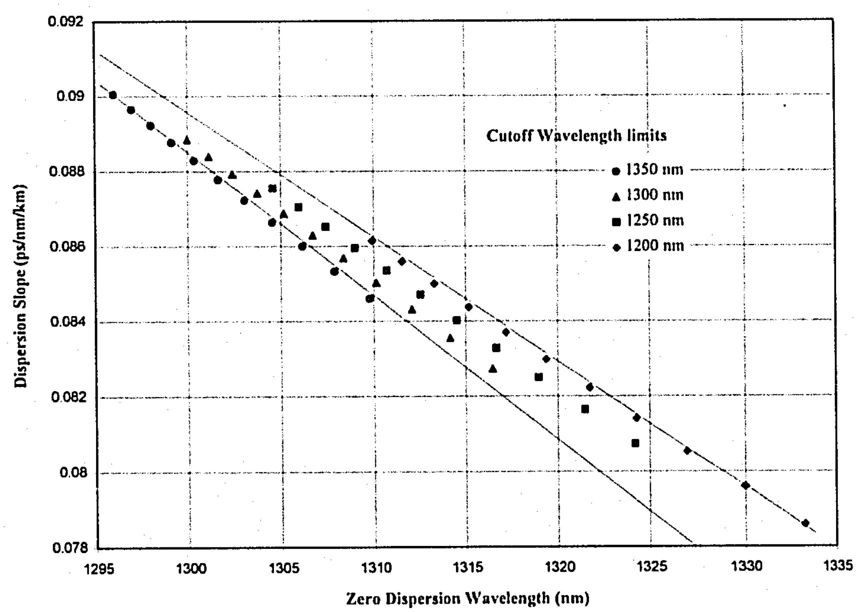

Figure 5.5: Dependence of dispersion slope on the zero dispersion wavelength.

This relationship was then determined experimentally by measuring the dispersion slope and the zero dispersion wavelength of several fibers. Since the cutoff wavelength measurement is not as accurate, it was considered as a random variable and was omitted in this study. The results are shown in Figure 5.6. The error bars indicate the one-standard deviation measurement error of the dispersion slope. A clear dependence of the dispersion slope on the zero dispersion wavelength is observed. These results indicate that fibers with a zero dispersion wavelength higher than the nominal value of 1310 nm are preferable to fibers with zero dispersion wavelength lower than 1310 nm.

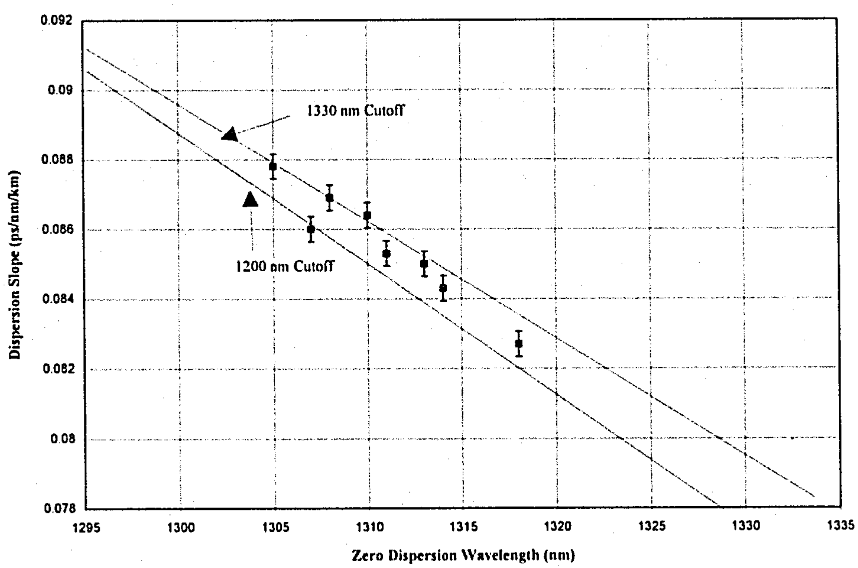

Figure 5.6: Experimentally determined dependence of the dispersion slope on the zero dispersion wavelength. The lower and upper limits are based on calculated values by using the most commonly adopted upper and lower cutoff wavelength values of 1330 nm and 1200 nm respectively.

5.3 Chromatic Dispersion of a Dispersion-Shifted Fiber

Even though this work is meant to define the design limits of step-index dispersion-unshifted fibers, it was felt that defining the chromatic dispersion characteristic of a dispersion-shifted fiber is the most demanding test to determine the capabilities of a model. In this section, a new design for a dispersion-shifted fiber was chosen, and the dispersion parameters were determined by properly adjusting the profile parameters.

The fiber design is shown in Figure 5.7. The fiber is a step index with an index depression at its center. In its two-dimensional form the fiber refractive index will have the shape of a ring. The fiber is characterized by the following parameters:

- The core size, b.
- The size of the central depression, a.
- The index difference between the core and the cladding.

This fiber type has the following advantages over conventional dispersion-shifted designs:

- The effective area of the field, A_{eff}, is large due to the dip in the core's center. Large effective areas are desirable since they can reduce the nonlinear properties of the fiber, a great concern in long-wavelength transmission.
- The scattering coefficient can be reduced. GeO_2 particles act as scattering centers and increase the Rayleigh scattering of silica. The contribution of each fiber section to the scattering coefficient depends on the field intensity in the section and its GeO_2 concentration. In conventional dispersion-shifted fibers the higher field intensity coincides with the high GeO_2 concentration. These two parameters are opposite in this fiber design. Therefore, low attenuation can be achieved even for high refractive index differences.

These characteristics do not come without penalties, however. This fiber design has lower bend loss performance. The bend loss is a function of the mode field diameter, which in turn is proportional to the effective area of the fiber. A careful choice of all the parameters is necessary in order to optimize the performance of the fiber. The bend loss characteristics of this fiber type are outside the scope of this work, and will not be evaluated.

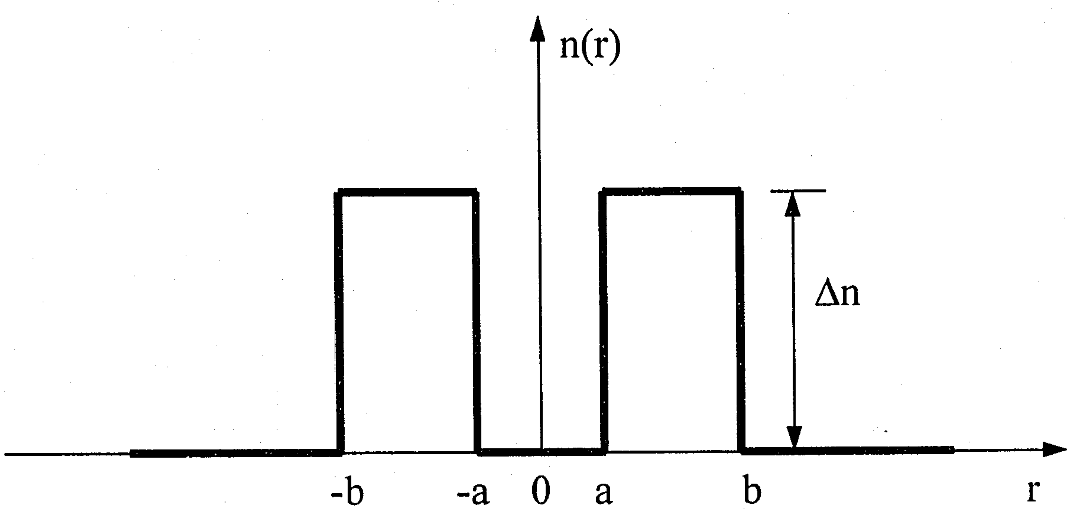

Figure 5.7: Refractive index profile of the dispersion-shifted fiber under study.

The dispersion properties of this fiber type were determined as a function of the cutoff wavelength, the numerical aperture, NA, and the ratio of the depression to the core size, b/a.

The numerical aperture is calculated using the following equation:

$$NA = \sqrt{2n\Delta n}$$

where n is the refractive index of the cladding.

It was also assumed that the cladding was composed of pure Silica, while the core was doped with GeO_2 only. Several variations of this structure can be fabricated, increasing the complexity of the design and the required calculations. These fiber designs are outside the scope of this work.

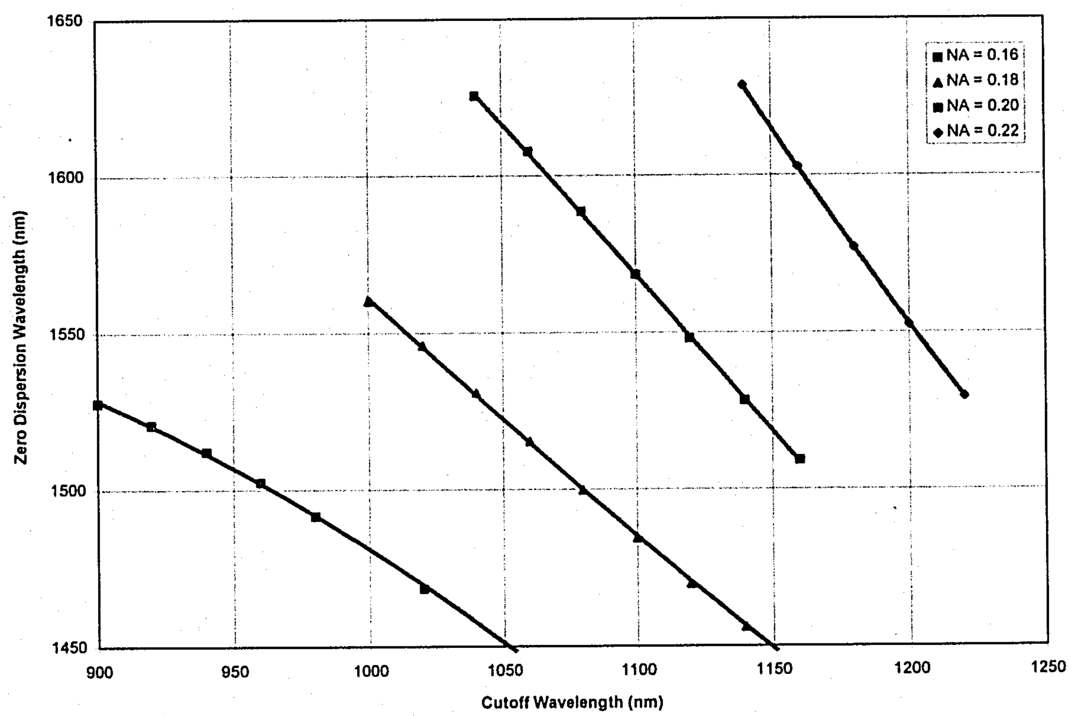

Figure 5.8: Zero dispersion wavelength as a function of cutoff wavelength for fibers with their numerical apertures varying from 0.16 to 0.22. These parameters were calculated for an *a/b* value of 0.375.

The zero dispersion wavelength as a function of the cutoff wavelength is shown in Figure 5.8. This parameter was determined for different values of numerical aperture. The figure demonstrates that the zero dispersion wavelength reduces as the cutoff wavelength increases and as the numerical aperture reduces. Cutoff wavelength and NA reductions result in higher bend loss, while higher NA results in higher attenuation due to an increased level of GeO_2 concentration yielding higher Rayleigh scattering. These plots demonstrate that the proper zero dispersion wavelength of 1550 nm is obtained for NA variations between 0.18 and 0.20 and cutoff wavelength variations of 1000 to 1150 nm. Under these conditions the bend loss has an acceptable value, i.e. without high attenuation increases.

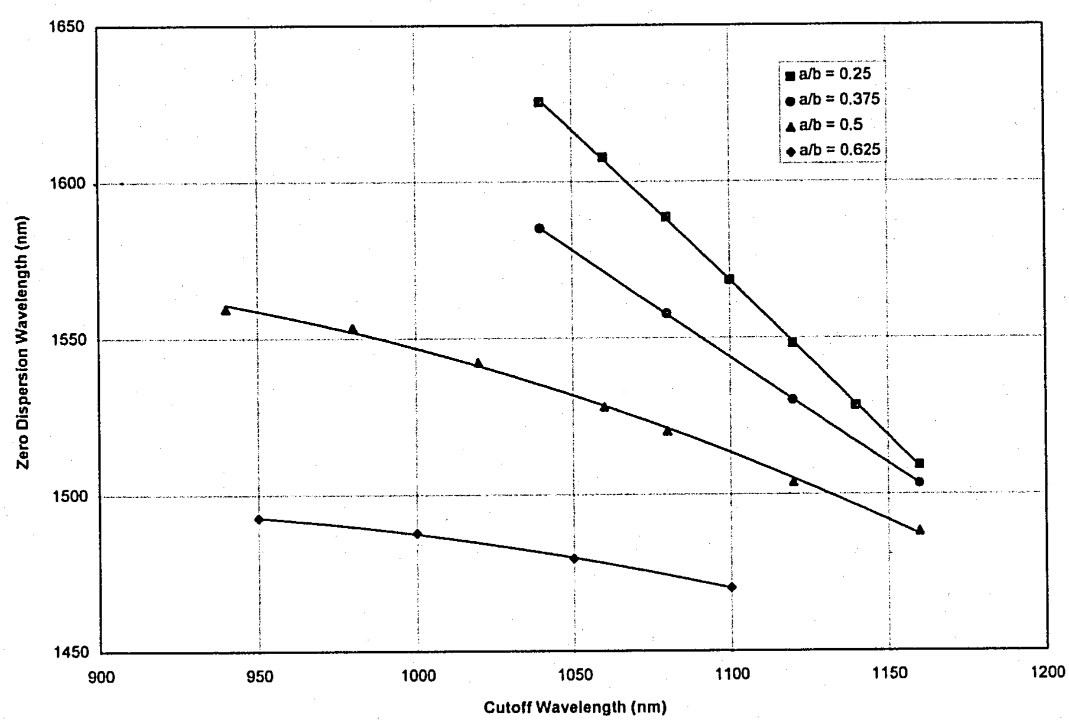

Figure 5.9: Zero dispersion wavelength as a function of cutoff wavelength for fibers with varying a/b values and NA of 0.2.

In Figure 5.9 the zero dispersion wavelength was calculated as a function of the *a/b* ratio by keeping the numerical aperture constant at 0.2. The zero dispersion wavelength has the proper value if the cutoff wavelength varies between 1000 and 1150 nm and the *a/b* ratio is less than 0.5. As the *a/b* ratio increases, the zero dispersion wavelength decreases. Higher effective areas and lower scattering coefficients result in lower zero dispersion wavelengths. From Figures 5.8 and 5.9 we can say that the optimum fiber parameters for the above design are:

- **Cutoff wavelength of 1050 to 1150 nm**
- ***a/b* ratio of 0.3 to 0.4**
- **NA of 0.18 to 0.20**

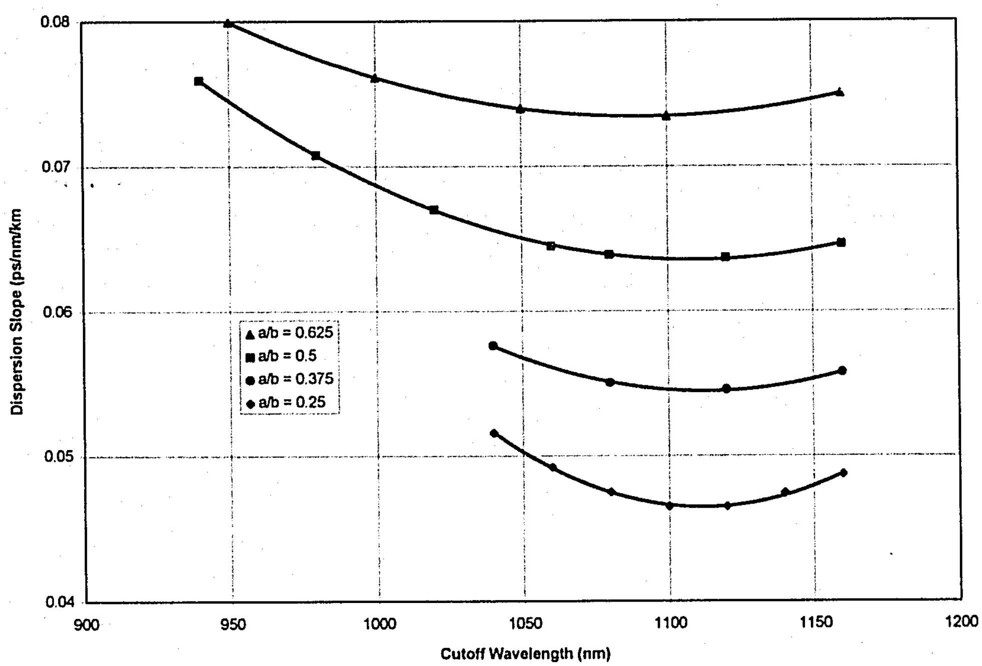

Figure 5.10: Dispersion slope as a function of cutoff wavelength for fibers with varying *a/b* value and NA of 0.2.

The other important dispersion parameter that was calculated is the dispersion slope. The results are presented in Figure 5.10, where the slope is plotted as a function of the cutoff wavelength for several *a/b* ratios. This figure demonstrates that the slope reaches a minimum value with the cutoff wavelength. This value varies between 1050 and 1100 nm, which are in the desired range. As the *a/b* values decrease, the dispersion slope decreases. A dispersion slope between 0.05 and 0.6 ps/nm/km is obtained for *a/b* ratio of 0.375. The low dispersion slope of this fiber type makes it an even more attractive alternative to the higher slopes of 0.07 to 0.08 ps/nm^2/km of the conventional dispersion-shifted fibers since they will result in lower chromatic dispersions over a wider operating wavelength range.

6. BENDING AND MICROBENDING LOSSES OF OPTICAL FIBERS

6.1 Introduction

The bending performance of an optical fiber is a significant parameter in optimizing the fiber's design criteria. This parameter becomes even more significant for fibers that operate at much longer wavelengths than their cutoff wavelength. During installation of a fiber optic link, tight bends are applied to the fibers in the splice organizer trays. In addition, accidental tight bends imposed on the fiber can result in very high bending losses, and, ultimately, system failures.

Many of the current optical cable designs impose a curvature of 5 to 6 cm radius on the fiber, by oscillating the fiber around the central strength member in a helical stranding process[52]. Since there can be thousands of these curvatures per kilometer of fiber, their effect on the overall fiber attenuation can be significant, especially at long operating wavelengths. Most of the current cable structures are affected by this macrobending loss rather than microbending loss. In this section we will define a curve where a constant bend loss is determined from the cutoff wavelength and the mode field diameter of the fiber.

The loss due to curvature can be explained by observing the plane wavefronts of the bent fiber. These wavefronts are pivoted at the center of curvature of the bent fiber, and their longitudinal velocity increases with the distance from the center of the fiber axis. Therefore, there is a distance at which the fiber's phase velocity is higher than that of a plane wave in the cladding. At this distance the electromagnetic field resists radiates away from the guide, causing the "bend-induced" loss[53].

The bending loss is represented graphically by a confocal transformation, where the bent fiber is transformed to a straight one and the refractive index changes according to the relationship[54]:

$$n_b(r) = n(r)\left[1 + \frac{r}{R}\cos\phi\right] \tag{6.1}$$

where R is the radius of curvature and r is the distance from the center of the core. Figure 6.1 demonstrates this relationship graphically, for a matched-cladding single-mode fiber with a step-index profile. In the same diagram the fiber's effective refractive index is presented as β/k. The refractive index of equation (6.1), $n_b(r)$, is called the "equivalent refractive index".

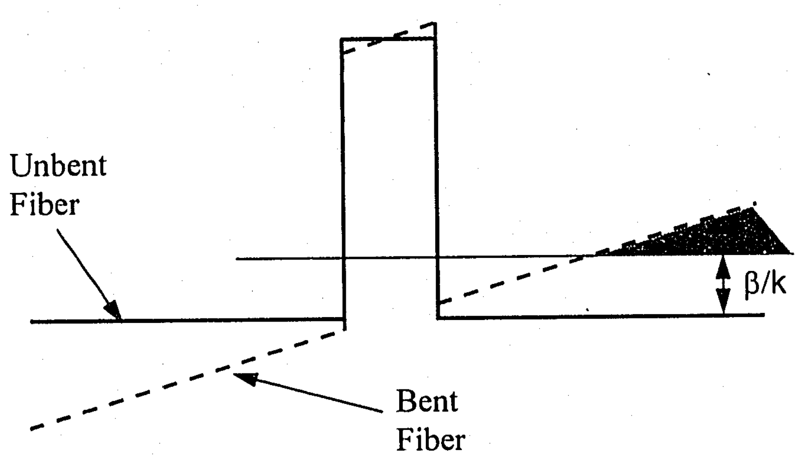

Figure 6.1: Refractive index profile of a matched-cladding single-mode fiber, and its equivalent index when the fiber is bent. The shaded area above the effective refractive index indicates the region where the mode is radiated.

This refractive index can be introduced into the scalar wave equation, and a complex propagation constant can be found, with the imaginary part contributing to the bending loss of the optical fiber.

There are two ways that the loss of the curved fiber can be approximated:

(i) By using a perturbation approach, the solution of the wave equation is found by using the scalar wave equation and assuming a straight fiber. Afterwards, the equivalent refractive index of the fiber due to bending replaces the actual refractive index and is integrated over a distance r where the calculation takes place. The loss due to bending is calculated by computing the power radiated from the fiber, and dividing it by the power carried by the mode. Of course, this is accomplished by using the Poynting Theorem.

(ii) By using a similar perturbation approximation, the field in the fiber is separated into two parts: The field due to the fundamental mode, and the one due to the radiated mode. The fiber curvature results in the coupling of the two modes. By calculating the coupling coefficient, the bending loss is derived. The coupling coefficient between the two modes is a strong function of the radius of curvature.

These methods are complicated and the resulting calculations have similar accuracies to the values assuming a step index approximation [55,56]. The bend loss obtained from these references is given below:

$$\alpha_b = A_c R^{-1/2} \exp(-UR) \tag{6.3}$$

with the parameters A_C and U given by the following equations:

$$A_c = \frac{1}{2}\sqrt{\frac{\pi}{a\chi^3}}\frac{\gamma}{(VK_1(\chi))^2}$$

$$U = \frac{4\Delta n\chi^3}{2aV^2n^2}$$

where

$$V = kan\sqrt{n\Delta n}$$

$$\chi^2 = n_c^2 k^2 - \beta^2 \qquad (6.4)$$

$$\gamma^2 = \beta^2 - n_{cl}^2 k^2$$

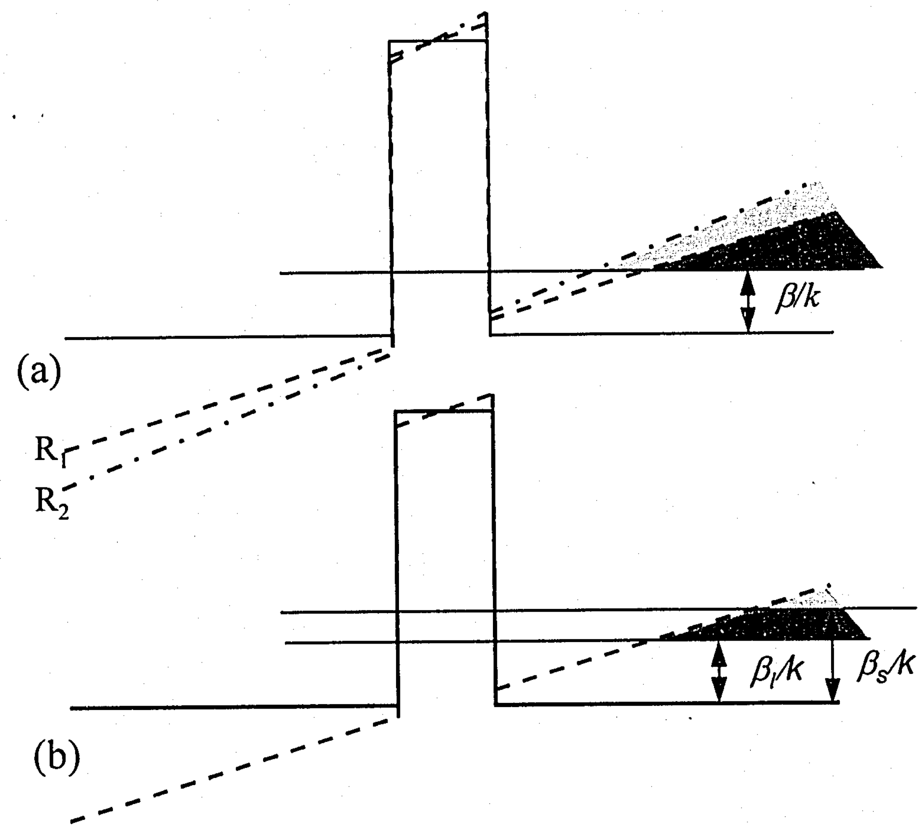

Figure 6.2: (a) By decreasing the bend radius of the fiber, the loss due to radiation increases as shown by the shaded area. (b) The effect of wavelength on the bending loss of single-mode fibers. As the wavelength increases from λ_s to λ_l, the fiber's effective index decreases, resulting to higher radiation losses.

This relationship is valid for matched-cladding fibers only. If the normalized propagation constant is calculated as a function of the normalized frequency for the case of the straight fiber, the bend performance of the matched-cladding fiber is known from the above expressions. In 6 6.2, the effect of the wavelength on the bending loss is shown, together with the effect of the bend radius.

For a depressed-cladding fiber a more complicated expression must be developed with which the fiber's bend performance can be analyzed only numerically[57]. In this case, the boundary between the inner and outer cladding plays a fundamental role in the excess bending loss. Graphically, this is shown in Figure 6.3 where the equivalent refractive index of a depressed-cladding fiber is plotted as a function of the distance from the fiber core. The effect of the ratio between the core and the inner cladding diameter as well as the curvature and wavelength effects on the bending loss can also be presented graphically as before.

Analytically, the bend loss is calculated by assuming that part of the field in the inner cladding region is is transmitted and part of it is reflected at the inner-outer cladding interface[57]. The bending loss is calculated from the ratio of the field amplitude transmitted in the outer cladding to the field amplitude in the core region.

In addition to the relationships given in equation (6.4), the following relationship is required:

$$\sigma^2 = n_{oc}^2 k^2 - \beta^2 \qquad (6.5)$$

where n_{oc} is the refractive index of the outer cladding.

The bend loss coefficient is calculated as the ratio of the power radiated to the power carried in the LP_{01} mode when the fiber is straight. The radiated power is found from the amplitude of the wave transmitted at the inner/outer cladding interface to the power carried by the fundamental mode. After several calculations, the following equation is derived [57]:

$$2\alpha(R) = \frac{4b\chi^2}{\beta V^2 K_1^2(\gamma a)} \int_0^{\pi} \frac{\bar{\sigma}(b)\bar{\gamma}^2(b)}{U[\bar{\gamma}^2(b) + \bar{\sigma}^2(b)]} \exp(-2U) d\varphi \tag{6.6}$$

where

$$\bar{\sigma}^2(r) = n_{oc}^2\left[1 + 2\frac{r}{R}\cos\phi\right]k^2 - \beta^2$$

$$\bar{\gamma}^2(r) = \beta^2 - n_{cl}^2\left[1 + 2\frac{r}{R}\cos\varphi\right]k^2 \tag{6.7}$$

$$U = \int_0^b \bar{\gamma}(r)dr$$

The above calculations are performed only numerically. A program where the bend loss of a depressed-cladding fiber is calculated is shown in Appendix 3. The results of these calculations are shown in the following section.

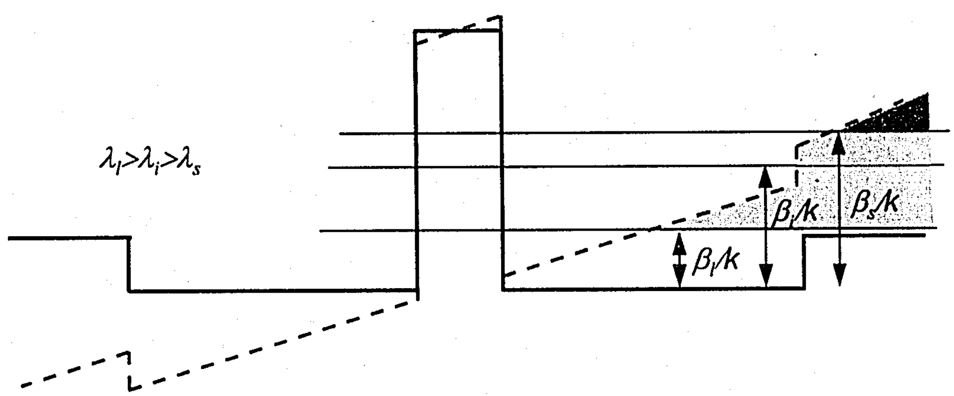

Figure 6.3: Bend loss effect on depressed-cladding single-mode fibers. Depending on the bend radius and the wavelength of operation, radiation may occur in the outer cladding, inner/outer cladding boundary, or inner cladding.

Up to now all the bend loss calculations performed on optical fibers have assumed a step-index approximation, and for the case of the index profiles deviating significantly from the step approximation, an equivalent step profile has been assumed[58]. Even though this assumption seems to be crude, it has provided excellent guidelines in the prediction of the fiber's bend loss.

An effect that can result in disagreements between theory and experiment, is the refractive index change due to tension and compression caused by bending[59]. The tension points will reduce the refractive index, while the compression points will increase it. These changes are opposite to change in the phase velocity, and will result in decreasing the effective radius of curvature of the fiber. This effect is shown in 6 6.4. If the refractive index change due to tension or compression is predicted accurately, the agreement between experiment and calculation should improve. Even though the change of the refractive index with curvature has been well documented in the literature, it has not been used previously in the prediction of the bending loss.

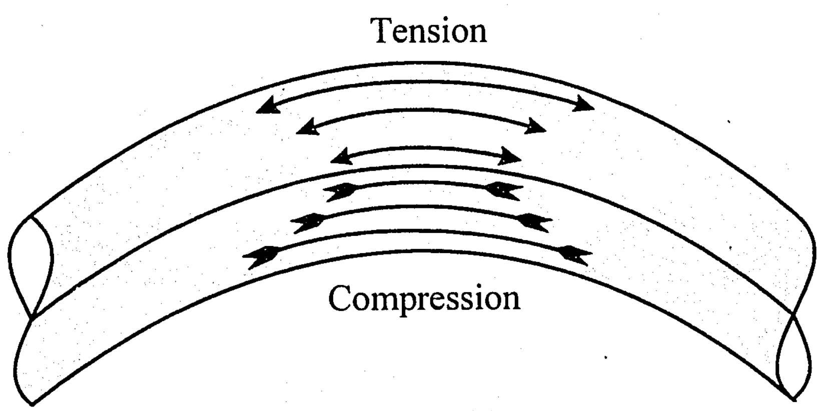

Figure 6.4: Tension and compression applied to the fiber during bending.

As mentioned previously, the bend characteristics of the fiber are significant in calculating losses caused due to installation. However, they cannot predict cabling losses and losses caused by low temperatures. In this case a microbending model needs to be developed. Microbends are defined as deviations of the fiber axis of the order of a few microns in amplitude. A microbending model is based on the second approach given previously. The loss that occurs between the fundamental and the second order mode is a function of the "profile of the microbends", or the curvature power spectrum. An example of the microbends is shown in 6 6.5, where the equivalent refractive index distribution is shown by using the confocal transformation presented earlier. The fiber loss due to microbending can be calculated from equations (6.3) and (6.4), if the spectrum of the microbends is known:

$$\Phi(\Omega) = \lim_{L \to \infty} \frac{1}{L} \left| \int_0^L \frac{1}{R(z)} \exp(-j\Omega z)\, dz \right| \tag{6.8}$$

With the recent trends towards larger repeater spacings and, subsequently, longer wavelengths, the fiber bending and microbending performance becomes even more significant than before. It has been found experimentally that fibers with good bend performance will have superior microbend performance. It is easier to determine the fiber's bend loss rather than relying on the more complicated microbend calculations and testing in order to determine the attenuation characteristics of the fiber at various environmental and layout conditions.

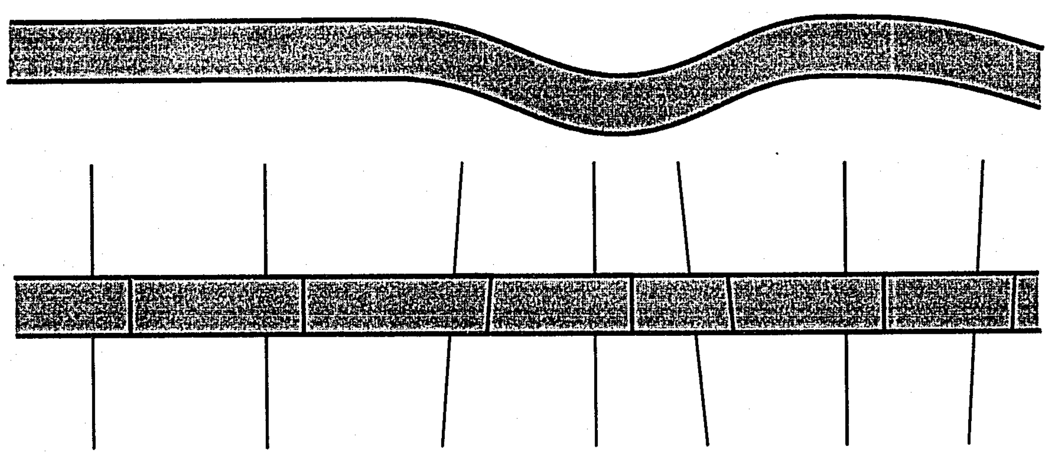

Figure 6.5: Fiber microbends and their transformation to equivalent refractive indices.

6.2 Bending Loss of Matched Cladding Fibers

The bend loss of the matched-cladding fiber is calculated from equation (6.4) above. This loss was calculated for the worst case of the following layout conditions:

- 100 bends of 2.5 cm constant bend radius. As explained below, this bend limit was set as the minimum diameter that a fiber can be bent without long term mechanical degradation due to fatigue
- 1 bend of 1.25 cm radius. This bend limit was set as a safety value for temporary tight bends imposed in the fiber without a significant power penalty.

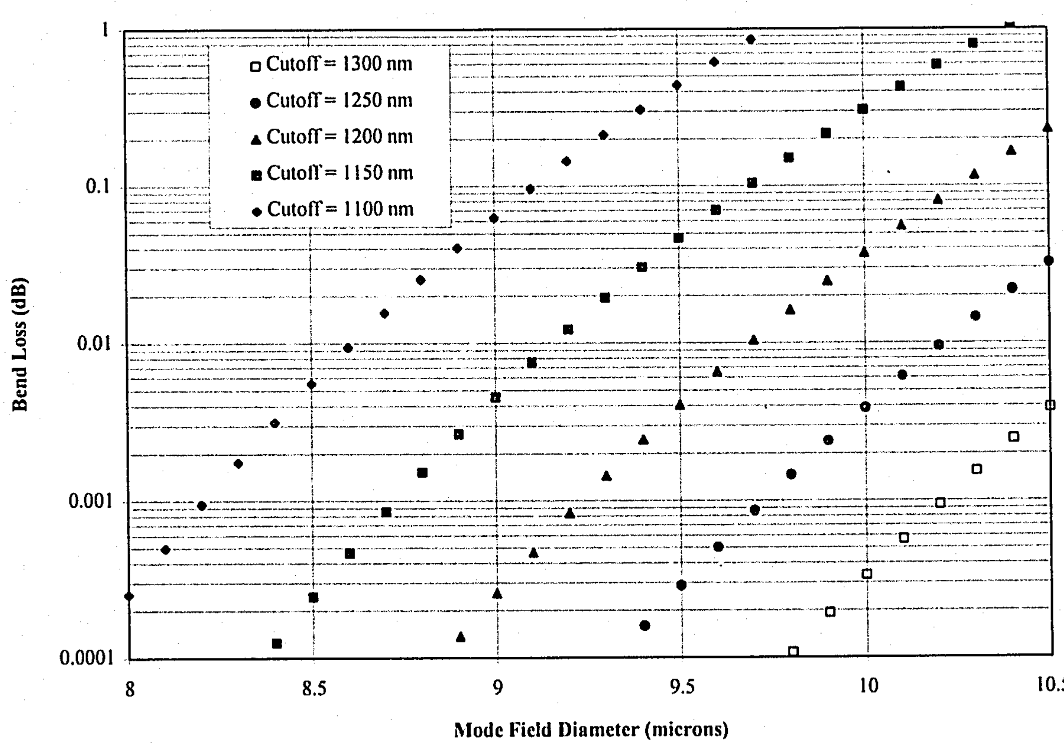

Figure 6.6: Bending loss of a step-index matched-cladding fiber as a function of the mode field diameter and the cutoff wavelength for 100 bends of 2.5 cm radius.

These calculations were performed using a spreadsheet program. The results of the calculations are shown in figures 6.6, 6.7 and 6.8. In all these calculations the bend diameter was corrected for the tension effects on the refractive index.

Figure 6.6 shows the bend dependence of cutoff on both the mode field diameter and the cutoff wavelength of the fiber. As seen, the bend loss increases as the mode field diameter increases or as the cutoff wavelength decreases. These trends can be predicted by using the graphical evaluation shown in Section 6.1. The case of varying cutoff wavelength with the same mode field diameter was explained in Figure 6.2b, by comparing the effective indices of the two cases. A similar explanation can be obtained by comparing fibers with identical cutoff wavelengths and varying MFDs.

In this section we want to establish a relationship between the cutoff wavelength and the MFD for constant bend loss. Up to now, elimination of fibers with poor bend loss was guaranteed by setting a limit only on the cutoff wavelength. This limit, set at 1180 nm, rejected fibers with good bend loss performance while it accepted fibers with poor performance. But most importantly, this limit was not based on the bend loss of optical fibers but rather was set arbitrarily, since it was determined empirically that lower cutoff wavelengths result in higher bend losses. The relationship that we will establish will define the limits on the cutoff wavelength and the mode field diameter in the design diagram for a constant bend configuration. This limit will define a curve in the design diagram in the vicinity of the low cutoff wavelength and large MFD below which the fiber should not be manufactured.

The relationship between the cutoff wavelength and mode field diameter was determined from the data of matched-cladding 6.6. The ratio between the MFD and the cutoff wavelength was taken for all data. In Figure 6.7 the bend loss was plotted as a function of the MFD to cutoff wavelength ratio for different cutoff wavelengths. As seen, the bend loss differs for different cutoff wavelengths and the relationship of MFD/λ_{co} cannot be used in the design diagram.

In this work the spread of the data as a function of $(MFD)^n/\lambda_{co}$ was evaluated for different values of the power n. It was found that the least amount of data spread was obtained if n equals 0.8. The results of this relationship are shown in Figure 6.8, where the bend loss as a function of $(MFD)^{0.8}/\lambda_{co}$ is plotted. As seen, the data spread for different cutoff wavelengths has been eliminated.

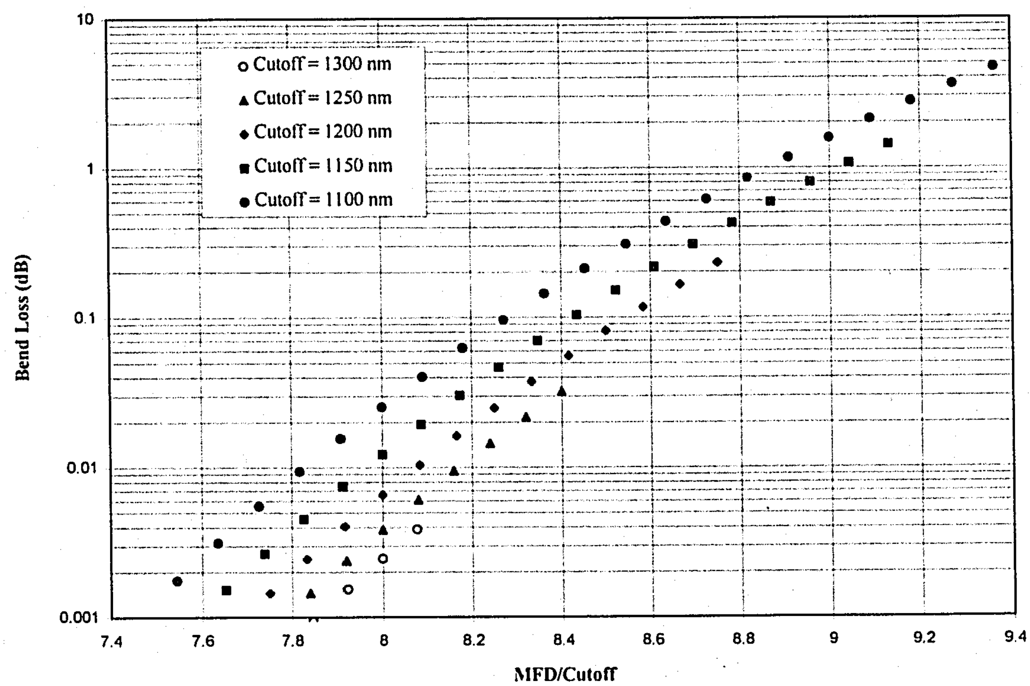

Figure 6.7: Bend loss of the fundamental mode of a matched-cladding fiber as a function of the MFD /λ_{co} for the same bend configuration.

In the same diagram the measured bend loss of the fiber is plotted. The experimental data were obtained by using a spectral attenuation test station described in Section 5.5. As seen, the theoretical results are slightly higher than the experimental ones. Even so, these results demonstrate the best agreement to date between theory and experiment. The disagreement is due to the worst case scenarios that were followed to obtain the theoretical calculations. If these theoretical results are used, though, to obtain the bend loss limit, the actual bend performance of the fibers will always surpass the predicted performance, even if measurement errors occur. These results also demonstrate that the use of the index correction factor can reduce significantly differences that were previously observed between theory and experiment.

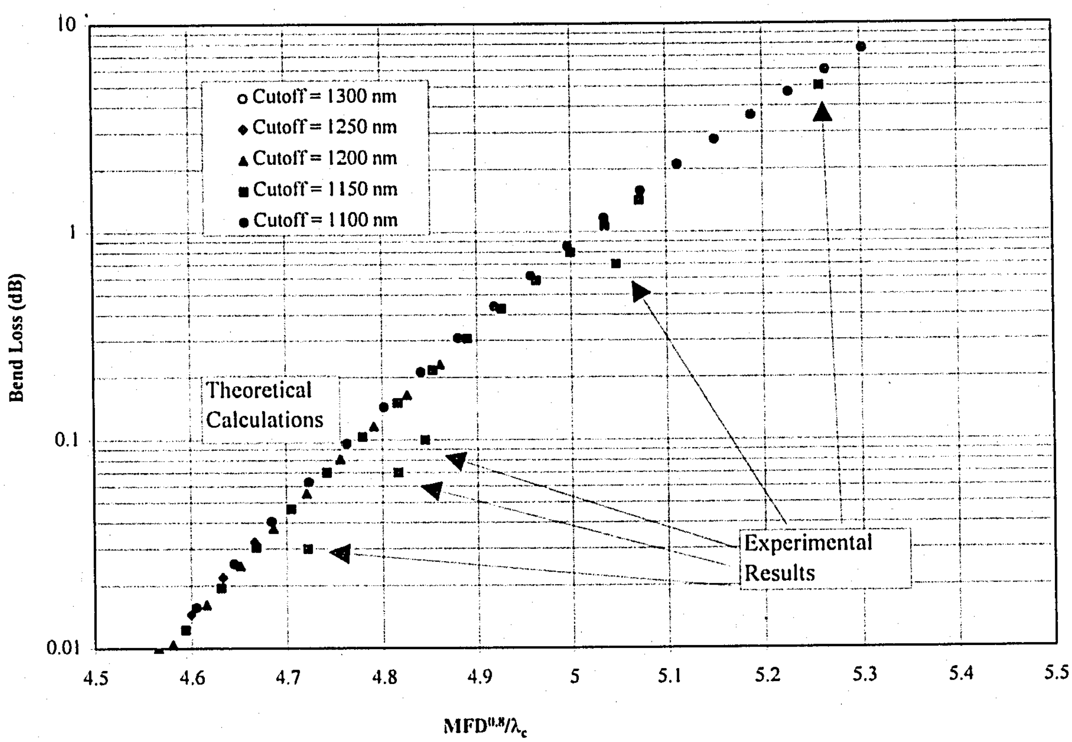

Figure 6.8: Bend loss of the fundamental mode of a matched-cladding fiber as a function of the "index correction factor" $(\mathrm{MFD})^{0.8}/\lambda_{co}$.

From Figure 6.8 it is observed that a value of 6.75 is required in order to achieve bend losses lower than 0.1 dB for 100 bends of 2.5 cm radius. This line is plotted in Figure 6.9 and the bend loss limit is defined.

In order to complete the study, the second limit discussed earlier will be studied in terms of the bend loss. By performing similar calculations as before, the results shown in Figure 6.10 were obtained. For a loss of 0.1 dB, an $(MFD)^{0.8}/\lambda_{co}$ of 6.7 is required. Since this is a lower ratio than the one determined earlier, this bend configuration will establish the bend limit in the design diagram. Both limits are shown in Figure 6.9, where it is observed that the limitations on the MFD and cutoff wavelength due to a single 1.25 cm bend is responsible for the worst case limitations on the fiber parameters

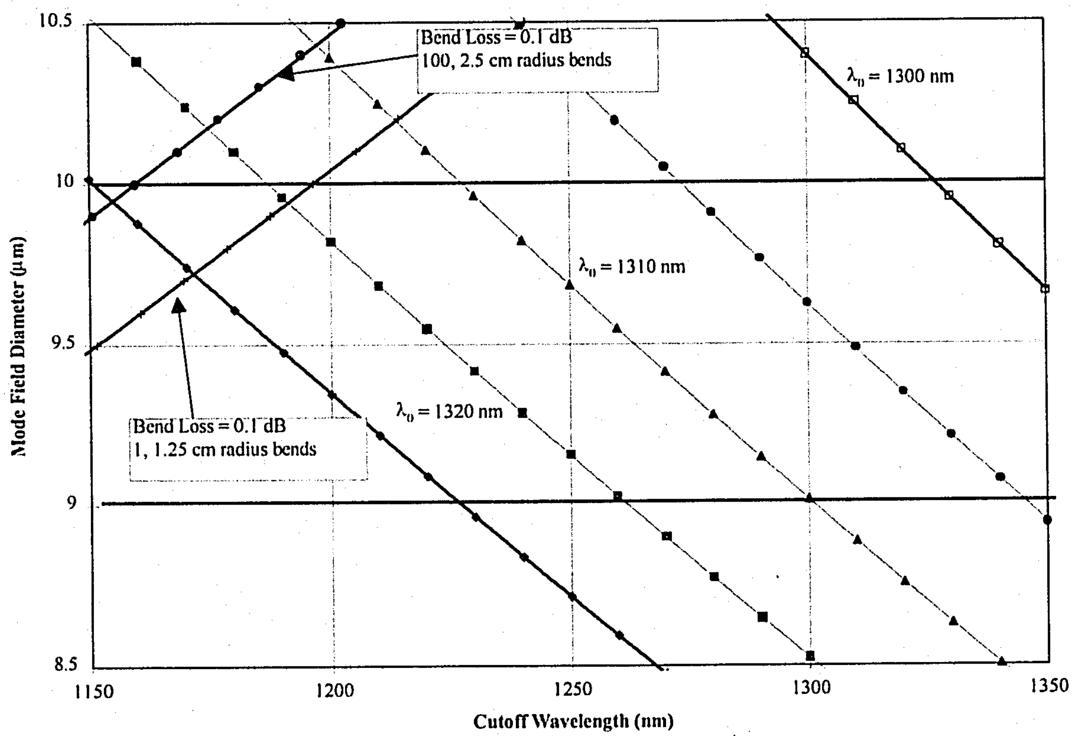

Figure 6.9: Design diagram of a matched-cladding single-mode fiber with the defined bend loss limit.

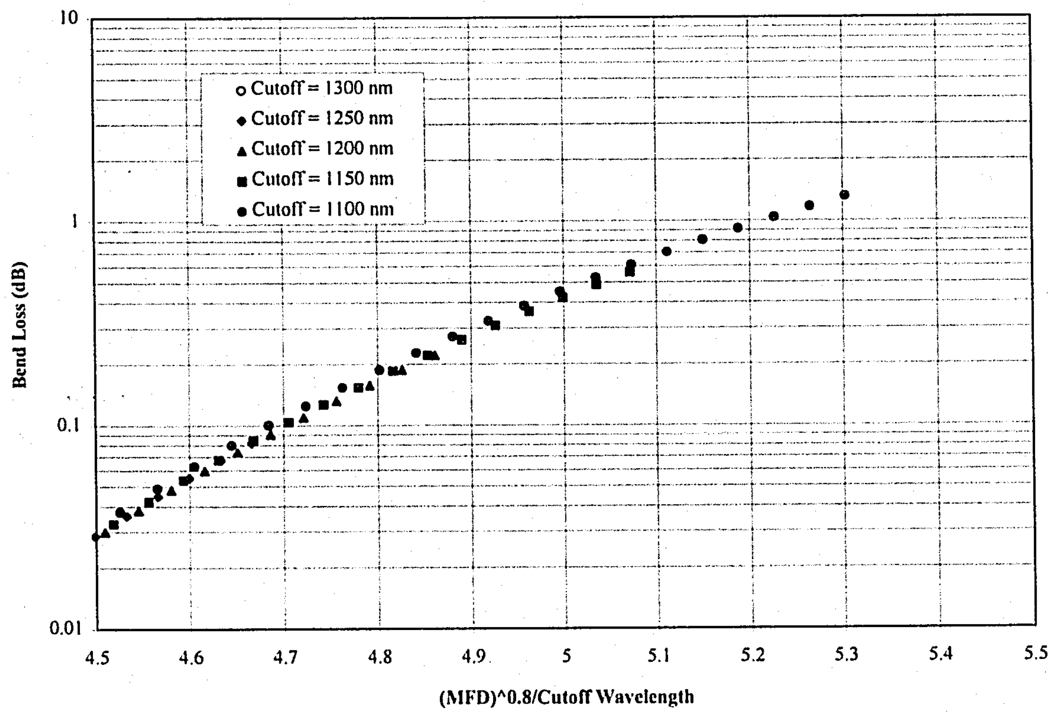

Figure 6.10: Bend loss as a function of the "index correction factor" $(MFD)^{0.8}/\lambda_{co}$ for the fundamental mode of a matched-cladding fiber. The bend configuration is one loop of 1.25 cm radius.

6.3 Bending Loss of Depressed-Cladding Fibers

The bend loss of a depressed-cladding fiber is calculated from equations (6.6) and (6.7) above. The same bend configurations as before were used, but it was found that in contrast to the matched--cladding case the 100 turns of 2.5 cm bend radius configuration was responsible for the loss contribution. The calculations are more involved than before, and for that purpose a program was written to determine the loss of the fiber numerically. The program is shown in Appendix 3.

The parameters of the fiber analyzed in this section had a outer-to-inner cladding ratio of 6 and a depression of 0.001. This type of fiber is used widely in telecommunications networks. It is capable of achieving low dispersion with reduced MFD, improving its bending sensitivity for small bends. For the same reasons, this design results in lower microbend sensitivity.

The design limitation of this fiber type is its bend performance at large bend diameters. In that case, the bend loss of the fiber is higher than the matched--cladding design. Contrary to the matched--cladding fiber case, the limiting bend sensitivity was found to be the 100 bends of 2.5 cm radius rather than the one 1.25 cm radius bend.

The results of the calculations using the program in Appendix 3 are shown in Figure 6.11, where, as before, the bend loss for 100 bends of 5 cm diameter loop is plotted as a function of the MFD^n/Cutoff ratio. A similar approach as in the matched--cladding section was taken to determine the value of n. The best fit obtained was for $n=1$. The calculations were corrected for the proper index changed caused by the tension and compression of the material.

Two major telecommunications companies manufacture this fiber type: AT&T and Northern Telecom. In this study, the bend sensitivity of actual production fibers was measured. The results of the measurements are presented in Figure 6.11. There is good agreement between theory and experiment, both qualitatively and quantitatively. The experimental results are close to the numerical ones, especially at the 0.1 dB bend loss. The large spread between experimental and theoretical results, especially at large bend loss values, are once again due to the conservative nature of the theoretical model. This slight disagreement helps establish a conservative upper limit that can account for measurement errors.

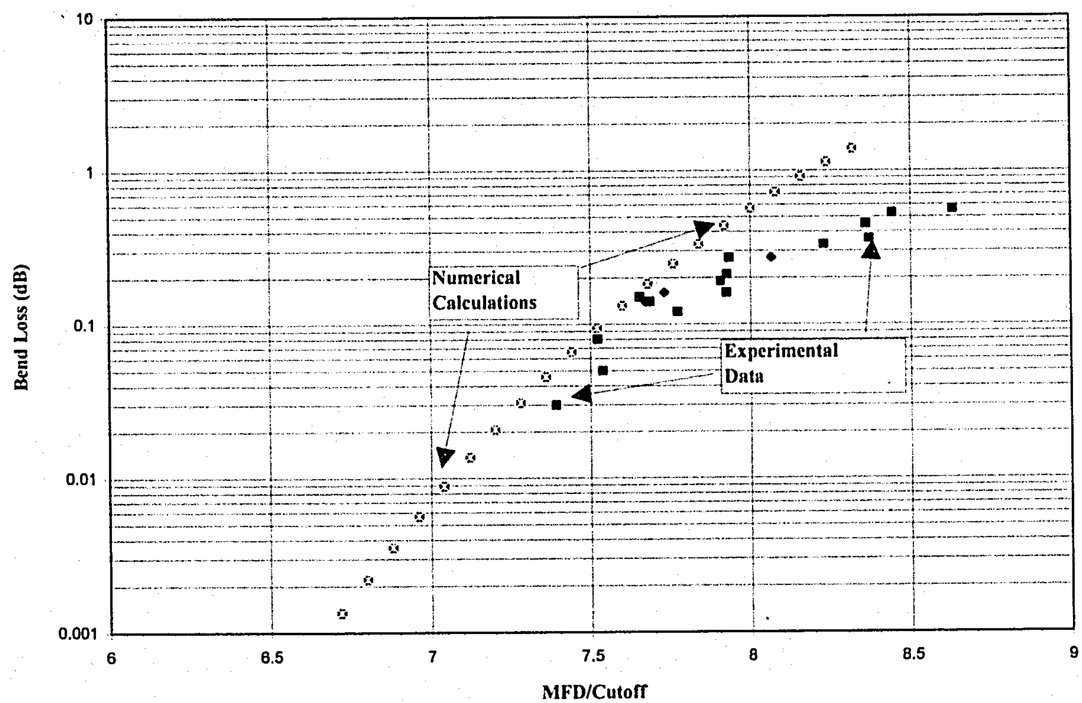

Figure 6.11: Bend loss of a depressed-cladding fiber as a function of the MFD/λ_c.

Figure 6.12 presents the design diagram limitations of depressed-cladding fibers. The bend loss limitations is determined for 0.1 dB bend loss. At this point the MFD/Cutoff value is 7.5. It is seen that the same bend loss requirement is obtained for lower MFDs compared to the matched--cladding fiber, as it is shown in Figure 6.9. The lower MFD requirements of 8.3 to 9.3 μm cause the design window to remain approximately the same as before.

As a summary, the worst case bend loss for matched and depressed-cladding fibers was measured at several bend diameters. The fibers selected had large MFD and low cutoff. The matched--cladding fibers had MFD of 10.2 μm and cutoff of 1180 nm, while the depressed-cladding fibers had MFD of 9.4 μm and cutoff of 1190 nm. The results of the measurements are shown in Figure 6.13. In this diagram the bend loss of the fibers with 100 bends of the corresponding diameter loop are plotted as a function of the bend radius. It is seen that for bend diameters approximately less than 4 cm, the depressed-cladding fiber outperforms the matched--cladding one. The opposite is true for diameters greater than 4 cm. By looking at figures 6.9 and 6.12 we observe that these values of MFD and cutoff are outside the defined window. These values were chosen due to the possibility that these fiber types can be manufactured and be implemented in the field if companies do not impose the design limits discussed in this section.

Figure 6.13 is used to define the minimum bend that a fiber can be imposed in splice organizers and distribution frames without any significant power penalty. For 100 bends of 5 cm diameter the maximum loss in a depressed-cladding fiber is 0.5 dB. The loss for matched--cladding fibers is below 0.1 dB. These losses can easily be tolerated in installed links with a great amount of safety. These are the bend configurations proposed in the next section, where the modal noise of the fiber is analyzed in order to define the maximum cutoff wavelength and thereby complete the fiber design diagram.

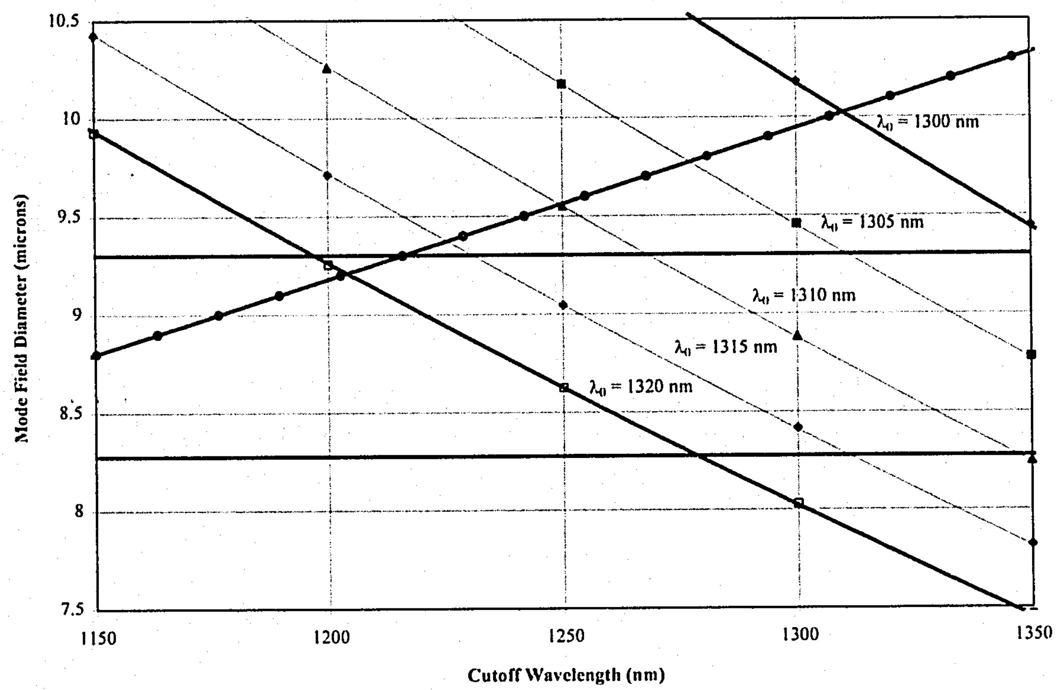

Figure 6.12: Design diagram of a depressed-cladding single mode fiber.

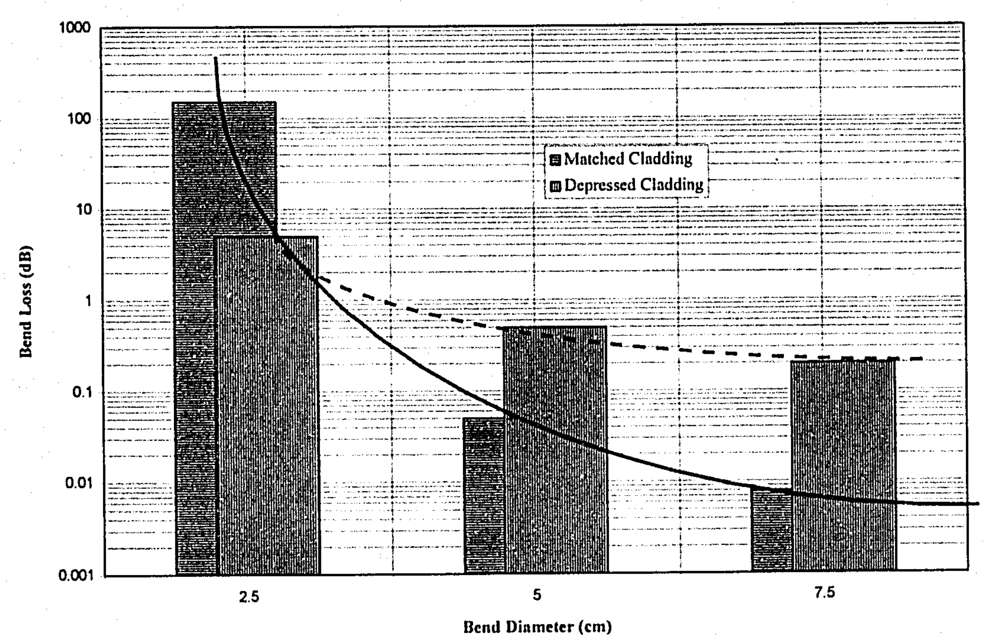

Figure 6.13: Worst-case bend loss comparison for matched- and depressed-cladding fibers.

7. MODAL NOISE OF SINGLE MODE FIBERS

7.1 Introduction

The cutoff wavelength of single mode fibers defines the minimum allowable wavelength of the light source without any noise degradation of the system performance.

The theoretical cutoff wavelength of the LP_{11} mode is found from the wave equation as the value at which the effective refractive index $\beta/$, equals the refractive index of the cladding, n_{cl}. The effective (or actual) cutoff wavelength that the system can operate at is always much smaller than the theoretical value. This wavelength is reduced further due to the fiber layout conditions, i.e. the curvatures that are imposed on the fibers (most of the time purposely) or its length. The latter can vary from a few centimeters to several kilometers. An exact determination of the effective cutoff wavelength dependence on the fiber curvature and length is very important for the proper deployment of the fiber in the field.

If systems designers use the theoretical, rather than the effective cutoff wavelength, the penalty in the system performance will be severe. This penalty is caused by excess loss due to the bend and microbend sensitivity at longer (i.e. 1550 nm) wavelengths. The theoretical cutoff wavelength has very little significance to practical system performance, while the effective cutoff wavelength is a parameter used continuously as a system design guideline.

As fiber penetrates into the central offices, interconnection density increases significantly. It is not unusual to find thousands of connectorized fibers in very small areas. Fiber management systems are currently designed to accommodate these high fiber densities. Long fiber lengths, required to reduce the modal noise effect, and large bends, that are set by the bend loss performance of the fiber, make this high fiber density difficult to accomplish. The reasons for these requirements are given below.

Fibers can improve their bend performance at long wavelengths if the normalized frequency is high. In a step index fiber, the closer the normalized frequency is to 2.4, the better the bend performance of the LP_{01} mode. This dependence was discussed in the Section 4. All commercially available fiber designs have theoretical cutoff wavelengths well above the operating wavelength. During standard testing, the fiber layout conditions reduce the cutoff wavelength further. These layout conditions were set arbitrarily by the international standardization bodies and are used around the world. They are based on one complete bend of 28 cm diameter and 2 meter length [60]. Even under these conditions, commercially available fiber systems operate at wavelengths below the measured cutoff wavelength. But how do we avoid noise arising from the presence of the LP_{11} mode? We achieve that by imposing more drastic layout conditions, such as a tighter bend or longer fiber lengths. There is a great desire in the industry to reduce the fiber length and increase the density in the fiber management system without any modal noise degradation.

The limit imposed on the fiber bend depends on two parameters: the space required by the distribution frame on the one hand, and the bend performance at 1550 nm, together with the fiber's mechanical reliability on the other. For these reasons the industry imposed an upper limit of two-meter fiber length limit and 7.5 cm bend diameter. Up to now both manufacturers and end users adhered to these limits faithfully. Due to recent space limitations end users and manufacturers alike question the value of these numbers.

In this section the minimum values of the bend and length configuration based on the wave propagation of the LP_{01} and LP_{11} modes are determined theoretically and experimentally. In combination with these parameters the maximum cutoff wavelength of the fiber will be determined. By defining this parameter, the single mode fiber design diagram will be completed.

Below an explanation of the poorly understood phenomenon of modal noise is given.

7.2 Phenomenological Explanation

The modal noise phenomenon is a special case of modal interference. It may occur when a short fiber section is connectorized between two longer fibers in a fiber optics transmission line. Modal interference, however, does not always cause modal noise. The phenomenon of modal noise can be explained more easily, from a proper analysis of the modal interference mechanism.

A diagram explaining the modal interference phenomenon is shown in Figure 7.1 where a short fiber section is connected to two longer fibers. Since the connection at each point is not perfect, light from the sending fiber in joint A will be partly lost from the LP_{01} mode. This light will excite the higher order modes of the short fiber length, that propagate with a different propagation constant than the light in the fundamental LP_{01} mode. At the second splice point B, part of this light is coupled back to the LP_{01} mode, if the connection loss is not perfect. Since the portion of the field that propagates in the LP_{11} mode of the short fiber section has a different propagation constant than the one propagating in the LP_{01} mode of the same section, the two modes will interfere with each other. This results in signal fluctuations at the fiber end, depending on the difference in propagation constants between the two modes. As the input of the fibers is wavelength-scanned, this propagation constant difference changes and causes the light intensity exiting the fiber to fluctuate. This is the well-known observation of electromagnetic field interference[61,62].

A complete characterization of the interference depends on the amplitude and the periodicity of the interference pattern.

The amplitude of interference depends on the following parameters:

- The connection loss at the two splice points. The higher this loss, the greater the coupling from the LP_{01} to the LP_{11} mode at the first splice and from the LP_{11} to the LP_{01} mode at the second splice.

- The loss of the LP_{11} mode. High LP_{11} mode attenuation will reduce its light intensity at the second splice point and reduced power will couple back to the LP_{01} mode. The LP_{11} mode loss depends on the waveguide parameters of the optical fiber, and the fiber length located between the two joints.

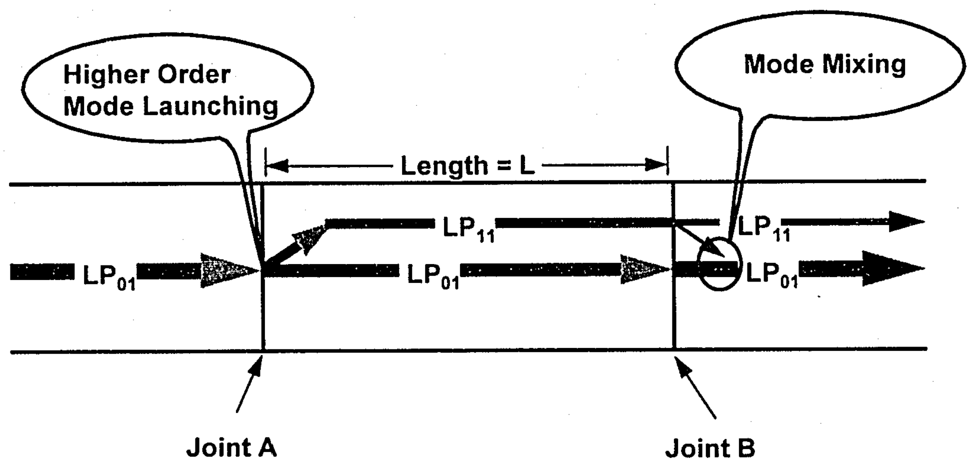

Figure 7.1: Generation of modal interference for two closely spaced connection points.

The first parameter can be reduced by optimizing the splice or connection loss at the two points. This is achieved with relative ease but the results can be unreliable. This work will focus on how to reduce the modal noise by increasing the attenuation of the LP_{11} mode. It is obvious that this must be achieved without increasing the loss of the fundamental mode, which would reduce the reach of the signal and decrease the repeater spacing.

The wavelength spacing of the interference fluctuations depends mainly on the fiber length. As the fiber length increases, this wavelength spacing becomes smaller. At the same time, though, the LP_{11} mode loss increases. An example of the intensity fluctuation after two consecutive joints of single mode fibers is shown in Figure 7.4.

The modal noise of a fiber optics system is related to the fiber characteristics mentioned above, and to the stability of the light source spectral intensity pattern. This pattern varies due to mode partitioning for multi-longitudinal mode lasers or mode hopping for single mode (such as DFB) laser structures.

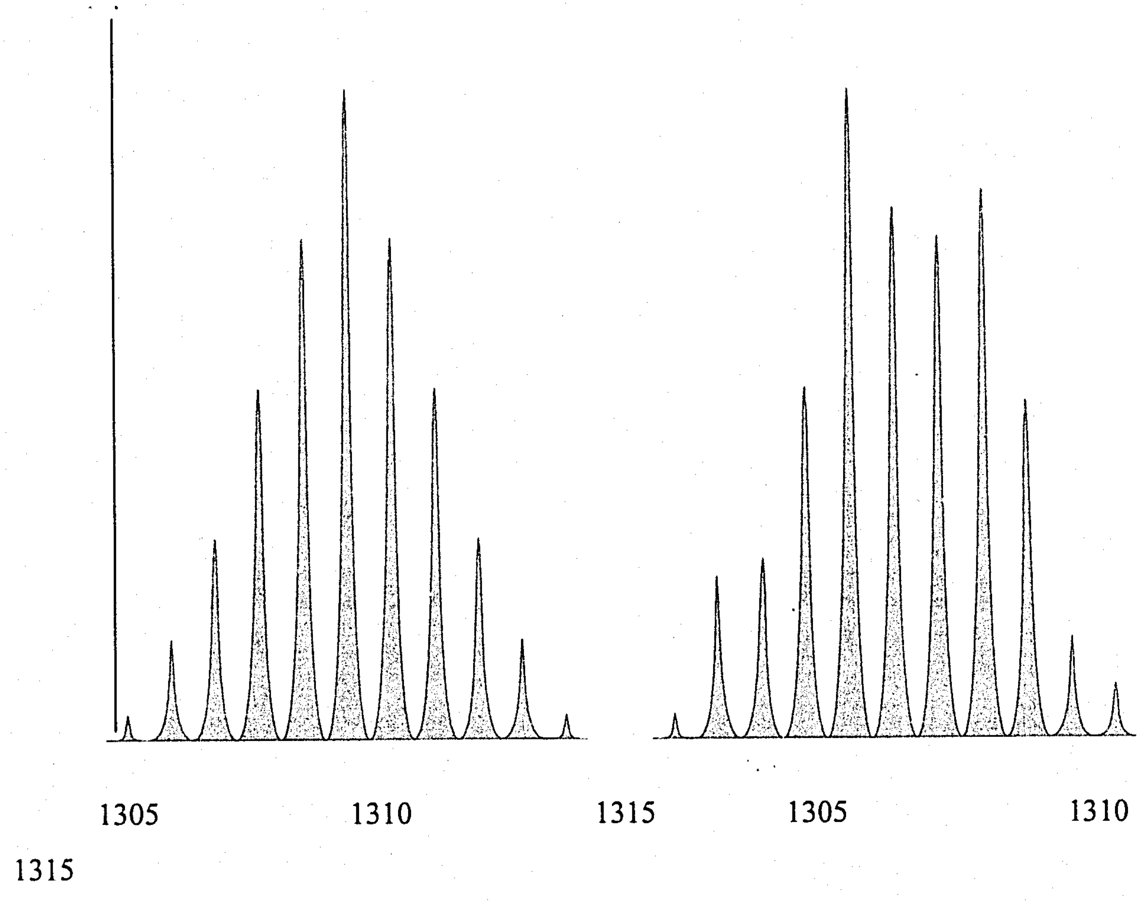

a b

Figure 7.2: a. Optical intensity output of a multi-longitudinal mode laser. The intensity fluctuates due to the Fabry-Perot effect of the laser structure. b. Mode partitioning noise in this laser type results in intensity fluctuations in specific modes, and therefore to modal noise.

An example of the output pattern of a multi-longitudinal semiconductor laser is shown in Figure 7.2. The intensity fluctuation of the laser with wavelength is caused by the interference of the modes in the laser cavity. It has been observed theoretically and experimentally that this light distribution changes randomly with time [63]. This light intensity fluctuation at each mode occurs during the modulation of the laser from the 0 to the 1 state. This phenomenon, called mode partition noise, has been studied in detail [64], [65], [66]. An example of mode partitioning noise is shown in Figure 7.2b.

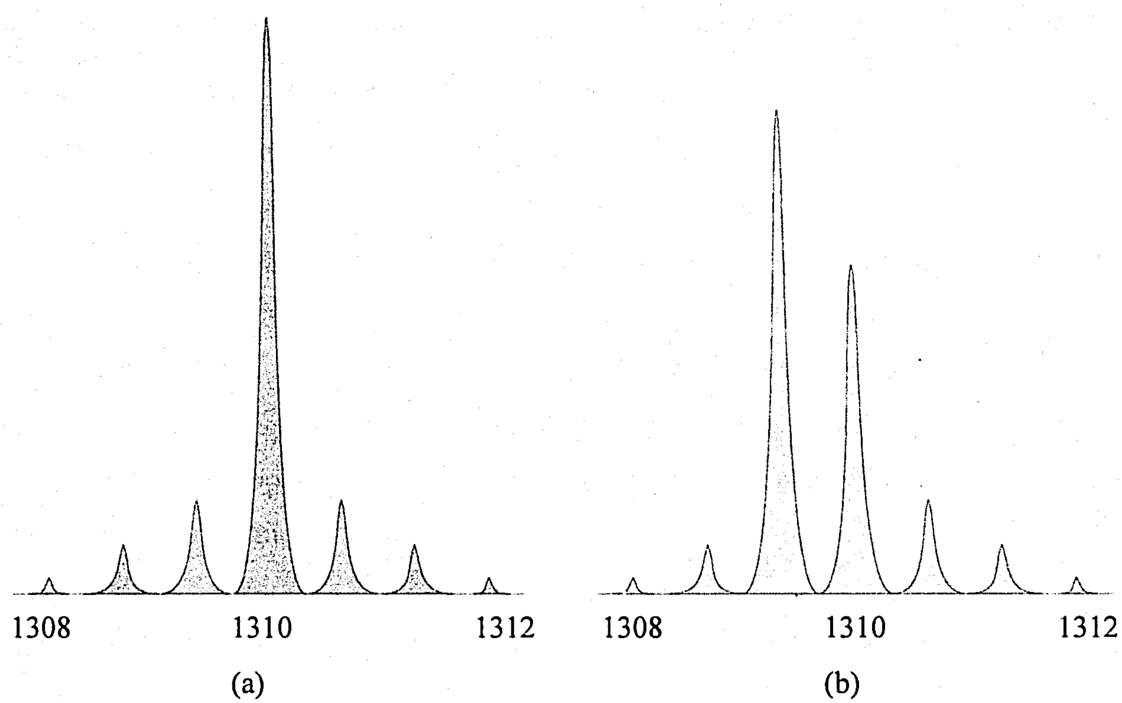

Figure 7.3: (a). Spectral output of single longitudinal mode laser. Most of the power is present in the first mode. (b). As the power hops from one mode to the other, the source wavelength fluctuates. This phenomenon, called mode hopping, also results in modal noise generation.

The output pattern of a single-mode laser structure is shown in Figure 7.3. As seen, the output pattern is similar to the multilongitudinal mode structure, but the side modes are suppressed[67], [68], [69]. In this case, power fluctuations from one mode to another, will result to significant variations of the intensity distribution with wavelength. This phenomenon, similar to the mode partitioning noise, is frequently called mode hopping [70], [71] or mode jumping [72].

The mode partitioning noise of the laser is characterized by the mode-partition noise parameter k, that varies in the range 0 to 1. Each mode in sources with a mode partitioning noise parameter of 0 varies independently, as is the case of LEDs. A mode partitioning noise parameter of 1 denotes that each mode is a mutually exclusive event.

Typical values of mode partitioning noise vary between 0.3 to 0.7, even in the case of single-mode lasers. The worst case is for lasers with two or three modes present, where great power fluctuations occur.

As the intensity of the laser fluctuates with the wavelength, the output of the fiber after the second joint changes. This change can occur abruptly or smoothly depending on the amplitude variation and wavelength spacing between the minima and maxima of the interference pattern. For large wavelength spacings, a change in the laser wavelength, caused by mode hopping or mode partitioning, will result to small variations in the output power and to small modal noise. This occurs for short fiber lengths.

As the length of the fiber between the two joints increases, the wavelength spacing of the intensity fluctuations decreases. The same mode hopping or partition noise effects will increase the modal noise sensitivity of the system. This dependence will continue until the power fluctuation wavelength spacing at the output of the third fiber matches that of the laser mode spacing. For greater fiber lengths, the penalty due to modal noise remains constant in terms of wavelength and the modal noise phenomenon is completely randomized. The next subject describes the theoretical analysis of this randomized modal noise penalty.

7.3 Modal Noise Theory

The modal interference can be calculated from the transmission efficiency η of the LP_{01} mode as it propagates through two closely spaced splice joints. This is given by the relationship[63]:

$$\eta = \eta_1\eta_2 + (1-\eta_1)(1-\eta_2)10^{-\frac{\alpha_{11}L}{10}} + 2\sqrt{\eta_1\eta_2(1-\eta_1)(1-\eta_2)}10^{-\frac{\alpha_{11}L}{20}}\cos\phi \quad (7.1)$$

where $\phi = L\Delta\beta$.

The angle ϕ is given approximately by the following relationship:

$$\phi = \frac{2\pi L\Delta n}{\lambda}$$

with η_1 and η_2 being the light transmission efficiencies at the first and second connection points respectively

λ the operating wavelength

L the length of the short fiber section

α_{11} the attenuation of the LP_{11} mode

$\Delta\beta$ the difference in propagation constant between the LP_{01} and LP_{11} modes.

Δn the index difference between the core and the cladding.

This relationship is valid at values close to the cutoff wavelength of the fiber where the effective index of the LP_{11} mode is close to the refractive index of the cladding. As explained previously, the effective index is given with respect to the propagation constant and the wavenumber by the relationship:

$$n_{eff} = \beta / k$$

The only parameter that is not known in equation (7.1) is the attenuation α_{11} of the LP_{11} mode. In this work this value is found experimentally from measurements of the length dependence of the cutoff wavelength. It can also be determined theoretically, but its prediction becomes very unreliable due to uncertainty in the measurement of the fiber parameters. A brief explanation of the LP_{11} mode for matched or depressed-cladding fibers is given in Section 7.4.

Experimentally it is shown in Section 7.5 that α_{11} is given by the empirical relationship:

$$\alpha_{11} L = 19.3 X^{\frac{\lambda - \lambda_c}{10}} \tag{7.2}$$

In the above relationship X is determined experimentally by measuring the length dependence of the cutoff wavelength.

By taking the logarithm of equation (7.1), we can calculate the splice loss. If this loss is plotted as a function of wavelength, an interference pattern will be observed. This pattern will reduce in amplitude as the wavelength increases since the attenuation of the LP_{11} mode increases and there is less light interfering with the LP_{01} mode at the second splice point. An example of the transmission efficiency variation as a function of the wavelength is given in Figure 7.4. In this figure the following assumptions are made: The fiber is a matched-cladding fiber design with a cutoff wavelength of 1250 nm. The fiber length is 50 cm. The splice loss at the first splice point is the identical to the second and is equal to 0.5 dB. A more detailed analysis of the splice loss will be presented later in this section.

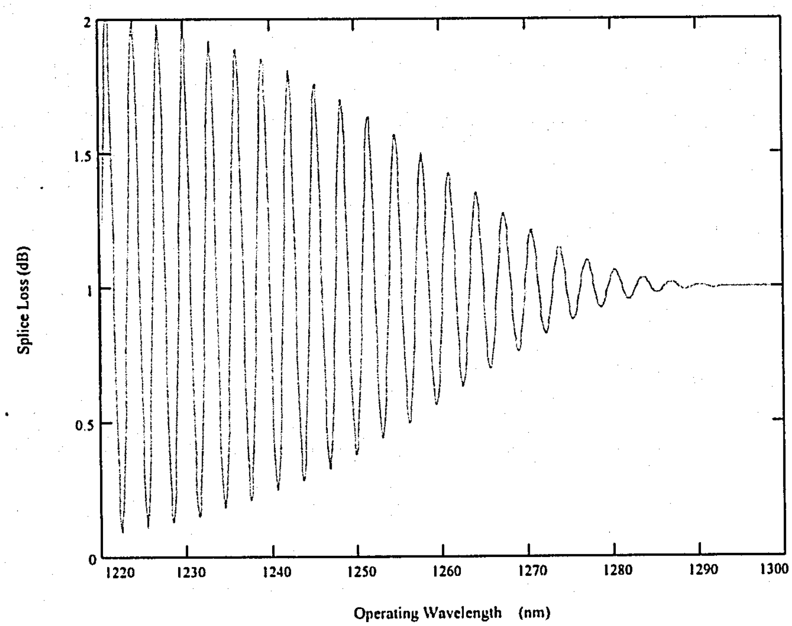

Figure 7.4: Modal interference pattern of a single mode fiber. The parameters used in these calculations are: $\alpha_{splice} = 0.5$ dB, $\lambda_c = 1250$ nm, L = 50 cm.

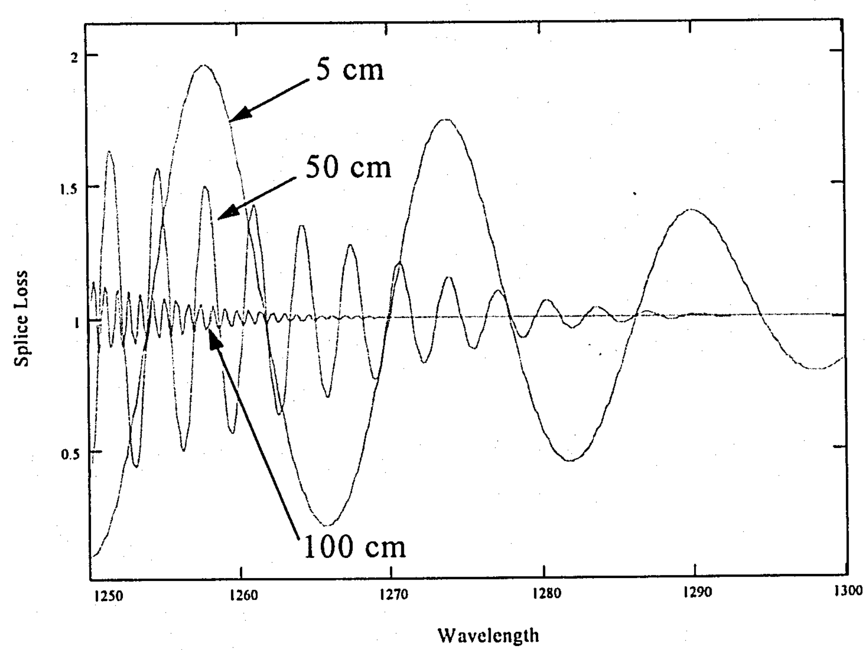

Figure 7.5: Splice loss as a function of wavelength for three different fiber stub spacings: 5, 50 and 100 cm.

Figure 7.5 shows the splice loss fluctuations for three different fiber stub lengths: 5 cm, 50 cm and 100 cm. As the fiber stub length increases, the power fluctuations for the same wavelength intervals increase. These fluctuations result in increased system sensitivity to modal noise. At the same time the amplitude of the oscillations decreases significantly due to the increased loss of the LP_{11} mode in the short fiber section. This will result in reduced modal noise.

The efficiency by which wavelength noise of the lasers is converted to modal noise is proportional to the derivative of equation (7.1) [73]. This derivative is given by the equation:

$$\frac{d\eta}{d\lambda} = 2\sqrt{\eta_1\eta_2(1-\eta_1)(1-\eta_2)}10^{-\frac{\alpha_{11}L}{20}}\frac{d(\Delta\beta)}{d\lambda}$$

$$= \frac{4\pi L\Delta n}{\lambda^2}\sqrt{\eta_1\eta_2(1-\eta_1)(1-\eta_2)}10^{-\frac{\alpha_{11}L}{20}} \qquad (7.3)$$

A plot of this equation as a function of wavelength is shown in Figure 7.6. We can observe that there are two areas of small modal noise sensitivity. One of them occurs at long fiber lengths where the fiber attenuation of the LP_{11} mode is large. In this case, the amplitude oscillations are small causing no power fluctuations for laser wavelength instabilities. For short fiber lengths, the wavelength separations between minima and maxima is large. In this case large wavelength changes are needed to cause amplitude fluctuations at the receiver.

Laser hopping or laser partitioning cause only small wavelength changes of the iaser source. These changes will result in small modal noise contributions. The most dangerous case in terms of modal noise is between the two extremes. For this case, significant modal noise is generated for small changes in the laser wavelength.

A program that calculates all the above results is presented in Appendix A. This program is written in MathCad. The results in the next chapter are used to calculate the attenuation of the LP_{11} mode at different wavelengths.

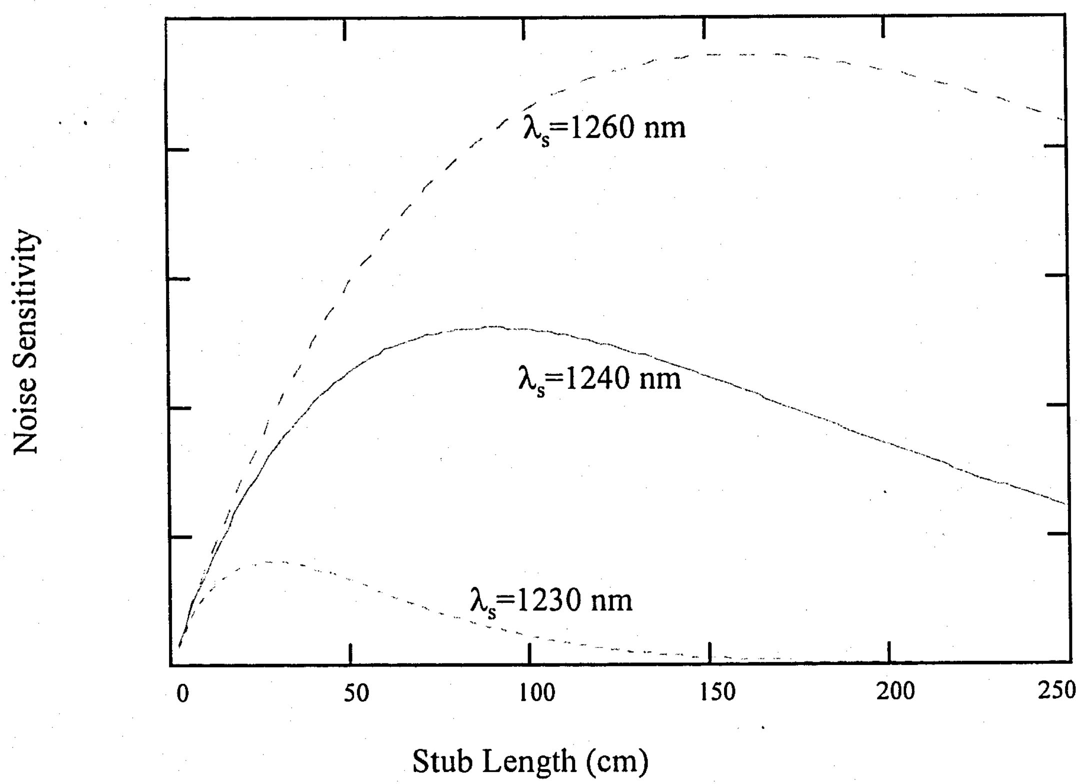

Figure 7.6: Modal noise sensitivity as a function of the fiber stub length. The three curves are generated for a fiber stub with the LP_{11} mode cutoff wavelength of 1240 nm and system operating wavelengths of 1230, 1240 and 1260 nm.

7.4 Theoretical investigation of the LP_{11} mode attenuation

7.4.1 Matched cladding fibers

The cutoff wavelength point of an optical waveguide is defined as the value at which the effective refractive index of that mode equals the refractive index of the cladding. For a perfect fiber, the LP_{11} or any other mode does not attenuate before it reaches the cutoff wavelength value. When the wavelength is higher than the cutoff wavelength of the mode, light in the mode continues to propagate. The difference between a dielectric and a metallic waveguide is that above the cutoff wavelength the power in the first case is being radiated while in the second it is being reflected. In metallic waveguides, due to the reflection phenomenon, the light in the mode attenuates exponentially above λ_c, while in dielectric waveguides the attenuation of the light of the mode is less drastic. Even above cutoff the mode continues to be a traveling wave in the longitudinal direction. The difference is in the radial direction where the light attenuates exponentially below cutoff and becomes a traveling wave above cutoff. We call this mode "leaky mode" since light does not escape abruptly but leaks out of the core at a steady pace.

Even though the waveguide can support light above the cutoff wavelength, it attenuates the light rapidly. As shown in [74], the mode attenuates extremely quickly above the cutoff wavelength. Figure 7.7 shows the attenuation of the mode as the normalized frequency, given by equation (2.18), increases beyond the normalized frequency at the cutoff wavelength, V_c. Theoretical calculations on depressed-cladding fibers have shown a more gradual increase. These calculations have been performed in cylindrical optical waveguides with the cladding extending to infinity.

In reality, however, a different phenomenon occurs. The cladding material in optical fibers extends to 125 μm, which corresponds to a cladding to core ratio of 15. The cladding is surrounded by a coating material that increases the size of the fiber to 250 μm. The fiber dimensions are shown in Figure 7.8.

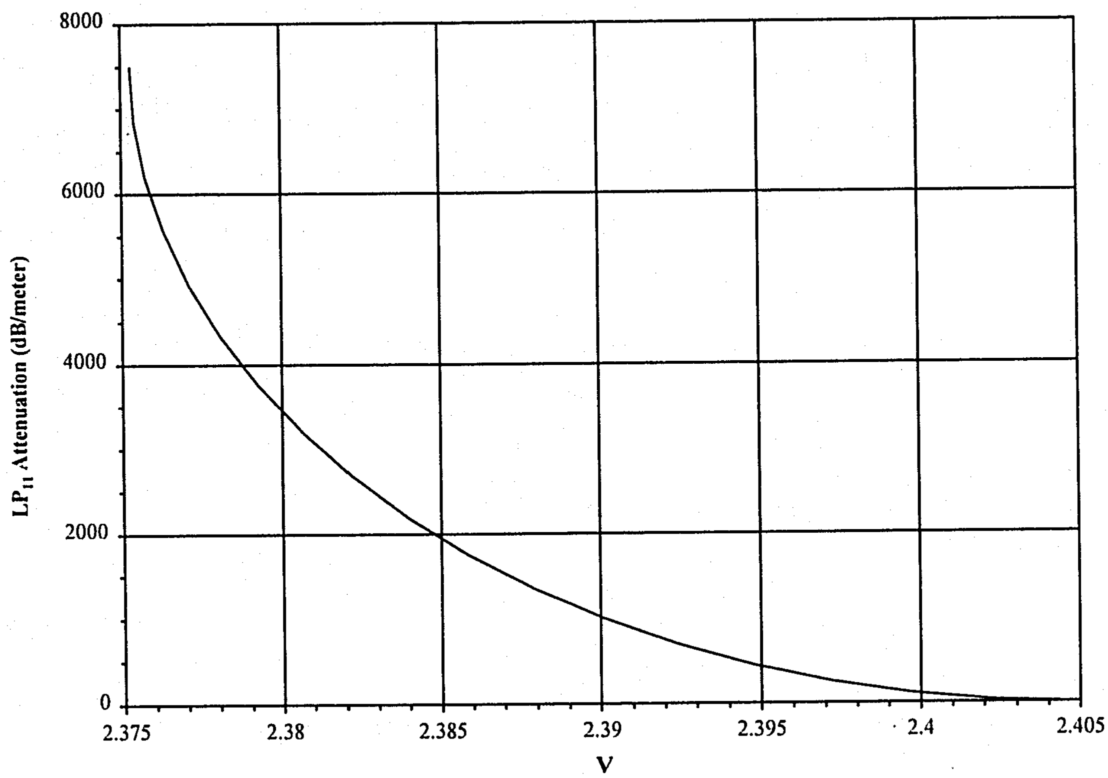

Figure 7.7: Attenuation of the LP_{11} mode for matched-cladding fiber with infinitely extended cladding

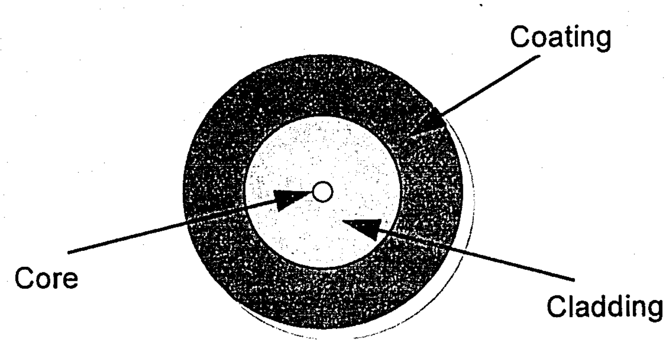

Figure 7.8: The actual structure of a matched-cladding single-mode optical fiber. The actual diameters are: Core = 8.5 μm, Cladding = 125 μm, Coating = 250 μm.

All currently available single-mode fibers are coated with material that has a refractive index greater than the index of pure silica. The material is usually UV cured epoxy applied to the fiber during the drawing process. UV radiation alters the molecular structure of the material and causes it to cure. This transformation affects the refractive index of the coating. Due to variations in the UV radiation, the refractive index of the material is not accurately known. It has been calculated that the refractive index of the coating material is approximately 1.55 to 1.6, compared with 1.447 for the refractive index of pure silica at a wavelength of 1310 nm.

Differences in the propagation properties of optical fibers are caused by the presence of the coating material. The field in the higher order mode hits the cladding/coating boundary at grazing angles. Part of the light will be transmitted inside the coating, and will be absorbed by the coating's high attenuation coefficient. The remaining light will be reflected back into the cladding and eventually recaptured by the core. The mode loss is caused by the light that escapes into the coating.

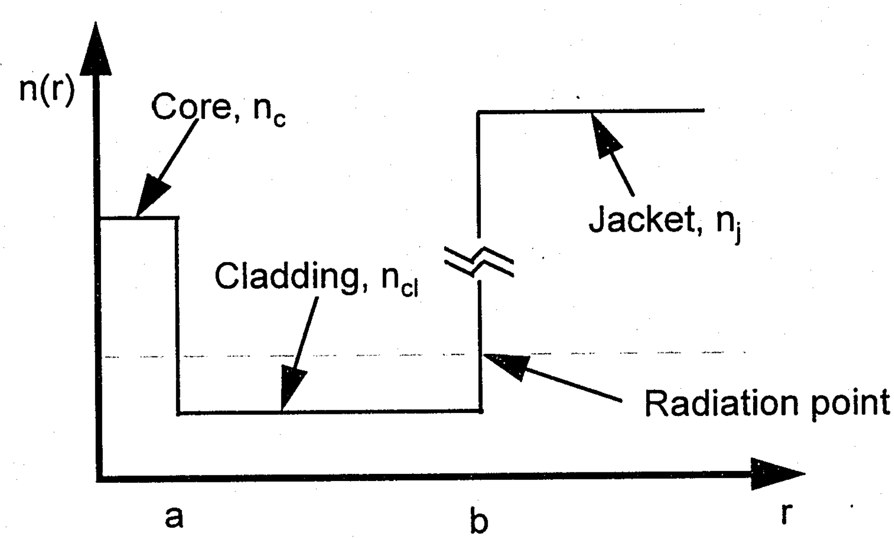

Figure 7.9: The actual refractive index profile of a matched-cladding single-mode fiber.

The LP_{11} mode loss can be calculated by solving the scalar wave equation and applying the proper boundary conditions. The refractive index structure of the optical fiber is shown in Figure 7.9.

The solution of the scalar wave equation of the LP_{11} mode for the three regions of the fiber is given by the following equations [4]:

$$\psi = AJ_1(\chi r)\cos\phi\exp(-i\beta z) \qquad r<a \qquad (7.4a)$$

$$\psi = \left[BK_1(\gamma r) + CI_1(\gamma r)\right]\cos\phi\exp(-i\beta z) \qquad a<r<b \qquad (7.4b)$$

$$\psi = DH_1^{(2)}(\rho r)\cos\phi\exp(-i\beta z) \qquad b<r \qquad (7.4c)$$

where

$$\chi^2 = k^2 n_c^2 - \beta^2$$
$$\gamma^2 = \beta^2 - k^2 n_{cl}^2$$
$$\rho^2 = k^2 n_j^2 - \beta^2$$

are the propagation parameters of the core, cladding and coating.

This problem can be solved by setting the field ψ at point b equal to zero. This approximation is correct, since the field is far away from the core and the refractive index of the coating is large enough and close to that of the core. We therefore obtain:

$$C = -\frac{K_1(\gamma b)}{I_1(\gamma b)}B \qquad (7.5)$$

The boundary conditions at $r = a$ dictate the continuity of the field and its derivative at this point, i.e. that:

$$
\begin{aligned}
AJ_1(\chi a) &= BK_1(\gamma a) + CI_1(\gamma a) \\
\chi AJ_1'(\chi a) &= \sigma BK_1'(\gamma a) + \sigma CI_1'(\gamma a)
\end{aligned}
\tag{7.6}
$$

By combining the above equations, the following eigenvalue equation is generated:

$$
\begin{aligned}
&\chi J_1'(\chi a)[K_1(\gamma a)I_1(\gamma b) - K_1(\sigma b)I_1(\gamma a)] \\
&= \sigma J_1'(\chi a)[K_1'(\gamma a)I_1(\gamma b) - K_1(\sigma b)I_1'(\gamma a)]
\end{aligned}
\tag{7.7}
$$

By solving this eigenvalue equation the propagation constant of the LP_{11} mode is found. The attenuation of the LP_{11} mode is calculated from the ratio of the radiated power, P_r, to the transmitted power, P_z. The radiated and transmitted powers are found to be:

$$
\begin{aligned}
P_r &= ib\int_0^{2\pi}\left[\psi^*\frac{\partial\psi}{\partial r} - \psi\frac{\partial\psi^*}{\partial r}\right]d\phi \\
P_z &= i\int_0^{2\pi} d\phi\int_0^{b}\left[\psi^*\frac{\partial\psi}{\partial z} - \psi\frac{\partial\psi^*}{\partial z}\right]r\,dr
\end{aligned}
\tag{7.8}
$$

The solution to the above problem can be found numerically. First, the eigenvalue equation is solved and the propagation constant β is calculated. Afterwards, the eigenfunctions are found in the core, cladding and coating. The radiated powers are calculated and finally the attenuation of the LP_{11} mode is found. The results of these calculations for a fiber with core radius of 5 μm are shown in Figure 7.10. As seen, the attenuation of the mode as compared to the approximation where the cladding material extends to infinity is significantly smaller for wavelengths above the cutoff wavelength. At wavelengths below the cutoff wavelength, the attenuation becomes larger. The singularity that appears at the cutoff wavelength for an infinite cladding fiber disappears when dealing with a finite cladding fiber.

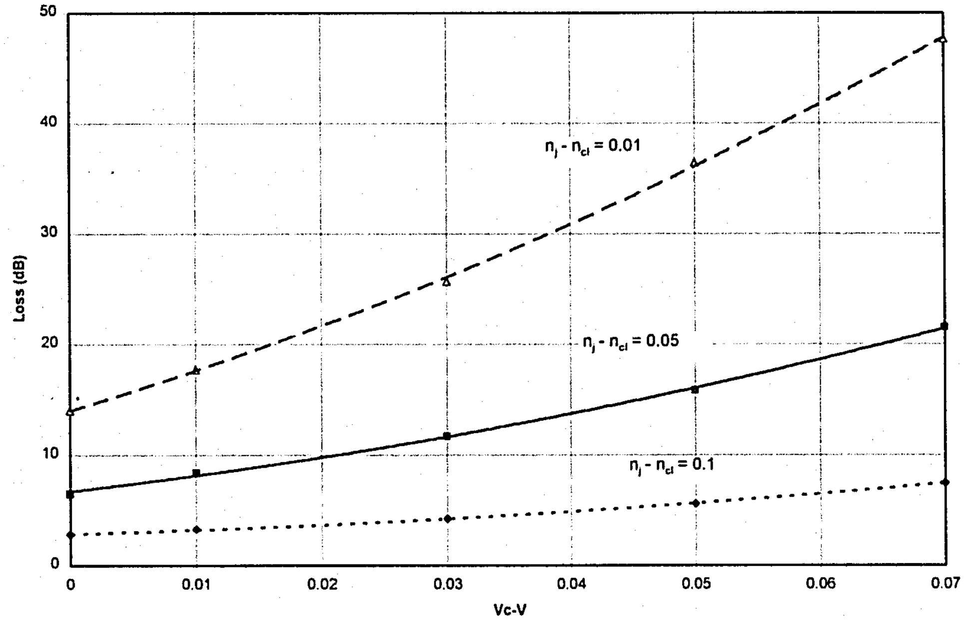

Figure 7.10: LP_{11} mode attenuation for one meter length of a matched-cladding fiber with finite cladding dimensions as a function of the difference between the normalized frequencies at cutoff wavelength and at the operating wavelength.

7.4.2 Depressed Cladding Fibers

The attenuation mechanism of a depressed-cladding fiber is very different from that of a matched-cladding fiber. Even though the fiber coatings are identical to the matched-cladding fibers, the coating/cladding interface contribution to the LP_{11} mode attenuation is negligible compared to the contribution of the inner and outer cladding interface. The refractive index profile of a depressed-cladding fiber is shown in Figure 7.11. In this graph the refractive index of the jacket is ignored due to its insignificant contribution to the attenuation of the LP_{11} mode.

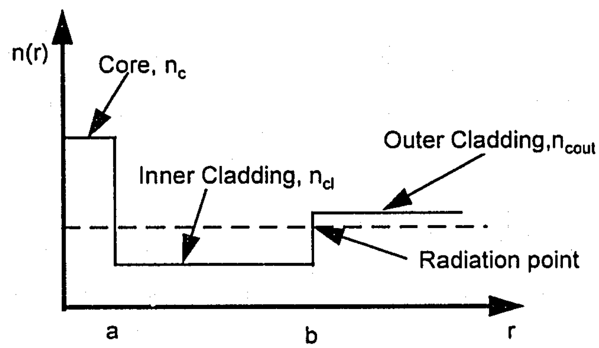

Figure 7.11: Refractive Index profile of depressed-cladding fiber.

Previously, Marcuse [75] used a perturbation method to calculate the leaky loss of the LP_{01} mode of depressed-cladding fibers. In this approximation he considered the outer cladding to be a perturbation of a matched-cladding fiber with the cladding refractive index being equal to the inner cladding one. The solution of this matched-cladding fiber structure is used to calculate the light reflection and transmission at the inner/outer cladding interface. The power loss coefficient is calculated by the ratio of the radiated (or transmitted) power per unit length compared to the power present in the LP_{01} mode.

In this work the same approach is used to determine the leakage loss of the LP_{11}, rather than the LP_{01} mode. The equations that are used to calculate the fields at the interfaces are similar to the ones given above with the major change being the refractive index designation.

$$\psi = AJ_1(\chi r)\cos\phi\exp(-i\beta z) \qquad r<a \qquad (7.9a)$$

$$\psi = \left[BK_1(\gamma r) + CI_1(\gamma r)\right]\cos\phi\exp(-i\beta z) \qquad a<r<b \qquad (7.9b)$$

$$\psi = DH_1^{(2)}(\sigma r)\cos\phi\exp(-i\beta z) \qquad b<r \qquad (7.9c)$$

with $\chi^2 = k^2 n_c^2 - \beta^2$

$\gamma^2 = \beta^2 - k^2 n_{cl}^2$

$\sigma^2 = k^2 n_{cout}^2 - \beta^2$

and n_c, n_{cl} and n_{cout} are the refractive indices of the core, inner cladding and outer cladding respectively.

By applying the proper boundary conditions at the inner/outer cladding interface, the attenuation of the LP_{11} mode is calculated to be:

$$2\alpha_{11} = \frac{8\sigma\gamma^2\chi^2 a}{\beta V^2(\gamma^2 + \sigma^2)K_0(\gamma a)K_2(\gamma a)}\exp[-2\gamma(b-a)] \qquad (7.10)$$

The plot of the above equation is shown in Figure 7.12. In this plot the attenuation of the LP_{11} mode is graphed as a function of the normalized frequency, V. Compared to the matched-cladding calculations, the attenuation of the LP_{11} mode is significantly higher for the same V values. For a normalized frequency of 2.405 and *b/a* of 6, the attenuation of the LP_{11} mode is 100 dB/meter. For matched-cladding fiber with the difference between the jacketing and the cladding refractive index being 0.1, the LP_{11} mode attenuation is 2.5 dB/meter. As the normalized frequency increases above this value, the LP_{11} mode attenuates very little in the matched-cladding fiber, but significantly more in the depressed-cladding one.

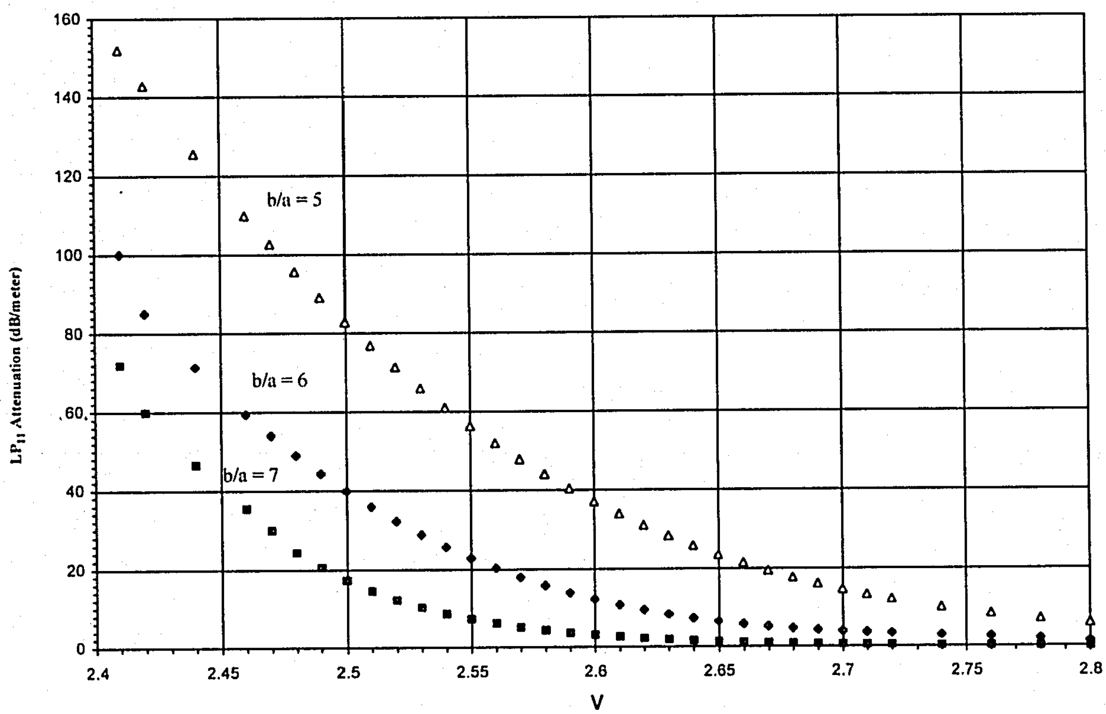

Figure 7.12: LP_{11} mode attenuation as a function of the V value for inner cladding to core ratios of 5, 6, and 7. The inner cladding depression is 20%.

7.5 Experimental Investigations

7.5.1 Measurement Apparatus

The theoretical analysis presented in Section 7.3 is an indication of the LP_{11} attenuation. Variations between the experimental and theoretical results are expected due to uncertainties in the fiber parameters.

In this section an experimental investigation on the attenuation of the LP_{11} mode for both the matched and depressed fiber cladding is presented. Two different experimental techniques are used and their results are compared.

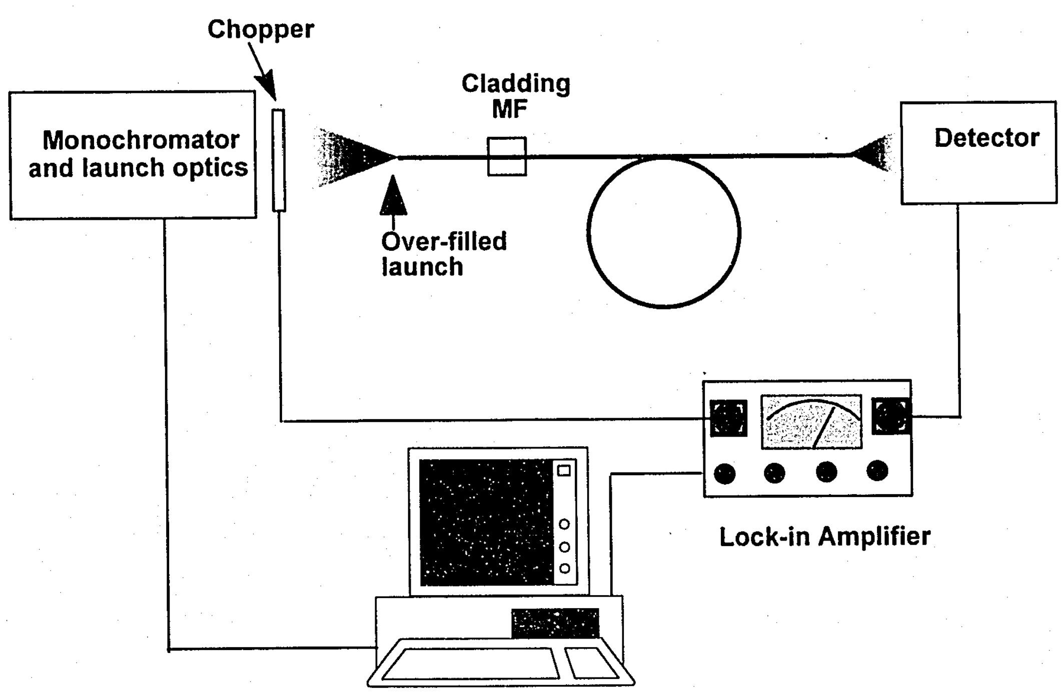

Figure 7.13: Measurement apparatus of the LP_{11} mode attenuation.

The measurement apparatus, shown in Figure 7.13, is composed of a launch optics apparatus with angular and spatial intensity distributions significantly larger than the numerical aperture and core of the fiber. This launch optics configuration overfills the optical fiber under test. An InGaAs detector senses the power level at the output of the fiber. Signals from the detector and the chopper are fed into a lock-in amplifier, whose output is connected to the computer

A more detailed description of the launch optics is shown in Figure 7.14. White light from a tungsten-halogen light source is coupled into a Jobin-Yvon monochromator. After several reflections in mirrors placed inside the monochromator, the white light is dispersed into the different colors by a grating. The number of mirrors increase the length of travel of the light beam which in return disperses the light further, while the grating's grooves per mm spacing is selected to optimize the output at the near infrared spectrum. A 1 mm slit is placed in both ends of the monochromator in order to select the proper spectral width at its output. The spectral width selected depends on two parameters: the width of the slit and the light dispersion of the monochromator's grating. The selected slit width corresponds to approximately 10 nm spectral width at the output of the monochrometor.

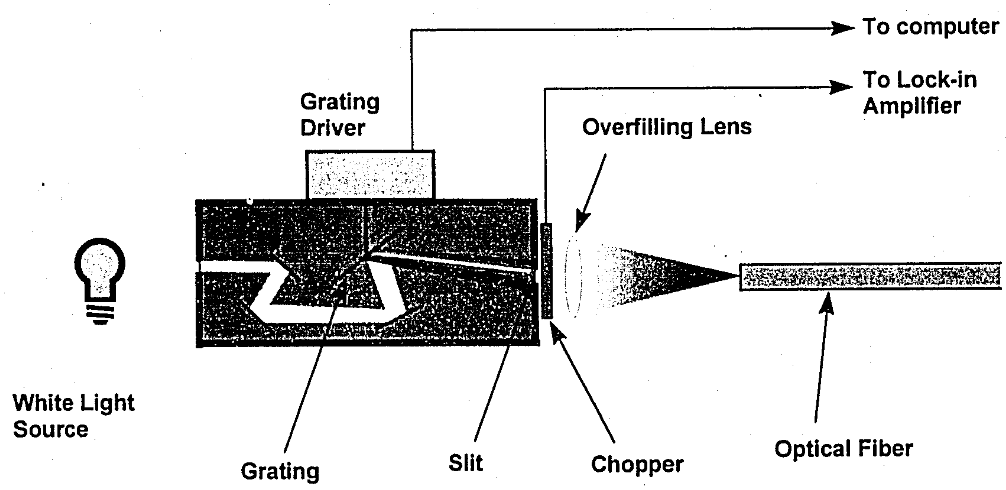

Figure 7.14: Light launching system of the measurement apparatus shown in Figure 7.13.

The wavelength of the monochromator is controlled by the computer which drives the grating. The output of the monochromator is chopped by either a rotating or a fork-type chopper. The chopped output is required in order to achieve synchronous detection, due to the low power of the output signal.

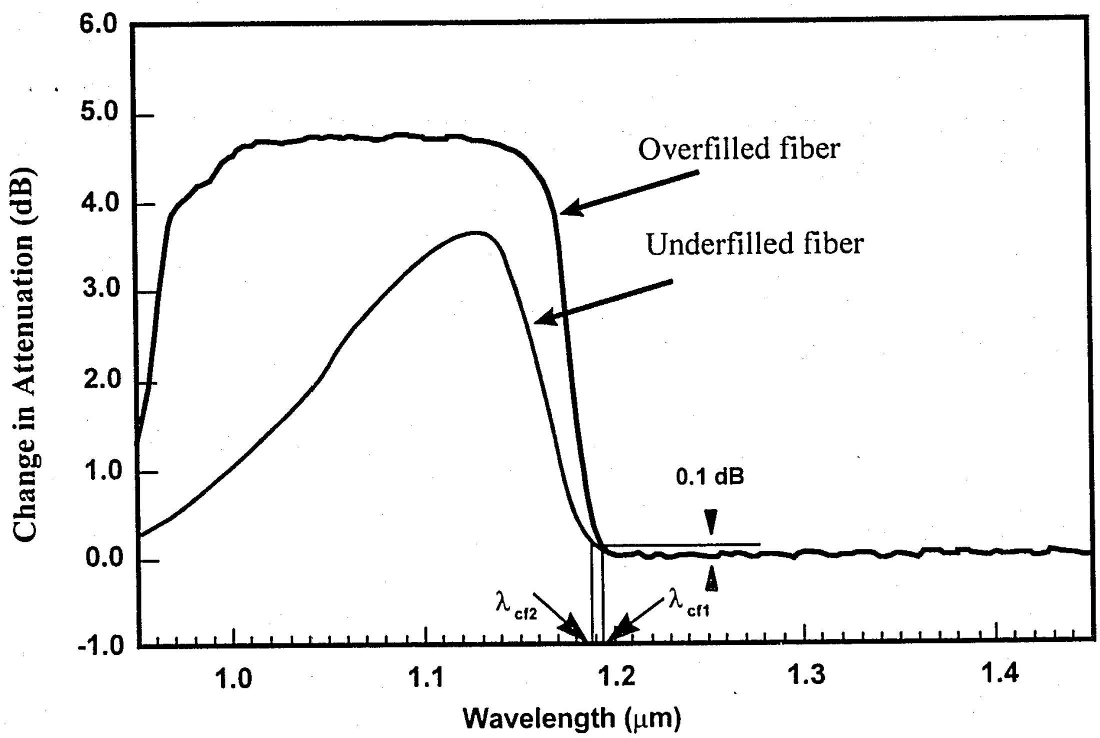

Figure 7.15: Changes of the cutoff wavelength measurement depending on whether the fiber is over-or underfilled.

The output of the monochromator is focused into the optical fiber with the use of a microscope lens. The magnification and the NA of the lens are selected to overfill the fiber input. This is of great importance in the measurements of the LP_{11} mode properties. Underfilled fibers result in excitation of only part of the LP_{11} mode, yielding incorrect measurement of the cutoff wavelength and of its attenuation as a function of wavelength. A 10x, 0.3 NA lens was used to launch the monochromatic light into the fiber and overfill it both spatially and angularly.

An example of measurement discrepancies resulting from the overfilled and underfilled conditions is shown in Figure 7.15. For the case of overfilled fibers, the maximum attenuation difference between the wavelengths where two rather than one mode propagates, is approximately 4.7 dB [76]. For underfilled fibers, this difference is smaller. As shown in Figure 7.15, underfilled fibers result in lower cutoff wavelength measurements. The difference in the cutoff wavelength is caused by the amount of excitation of the LP_{11} mode. As we will see later, the attenuation difference before and after the fiber cutoff can be used to measure the actual excitation of the LP_{11} mode.

7.5.2 LP_{11} Mode Attenuation Measurements

Measurements of the LP_{11} mode attenuation require a careful configuration of the fiber's layout conditions. Changes in the layout conditions will result to additional loss of the LP_{11} mode due to bending or microbending phenomena and smaller measurement values.

A direct way of measuring the LP_{11} mode attenuation was developed based on the three-measurement method. This measurement scheme is shown in Figure 7.16 [77]. The power output as a function of wavelength is measured for a length of fiber approximately 7 meters long with a 3 cm bend imposed on it. The fiber is kept in a spool of bend diameter greater than 30 cm. The second power measurement is acquired in the same fiber length with the bend removed from the fiber. Finally, the fiber is cut to a length of 2 meters. The power output as a function of wavelength is measured once again. From these three measurements, the attenuation of the LP_{11} mode is obtained. The last two measurements determine the relative power output. The first one subtracts the power level of the LP_{01} mode, since the 3 cm bend will eliminate completely the presence of the LP_{11} mode.

If we symbolize as $P_{01}(\lambda)$ the power output of the first measurement and $P_{11}(\lambda,L_1)$ and $P_{11}(\lambda,L_2)$ the second and third measurements, we find that they are given by the relationships:

$$P_{11}(\lambda, L_1) = P_{01}(\lambda) + P_{11}(\lambda)\exp[-\alpha_{11}(\lambda)L_1] \tag{7.11}$$

$$P_{11}(\lambda, L_2) = P_{01}(\lambda) + P_{11}(\lambda)\exp[-\alpha_{11}(\lambda)L_2] \tag{7.12}$$

In the above equation $P_{01}(\lambda)$ and $P_{11}(\lambda)$ are the launching powers of the LP_{01} and LP_{11} modes. Since the loss of the LP_{01} mode is very small compared with the LP_{11} at wavelengths close to the cutoff wavelength, the power in the LP_{01} mode is assumed to be constant.

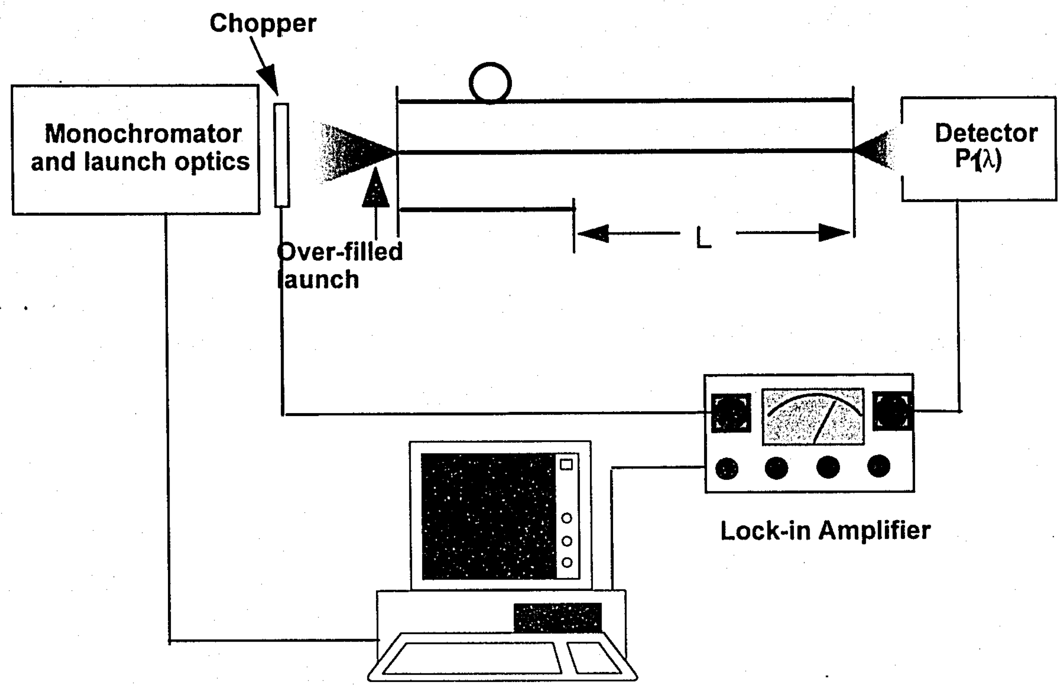

Figure 7.16: Measurement of the LP_{11} mode attenuation

From the above equations the LP_{11} mode attenuation is obtained:

$$\frac{P_{11}(\lambda, L_2) - P_{01}(\lambda)}{P_{11}(\lambda, L_1) - P_{01}(\lambda)} = \exp[\alpha_{11}(\lambda)L] \tag{7.13}$$

Using this method, the LP_{11} mode attenuation for the matched as well as depressed-cladding fiber types was measured. A plot of the LP_{11} mode attenuation as a function of wavelength for matched and depressed-cladding fiber designs are shown in Figure 7.17. As seen, the LP_{11} mode attenuation before and after the cutoff wavelength for matched and depressed-cladding fibers are different even if the cutoff wavelength of the two fiber types is the same. For wavelengths shorter than cutoff the attenuations of the LP_{11} mode for the depressed fiber type is larger. For wavelengths above the cutoff wavelengths, however, the LP_{11} mode attenuation of the matched-cladding fiber type are higher than that of the depressed fiber. Even though the above method gives a direct measurement of the LP_{11} mode attenuation as a function of wavelength, it lacks the accuracy required to establish the modal noise penalty. The measurement is very sensitive to the layout conditions, since it is difficult to keep it consistent during all three data acquisitions.

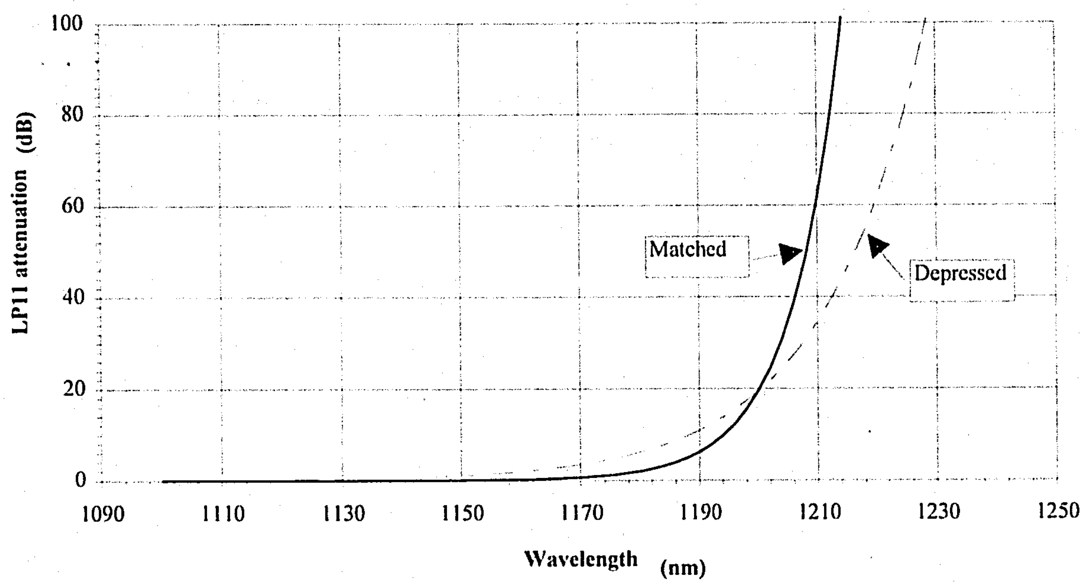

Figure 7.17: LP_{11} mode attenuation as a function of wavelength for matched and depressed-cladding fibers.

A less sensitive method based on the length-dependence of the cutoff wavelength was developed. We can approximate the length dependence of the cutoff wavelength by the following equation:

$$\lambda_c(L_2) = \lambda_c(L_1) + C\log\left(\frac{L_2}{L_1}\right) \tag{7.14}$$

where $\lambda_c(L_2)$and $\lambda_c(L_1)$ are the cutoff wavelengths of L_1 and L_2 fiber lengths. The parameter C is the length dependence constant. The constant C is obtained by fitting the cutoff wavelength data as a function of the fiber lengths to a logarithmic curve using regression analysis methods. Measurements performed on three different fiber types are shown in Figure 7.18. From this plot we see that for depressed-cladding fibers the length dependence constant C is much greater than for matched-cladding. This is due to the leaky mode loss in depressed-cladding fibers, compared to the loss due to the coating in matched-cladding fibers. As was shown in the theoretical section, the attenuation of the LP_{11} mode depends on the *b/a* ratio and on the amount of depression of the depressed-cladding fiber and on the fiber's mode field diameter. Depressed cladding fiber types I and II show the dependence on these parameters. Fiber I, which has lower depression and larger *b/a* ratio, has a lower C value compared to fiber II. The matched-cladding fiber has yet a lower C value.

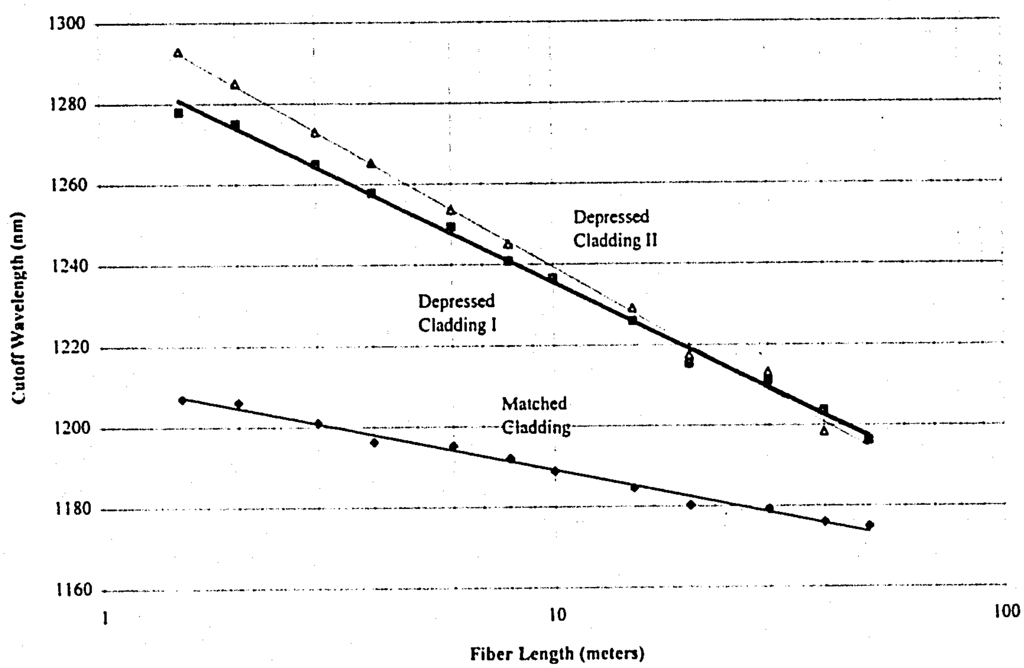

Figure 7.18: Length dependence of cutoff wavelength for three different matched and depressed-cladding fibers.

7.6 Correlation between the length dependence and the LP_{11} mode attenuation

It has been shown that the LP_{11} mode attenuation is approximated by the equation[78,79]:

$$\alpha_{11}L = 19.4X^{\frac{\lambda-\lambda_c(L)}{10}}$$

where X is a constant related to the fiber type and λ the operating wavelength. The parameter X is determined from the three-way measurement mentioned in the previous chapter. For a matched-cladding fiber type, with small length dependence of cutoff, the measurement of the X parameter is not accurate. In this case, the spectral transmission curves of the original and the cutback length almost always overlap.

By using the above equation for fiber lengths L_1 and L_2 we obtain:

$$\alpha_{11}(L_1) = \frac{19.4}{L}X^{\frac{\lambda(L_1)-\lambda_c(L)}{10}} \tag{7.15}$$

$$\alpha_{11}(L_2) = \frac{19.4}{L}X^{\frac{\lambda(L_2)-\lambda_c(L)}{10}} \,. \tag{7.16}$$

In the above equations $\lambda_c(L)$ is the effective cutoff wavelength as measured in the factory, i.e. in a fiber sample with a 2 meter length and a 28 cm bend diameter [60]. The cutoff wavelength is defined as the point at which the LP_{11} power relative to the LP_{01} power has dropped by 0.1 dB. From this determination of the cutoff wavelength, the following relationship is found:

$$\lambda_c(L_2) = \lambda_c(L_1) - 10\frac{\log(L_2/L_1)}{\log X} \tag{7.17}$$

and therefore,

$$C = -\frac{10}{\log X} \qquad (7.18)$$

From this equation we can calculate the LP_{11} mode attenuation if we measure the length dependence of the cutoff wavelength. In Figure 7.19, the attenuation of the LP_{11} mode for a depressed-cladding fiber, as it is calculated from the length dependence of the cutoff wavelength, is compared to the one measured directly using the method described earlier. Figure 7.20 shows the same comparison but for a matched-cladding fiber.

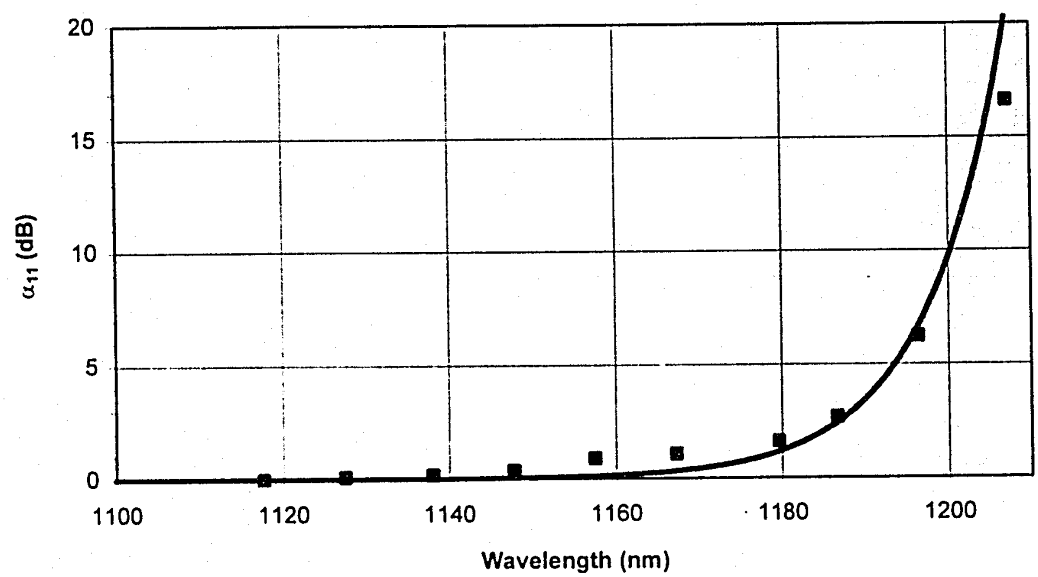

Figure 7.19: Calculated and experimental results of the LP_{11} attenuation for depressed-cladding fiber

We observe that the calculated and the measured attenuation values are in good agreement. As was mentioned earlier, the length dependence of the cutoff wavelength provides us with a more repeatable measurement that is not dependent to the fiber layout conditions. This measurement is preferred, even though it is more time consuming.

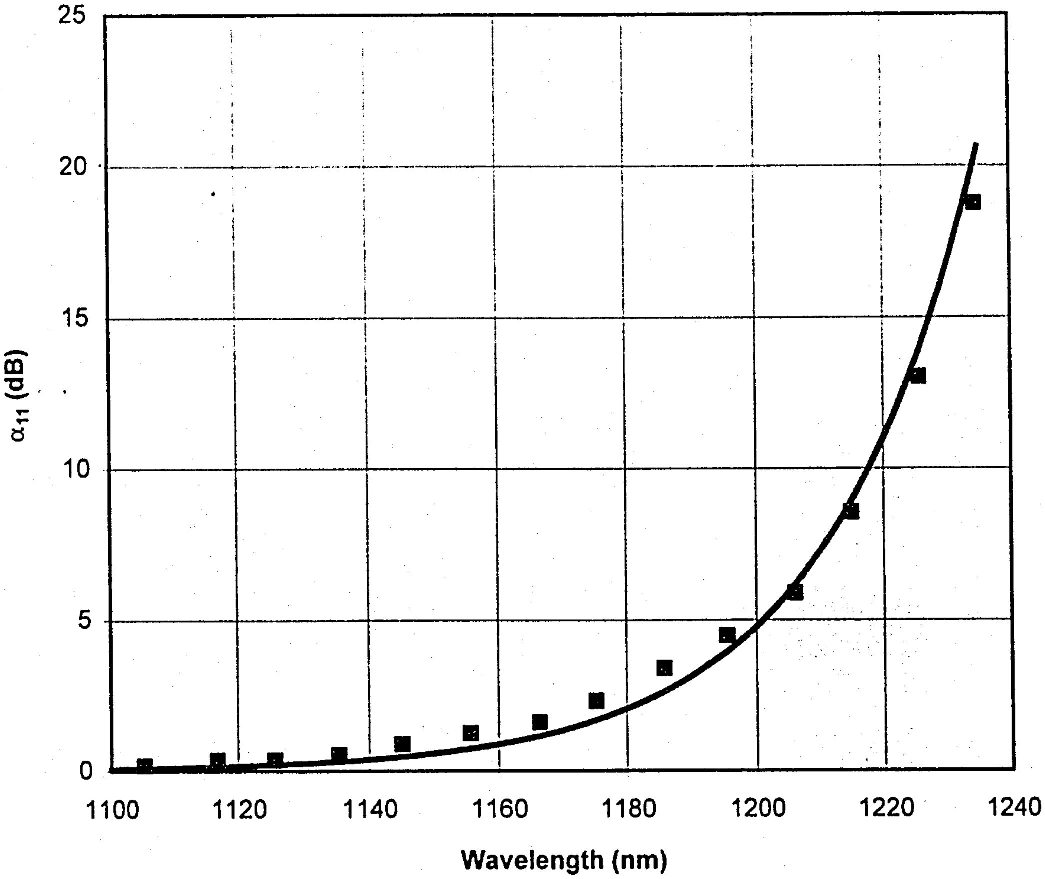

Figure 7.20: Calculated and experimental results of the LP_{11} attenuation for matched-cladding fiber

7.7 Curvature Dependence of Cutoff Wavelength

7.7.1 Minimum bend diameter - Limitations due to bend loss

As discussed earlier, the optimum bend diameter of a fiber is always set between an upper and lower limit. The upper limit is set by the space limitations of the splice organizers, distribution frames and fiber panels. Large bend diameters introduce design limitations that are difficult to implement without a penalty on the reduction fiber density. On the other hand, small bend diameters cause stresses on the fiber's surface that affect its mechanical reliability. Small bends can attenuate the light that propagates in the LP_{01} mode. The determination of the minimum bend diameter is of extreme importance on the practical implementation of optical fibers and will be specified in the next chapter.

From the modal noise point of view, the bend configuration has a similar effect on the LP_{11} mode as it has on the LP_{01} mode. The smaller the bend diameter, the higher the attenuation of the LP_{11} mode, and the smaller the modal noise penalty. It is desirable to induce as small bends as possible on the optical fibers. These bends will allow the specified cutoff wavelength to increase and improve the bend sensitivity of the optical fibers, while at the same time reduce the modal noise sensitivity of the optical fibers and increase the fiber density of the frames.

It was shown experimentally and theoretically in Section 4, that the minimum bend diameter of matched and depressed-cladding fibers can be 5 cm. For bends larger than 4 cm in diameter the bend loss performance of the matched-cladding fiber is lower compared to depressed-cladding fiber if their mode field diameter and cutoff wavelength are identical. The same can be said for commercially available matched and depressed-cladding fibers with known differences in MFDs. It is, therefore, important to determine whether the limitation imposed on the minimum bend diameter due to permanent stresses caused by the bend overcomes the one caused by the bend loss of the fundamental mode.

7.7.2 Minimum bend diameter - Limitations due to Fiber Stress

The effect of fiber bend on fiber reliability has been analyzed earlier [78][79][80]. However, the analysis has not been applied to study the minimum bend requirements. In this study it will be determined whether the imposed bend limits are established by the mechanical reliability of the fiber or by the minimum bend loss requirement.

When the optical fiber is bent, its outer surface is under tension while the inner surface is under compression. The maximum tension is on the outer surface of the fiber, i.e. for angles of 180°. The maximum compression occurs in the inside part of the bend, for angles of 0°. The tension and compression effect is shown in Figure 7.21.

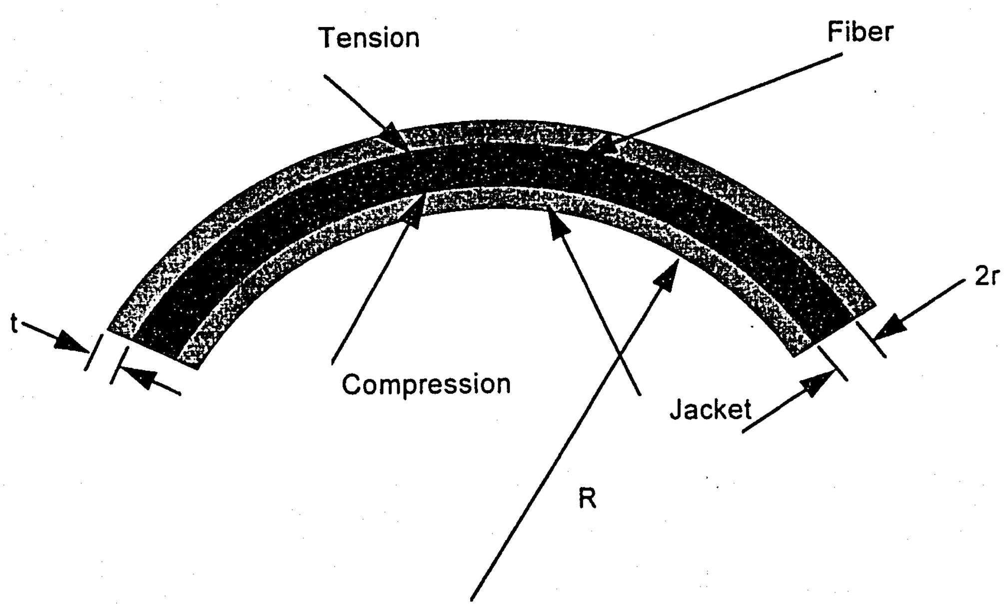

Figure 7.21: Stresses applied on a bent optical fiber.

The fiber will fracture at the points that are under tension. The maximum stress, calculated from the applied strain on the fiber's surface, is:

$$\varepsilon = \frac{L - L_0}{L} = \frac{(R + t + 2r)\theta - (R + t + r)\theta}{(R + t + r)\theta} \tag{7.19}$$

$$\varepsilon = \frac{r}{R + t + r} \cong \frac{r}{R} \tag{7.20}$$

and therefore,

$$\sigma_{max} = \varepsilon E = \frac{Er}{R} \tag{7.21}$$

We observe from this relationship that the radius of curvature is inversely proportional to the maximum stress. We also make the following conservative approximations: rather than assuming that the maximum tension is applied to the outer surface of the fiber, it is assumed to be equally distributed around the whole fiber surface. The probability of a defect occurring at the outer surface of the optical fiber is significantly smaller compared to a fiber under uniform stress.

The current standard industry proof test level is 100 ksi. This is applied to the entire fiber length either during drawing or off-line proof testing. The fiber is proof tested in the factory in order to eliminate all flaws that can cause failures at stresses below 100 ksi.

Theoretical and experimental work has demonstrated that fiber can withstand stresses for a period greater than 25 years, if the permanent stress level is less than 1/3 of the factory proof test level. By applying this rule to equation (7.21) we find that the 1/3 stress level corresponds to a bend diameter of 3.75 cm. Of course, this minimum bend diameter can be reduced further if we assume non-uniform stress changes due to fiber bending.

From the above work we can determine that the minimum bend diameter is imposed by the 1550 nm bend loss of the LP_{01} mode rather than the long-term mechanical reliability of the optical fiber. As it was explained earlier, this minimum bend is 5 cm.

Currently the standardized minimum bend diameter on optical fibers is 7.5 cm. This limit was set by the inferior bend performance of 10-year-old commercially available fibers and a 50 ksi proof test level used several years earlier. In this study the two limits will be compared and the penalty caused by such a conservative limit on the implementation of optical fibers in the field will be assessed.

7.7.3 Bend Dependence of Cutoff - Theoretical Calculations

To a first order approximation, the bend dependence of cutoff can be calculated from the following equation [62]:

$$\lambda_c(D_2) = \lambda_c(D_1) + S\left(\frac{1}{D_2} - \frac{1}{D_1}\right) \tag{7.22}$$

where $\lambda_c(D_1)$ and $\lambda_c(D_2)$ are the cutoff wavelengths at bend radii of D_1 and D_2. S, the proportionality constant, is the curvature dependence of cutoff. In this section the bend dependence of cutoff will be calculated theoretically for matched-cladding fibers, and the results will be compared to experimental data.

The bend effect on the higher order modes is similar, but not identical to that on the LP_{01} mode. As soon as the fiber is bent, the radiation does not occur at the cladding/jacketing interface for the case of the matched-cladding fiber or the inner cladding/outer cladding interface of the depressed-cladding fiber, but almost always inward of these interfaces. At the same time, light lost at each splice point is coupled not only to the LP_{11} mode but also to higher-order modes. Some of these modes have low loss and the field can propagate unaffected for relatively long distances. Bends in the fiber will cause these modes to disappear more rapidly.

As with the case of the LP_{01} bend loss calculations, the LP_{11} mode attenuation can be calculated by solving the wave equation in a toroidal coordinate system as shown in Figure 7.22. Of course, these calculations are very difficult to perform. The preferable method is an approximation that transforms the refractive index profile of the fiber. Rather than assuming that the refractive index is constant along the fiber length and the fiber is curved, we can assume that the fiber is straight while the refractive index changes. The refractive index of the fiber is given by the relationship:

$$n_b(r,\theta) = n\ (r)\left[1 + 2\frac{r}{R}\cos\theta\right] \quad (7.23)$$

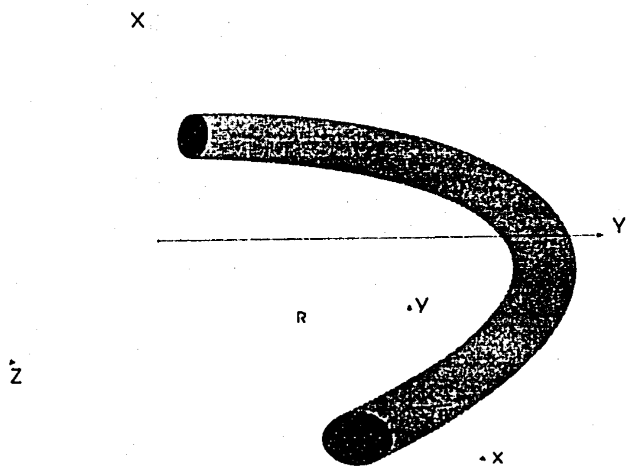

Figure 7.22: Toroidal coordinate system used in the bend analysis of optical waveguides.

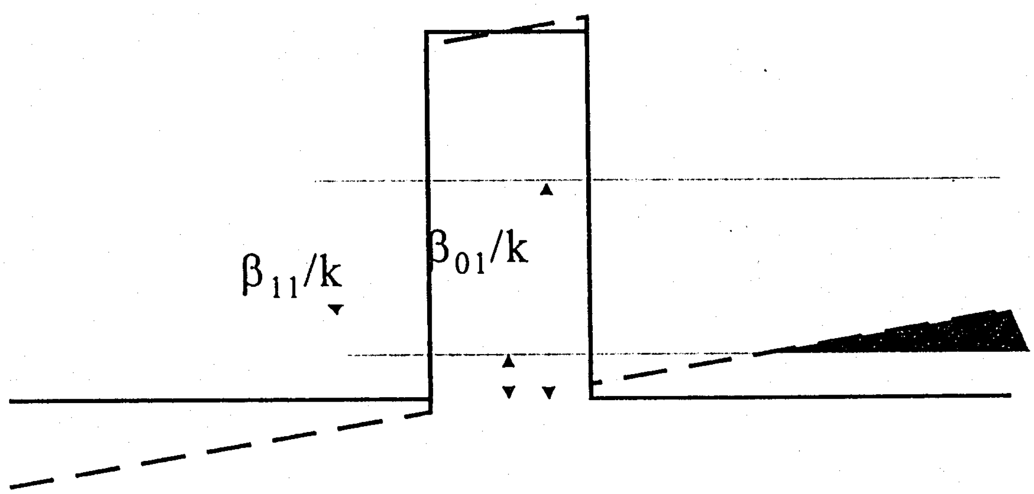

Figure 7.23: The effect of bend on the loss of the LP_{01} and LP_{11} mode.

The above equation can be plotted as shown in Figure 7.23. A similar diagram was presented for the bend performance of the LP_{01} mode.

The bend loss of the LP_{01} mode for matched-cladding fiber was previously calculated by Marcuse [42]. The bend loss formula was given in Section 4.1. The same principles can be applied to calculate the bend loss of the LP_{11} mode. The LP_{11} mode bend loss is found to be:

$$2\alpha(R) = \frac{\sqrt{\pi}\,\chi^2 \exp\left[-\frac{2}{3}(\gamma^3/\beta^2)R\right]}{\gamma^{3/2}V^2\sqrt{R}\,K_0(\gamma a)K_2(\gamma a)} \tag{7.24}$$

The bend loss of the LP_{11} mode for matched-cladding fiber has been calculated using a Mathematica program shown in Appendix 4. Below, a brief explanation of the program is presented.

The eigenvalue equation of the step-index matched-cladding fiber is:

$$U\frac{J_2(U)}{J_1(U)} = W\frac{K_2(W)}{K_1(W)} \tag{7.25}$$

$$V^2 = U^2 + W^2$$

By solving this equation, U and W are calculated as a function of V. From these values the parameters χ, γ, β are found if the core radius of the fiber is known. By using the values in the above equation, the bend loss for a known bend radius is calculated. The fiber core is found from the mode field diameter and the cutoff wavelength. The cutoff wavelength for all fibers was kept constant at 1250 nm. The equations used to calculate the core and NA of the fiber are based on the step-index approximation and are[92]:

$$\frac{w}{a} = 0.65 + 0.434V^{3/2} + 0.0149V^6 \qquad (7.26)$$

$$V_c = 2.405 = \frac{2\pi}{\lambda_c} aNA \qquad (7.27)$$

In the above equations w is the mode field radius, a is the core radius, V_C is the V-value at cutoff and λ_C is the cutoff wavelength. For a step-index profile, the V-value at cutoff is 2.405.

The bend loss of a matched-cladding fiber as a function of the V-value for several bend radii, calculated using the above Mathematica program, is shown in Figure 7.24 for a fiber with MFD of 8.5 microns.

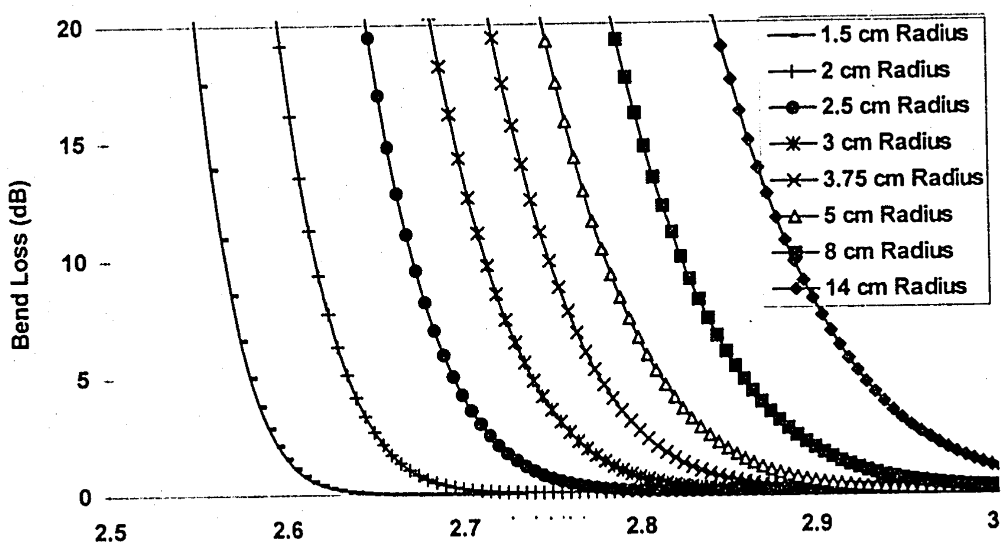

Figure 7.24: Bend loss of matched-cladding fiber as a function of the V-value for MFD

The bend loss for fibers with MFDs ranging from 8 to 10 microns was calculated using the above Mathematica program. From the cutoff wavelength value, corresponding to a loss of 4.77 dB, the V-value is obtained. The change in V-value is used to calculate the cutoff wavelength change as a function of the bend radius.

of 8.5 microns and several bend diameters.

A plot of the cutoff wavelength as a function of the bend diameter is shown in Figure 7.25. This graph shows that the cutoff wavelength does not change linearly with the reciprocal of the bend radius. Therefore, the proportionality constant *S*, as defined by equation 7.22, changes with the bend radius. It is important to specify the bend radius where the bend dependence of cutoff is measured, in order to determine the *S* value accurately.

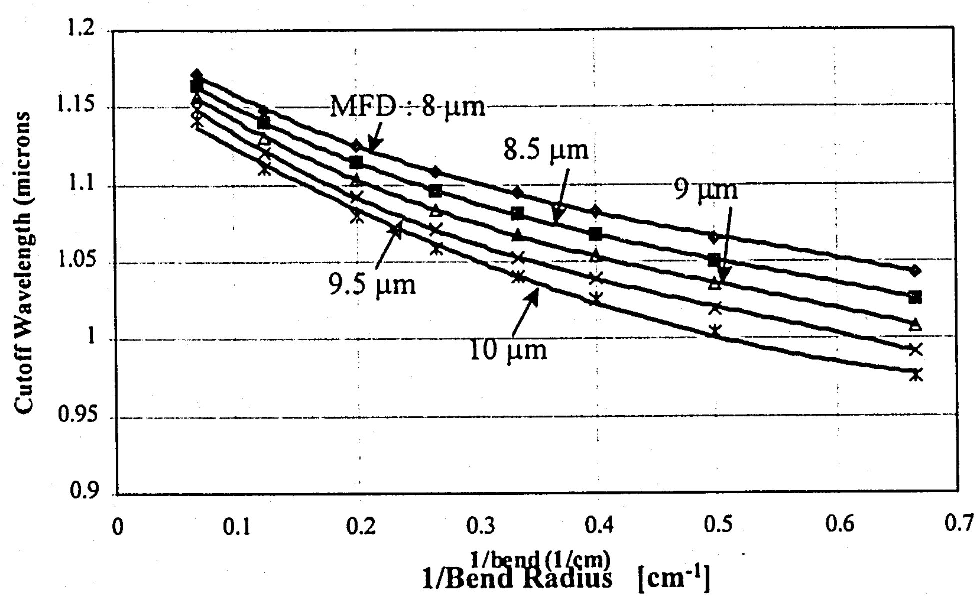

Figure 7.25: Calculated values of bend dependence of cutoff wavelength for fibers with MFDs of 8, 8.5, 9, 9.5, and 10 microns.

The curvature-dependence parameter *S* is shown in Table II. In this table a polynomial fit to the bend dependence of cutoff is shown for different mode field diameters.

An empirical polynomial fit to the calculated points is given by the relationship:

$$\lambda_c = A\left(\frac{1}{D_1}\right)^3 + B\left(\frac{1}{D_1}\right)^2 + C\left(\frac{1}{D_1}\right) + D \qquad (7.28)$$

The parameter S is found from the derivative of the above equation. The parameters of this equation, together with the previous one, are shown in Table II. In this table the constant S is calculated at two values: at a bend radius of 2.5 cm and at a bend radius of 14 cm. The plot of the parameter S as a function of the mode field diameter is shown in Figure 7.26.

Table II: Polynomial fit to the curvature dependence of cutoff. The slope of the curve is shown at two different bend radii of 2.5 and 14 cm.

	Polynomial Fit				***Slope (S)***			***Slope (S)***	
MFD	***A***	***B***	***C***	***D***	***3A***	***2B***	***C***	***at 2.5 cm***	***at 14 cm***
8	-0.410	0.678	-0.514	1.204	-1.230	1.355	-0.514	169	391
8.5	-0.427	0.713	-0.546	1.199	-1.280	1.427	-0.546	180	416
9	-0.478	0.713	-0.546	1.199	-1.435	1.427	-0.546	205	418
9.5	-0.552	0.895	-0.649	1.190	-1.657	1.789	-0.649	199	530
10	-0.550	0.908	-0.674	1.184	-1.651	1.815	-0.674	211	552

We can observe from the above figure, that the cutoff dependence on the radius of curvature increases as the mode field diameter of the fiber increases. It was previously believed that the parameter S depends only on the fiber design, i.e. whether the fiber is matched or depressed-cladding. The above calculations show that the mode field diameter is the only parameter that affects the bend performance of the cutoff wavelength rather than the fiber design.

A simple explanation of the above phenomenon is as follows: as the mode field diameter of the fiber increases, the core diameter increases as well. For the case of constant cutoff wavelength, the index difference between the core and the cladding will decrease in order to keep the cutoff wavelength of the fiber constant. This change in the relative index difference results in a smaller effective refractive index, which will cause the radiation of the mode to occur closer to the core. Therefore, the bend loss of the LP_{11} mode will increase. A graphical explanation of the above phenomenon is shown in Figure 7.27.

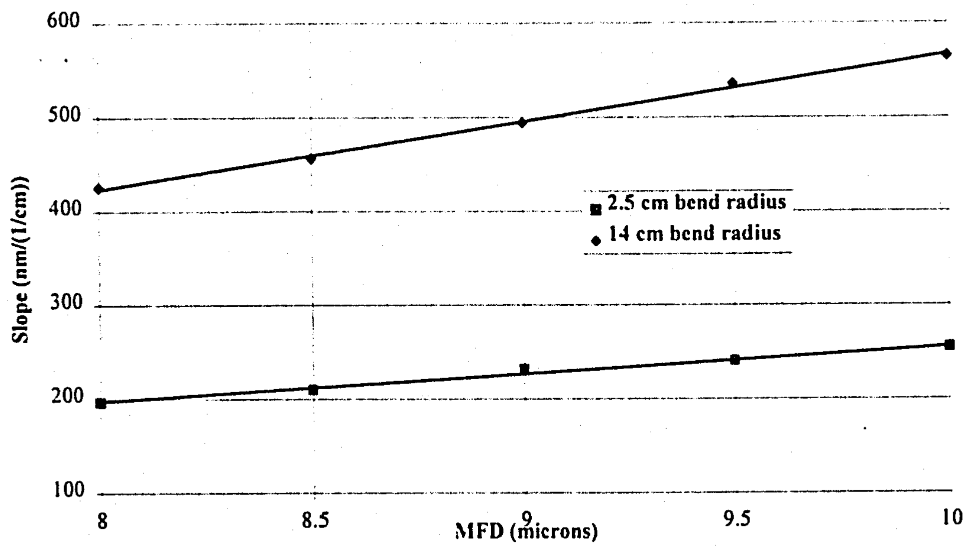

Figure 7.26: Curvature dependence of cutoff for bend radii of 2.5 and 14 cm. The lines shown are linear fit to the calculated points.

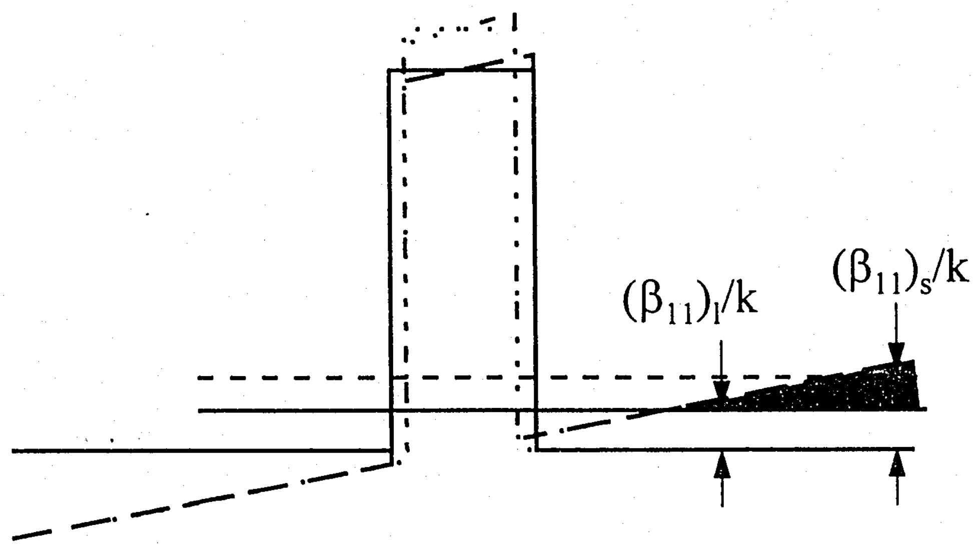

Figure 7.27: The effect of the mode field diameter on the bend loss of the LP_{11} mode. $(\beta_{11})_l$ is the propagation constant of the large MFD, while $(\beta_{11})_s$ is the one for small MFD.

7.7.4 Bend Dependence of Cutoff - Experimental Results

Due to the presence of the LP_{01} mode, the bend loss of the LP_{11} mode is difficult to determine. The behavior of the LP_{11} mode under bent conditions can be understood by studying the bend dependence of the cutoff wavelength.

In order to quantify the results mentioned above, several cutoff wavelength measurements were made as a function of the bend radius. Afterwards, the parameter S was calculated and compared with the theoretical results.

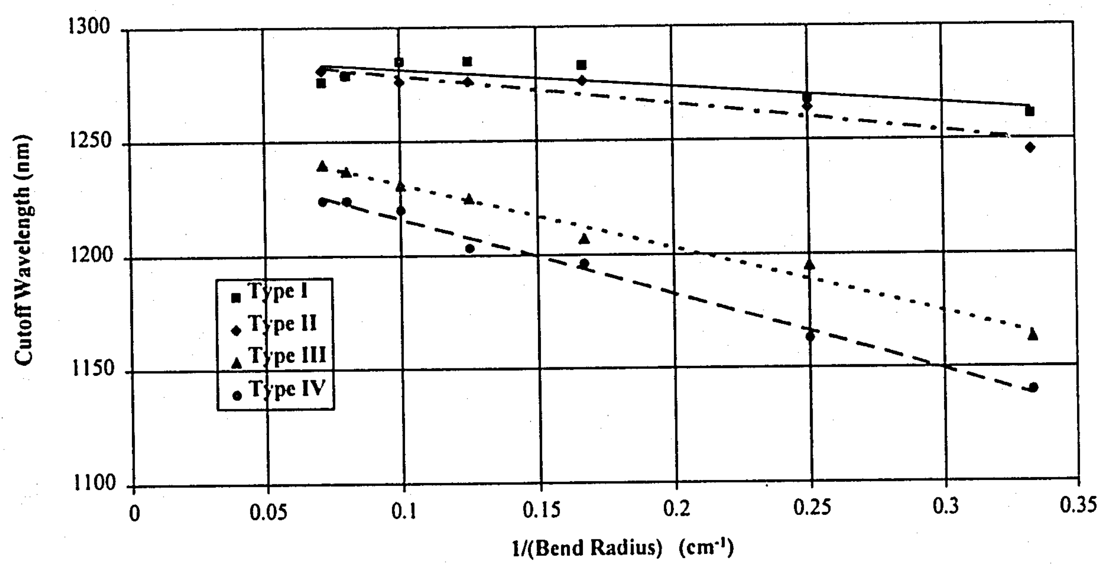

Figure 7.28: Measured bend dependence of cutoff wavelength for four different types of single-mode fibers.

In Figure 7.28, the measured cutoff wavelength as a function of the reciprocal bend radius is presented for four different fiber types. Linear regression lines are generated for each set of data representing the four fiber types. The four different fibers are shown in Table II. As seen, fiber type I and II are depressed-cladding single-mode fibers, while fiber type III is matched-cladding design and fiber type IV is a pure silica core fiber. In this table the parameter C is defined by equation (7.14) while the parameter S is given by equation (7.22).

Table III: Experimental determination of parameters C and S for two depressed and one matched-cladding fiber

Fiber Type	MFD (μm)	b/a	C nm/dec.	S nm/(cm^{-1})
Δ^+=0.25% Δ^-=0.09%	9.52	6.6	-55	-250
Δ^+=0.25% Δ^-=0.12%	8.95	6	-63	-160
Δ^+=0.25% Δ^-=0.00%	10.12	9.5	-22	-670

The following conclusions can be drawn:

For matched-cladding fibers, the cutoff wavelength changes drastically with the bend diameter. The calculated and experimentally determined parameter S have similar values, especially for large bend diameters. For small bend diameters the calculated parameter S is smaller than the measured one. The cutoff wavelength for matched-cladding fibers changes by 90 nm when the bend radius changes from 14 to 2.5 cm.

This is not the case of depressed-cladding fibers. The cutoff wavelength of fiber types I and II changes only slightly with wavelength. These results indicate that in the depressed-cladding fiber the dominant loss mechanism of the LP_{11} mode is due to leakage. This effect causes the "theoretical" cutoff wavelength in the absence of depression to be as high as 200 nm above the measured value. At the same time the mode field diameter is significantly smaller than the matched-cladding fiber. Both of these phenomena will reduce the LP_{11} bend loss, since the mode will be bound much closer to the core.

From the above discussion we see that a depressed-cladding fiber has a stronger length-dependence of cutoff wavelength, while the matched-cladding fibers have stronger bend dependence. In order to increase the LP_{11} mode attenuation and reduce the chance of modal noise, a longer fiber length for depressed-cladding fibers and a tighter bend for matched-cladding fibers are required. Tighter bends are easier to implement, making these fiber types more attractive in areas where short lengths are required in order to incorporate a large number of patchcords.

As seen in the Figure 7.28, the cutoff wavelength does not follow the curves predicted by the theoretical estimations given in Figure 7.25, where the relationship of the cutoff wavelength as a function of the reciprocal of the bend radius deviates slightly from being linear. It is believed that the difference in attributed to the accuracy by which the cutoff wavelength is being measured. In order to evaluate the theoretical predictions, an experiment was carried out where the cutoff wavelength was measured accurately for a few bend radii.

The results of the cutoff wavelength as a function of the bend configuration is shown in Figure 7.29 for the case of matched-cladding fiber only. In order to improve the repeatability, the measurement of the cutoff wavelength for the each of the four bend radii was measured 5 times. The agreement between theory and experiment is improved significantly.

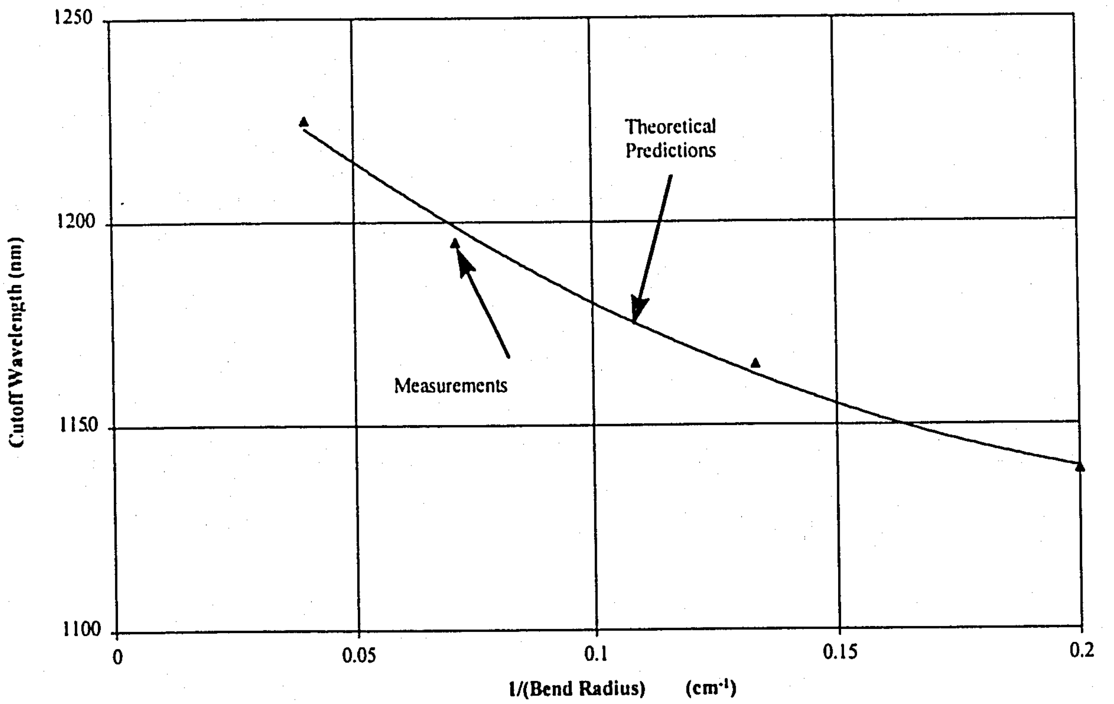

Figure 7.29: Correlation between the measured bend dependence of cutoff and theoretical calculations for matched-cladding fiber. The theory is in good agreement with the experiment.

7.8 Modal Noise Calculations

7.8.1 Noise-to-Signal ratio

The modal noise penalty is calculated from the signal-to-noise ratio that is generated after three successive splices, as shown in Figure 7.1. The signal-to-noise ratio is calculated by the following method.

For simplicity we assume that the splice at each point is identical. Since the light transmission efficiency of each splice point is the same, the LP_{01} transmission after the three splice points becomes:

$$T = \eta^2 + (1-\eta)^2 e^{-\alpha_{11}L} + 2\eta(1-\eta)e^{-\alpha_{11}L/2}\cos(\Delta\beta L) \qquad (7.29)$$

where η is the transmission efficiency of each splice.

In this expression the first and second terms are equivalent to the signal, while the last term is related to the noise due to modal interference. Therefore, the noise-to-signal ratio due to the presence of the LP_{11} mode is given by the relationship:

$$\sigma_m = \frac{Noise}{Signal} = \frac{2\eta(1-\eta)e^{-\alpha_{11}L/2}\cos(\Delta\beta L)}{\eta^2 + (1-\eta)^2 e^{-\alpha_{11}L}} \qquad (7.30)$$

In the above equations the following assumptions can be made:

- The splice loss is relatively small (usually smaller than 1 dB)
- The operating wavelength is close to the cutoff wavelength, contributing to high loss of the LP_{11} mode

- Each value of $\Delta\beta L$ occurs with the same probability, which corresponds to the worst signal-to-noise ratio (SNR). In that case, the cosine term can be replaced by its RMS value,

$$\cos(\Delta\beta L) = \frac{1}{\sqrt{2}}$$

and therefore,

$$\sigma_{ml} = \frac{\sqrt{2}(1-\eta)}{\eta} e^{-\alpha_{11}L/2}$$

The noise-to-signal ratio depends on two additional parameters: the mode partitioning noise, k, which was described in Section 7.2, and the excitation efficiency, A, of the LP_{11} mode. By taking these two parameters into consideration, the following is obtained:

$$\sigma_{ml} = kA\frac{\sqrt{2}(1-\eta)}{\eta} e^{-\alpha_{11}L/2} \tag{7.31}$$

The modal noise penalty, ΔP, is calculated from the value of the noise -to-signal ratio, σ_m, by the relationship [81]:

$$\Delta P = -5\log[1 - 72\sigma_{ml}^2 + 1296\sigma_{ml}^4] \tag{7.32}$$

From the above equations, the modal noise penalty can be calculated if the laser mode partition noise, the LP_{11} excitation efficiency, the splice loss at each point, the fiber length, and the LP_{11} mode attenuation are known. In the next section we will determine the LP_{11} mode excitation efficiency.

7.8.2 Excitation efficiency of the LP_{11} mode

At each splice point, part of the lost power couples into the LP_{11} mode and part into the higher-order cladding and radiation modes. We define the excitation efficiency of the LP_{11} mode at a splice as follows:

$$A = \frac{P_{11}}{P_{11} + \Sigma P} \tag{7.33}$$

where P_{11} is the power of the LP_{11} mode after the splice and ΣP is the total power coupled to all the excited modes except the LP_{01} and LP_{11} modes after the splice.

The parameter A was determined experimentally by the following technique: The test setup described in Section 7.5.1 was utilized, with a short piece of fiber inserted between the launch optics and the test fiber. The experimental setup is shown in Figure 7.30. As seen, a fiber is butt-joined to the test fiber with index-matching liquid. A loop of 2 cm is applied to the short fiber in order to avoid the presence of the LP_{11} or other higher order modes at the joint point. If there is no offset between the launch and the receive fiber and there is no loss at the splice point, only the LP_{01} mode will be generated after the splice. By increasing the transverse offset at the splice point, the splice loss will increase. This loss will excite the LP_{11} and additional higher-order modes. For a short fiber length, the power loss at the LP_{11} mode can be determined by comparing the output power with and without a small loop in the second fiber. In that case we find:

$$P_{01}^{in} = P_{01}^{out} + P_{11} + \Sigma P$$

$$\eta = P_{01}^{out} / P_{01}^{in}$$

$$R = (P_{01}^{out} + P_{01}^{in}) / P_{01}^{out}$$

In the last equations $1/R$ is the fractional loss caused by the loop in the receiving fiber. By performing separate power measurements with and without the loop in the receiving fiber, and a third including only the transmitting fiber, the parameters R and η can both be determined. R is calculated from the power ratio with and without the loop in the receiving fiber. The efficiency η is calculated from the power ratio with the loop in the receiving fiber and by removing the receiving fiber completely.

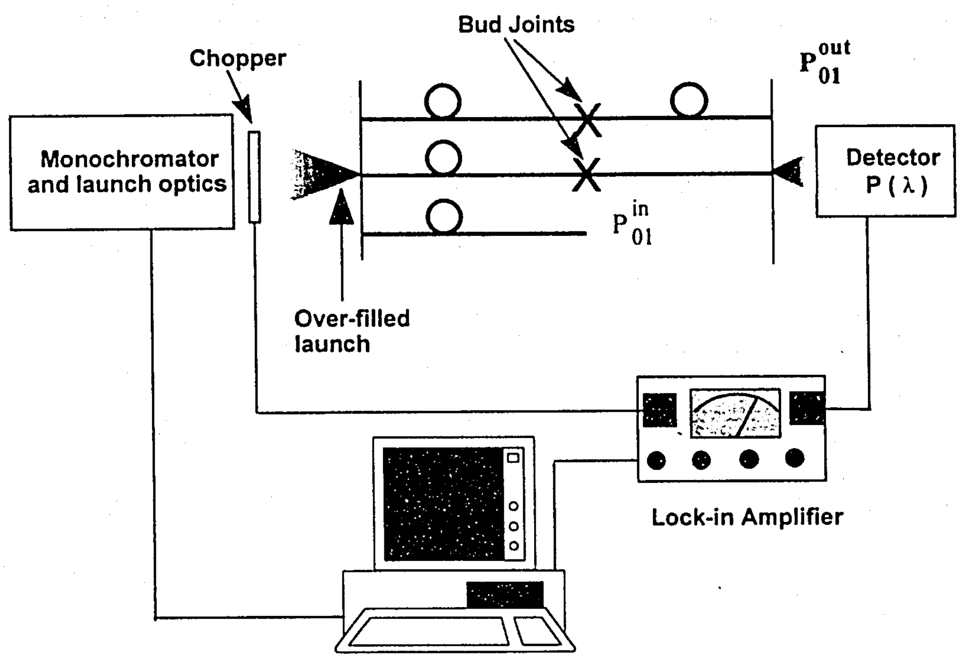

Figure 7.30: Experimental setup to evaluate the excitation coefficient of the LP_{11} mode.

By combining the above equations we obtain:

$$A = (R-1)/(1-1/\eta) \tag{7.34}$$

The excitation efficiency A is obtained as a function of the splice loss by misaligning the transmit to the receive fiber at the splice point. By using non-linear regression analysis we obtain an empirical relationship between the excitation efficiency A of the LP_{11} mode and the transmission efficiency at the splice point η. This relationship is given by the following equation:

$$A = 1 + \log \eta . \tag{7.35}$$

7.8.3 Experimental verification of Modal Noise

The effect of modal noise on the system performance was evaluated in an experimental 1.2 Gb/sec system. The experimental results were compared with the calculated ones in order to establish the validity of the foregoing calculations. The measurement system degradation was performed using a 10-meter section of depressed-cladding fiber (similar to type II in Table I).

For the purpose of these experiments several unconventional fibers were fabricated by the modified chemical vapour deposition (MCVD) method. These fibers had the standard refractive index profile shown in Table II. During the drawing process the cladding diameter was modified in order to adjust the cutoff wavelength. Adjustments in the cladding diameter modify the core size proportionally, which results in cutoff wavelength changes as given by the relationship:

$$\lambda_c = \frac{2\pi}{V_c} aNA .$$

Four fibers with cutoff wavelengths of 1350, 1380, 1400 and 1450 nm were fabricated by the above method. The fibers were drawn from the same preform, in order to keep the refractive index profile constant.

The measurement of modal noise can be performed using the concept of eye closure or a direct bit-error-rate (BER) measurement. Since the eye diagram is sensitive to the generated noise and to the user's interpretation, the more accurate direct measurement of BER was used in this section.

The modal noise measurement apparatus is shown in Figure 7.31. As seen, the fiber under test was inserted between the transmitter and the receiver pigtail. The receiver fiber was connected to a variable optical attenuator, which was used to adjust the power at the receive end. The variable optical attenuator was connected to the BER tester. The system BER was measured for different power levels in order to determine the power differences more accurately. The power penalty was calculated at BER levels of 10^{-9}. At this level, the received power difference was calculated with and without the presence of the fiber under test and the corresponding splice loss.

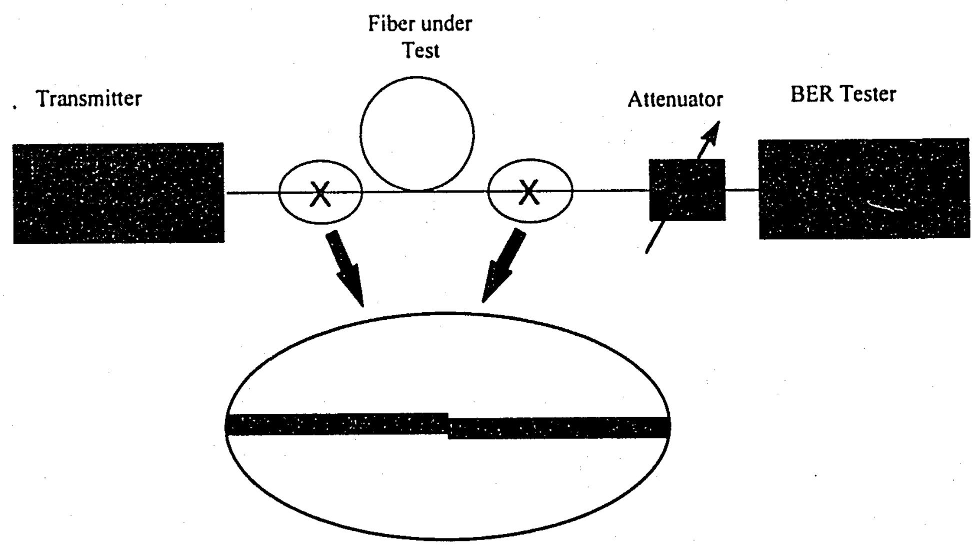

Figure 7.31: Apparatus for measuring modal noise penalty.

Initially the BER characteristic of the system was determined by connecting the transmitter pigtail to the receiver. Care was taken to assure that the cutoff wavelength of the pigtails was below the laser operating wavelength. The BER was measured by adjusting the received optical power with the help of the variable optical attenuator. Afterwards, a line was fitted to the data by using an exponential regression analysis. The results of this measurement were found to be identical to the zero-dB curve of Figure 7.32.

After the initial evaluation of the system performance, two experiments were performed to determine the modal noise penalty:

In the first, the BER was measured as a function of splice loss for a fiber with cutoff wavelength of 1350 nm. The system operating wavelength was 1300 nm. In this case no modal noise penalty was observed even when the splice loss was increased to 5 dB at each splice point. As a result, another fiber with cutoff wavelength of 1400 nm was inserted between the transmit and receive fiber. The BER as a function of the receive power P_r was measured for splice losses ranging from 0 to 4 dB at each splice point. The results of this experiment are shown in Figure 7.32 for all splice losses.

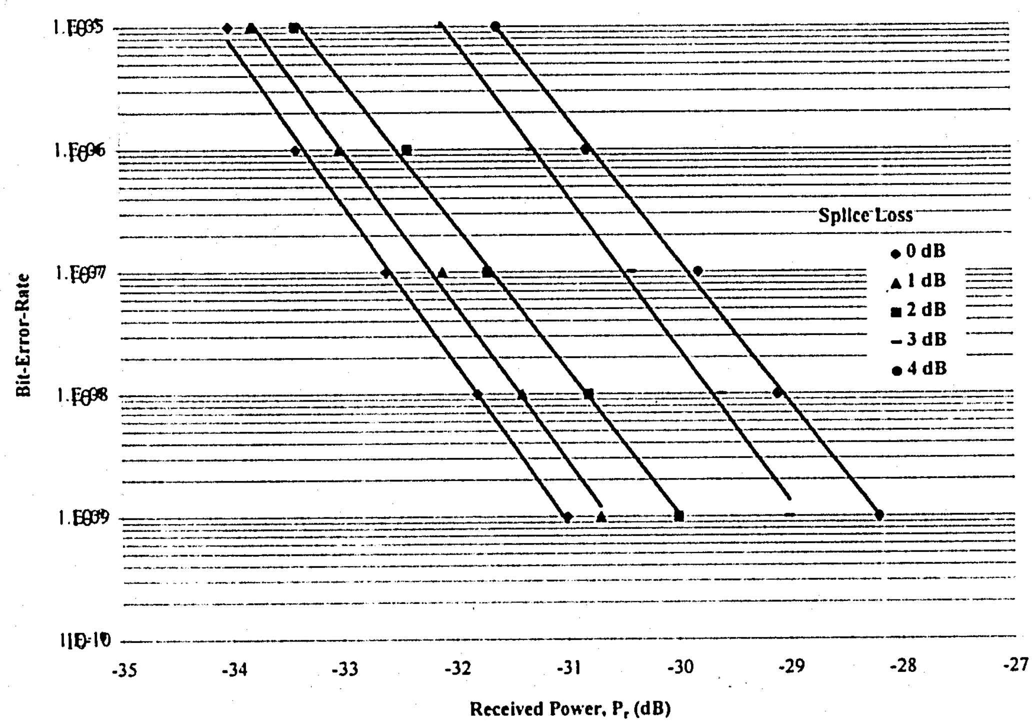

Figure 7.32: Measured bit-error-rate (BER) as a function of received power for splice losses ranging from 0 to 4 dB.

At a BER of 10^{-9}, the power penalty was determined by measuring the difference in the required received power for a splice loss of zero and for the imposed splice loss.

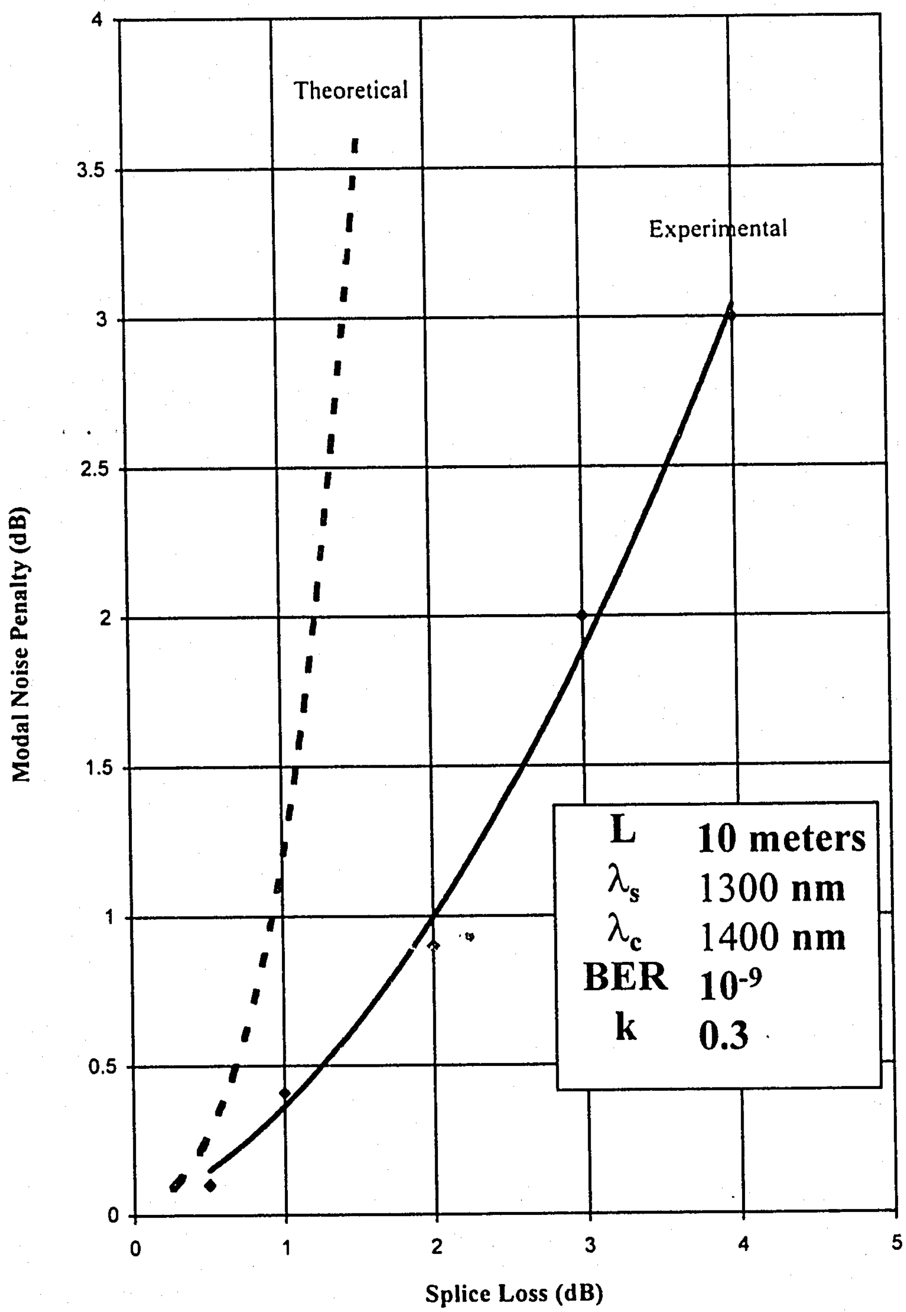

Figure 7.33: Measured and calculated modal noise penalty as a function of splice loss for a constant BER of 10^{-9}.

In Figure 7.33, the theoretical values calculated from (7.31) and (7.32) are shown. From this plot we observe that the power penalty for zero splice loss is zero. This occurs since, at zero splice loss all the power is coupled to the LP_{01} mode at both splices and no modal noise is generated. For a splice loss of 1 dB the calculated penalty is approximately 1.1 dB while the experimental penalty is 0.4 dB. This difference between theory and experiment increases even further for higher splice losses.

In a second experiment, all four high-cutoff-wavelength fibers were used to determine the modal noise dependence on the fiber cutoff wavelength. For this experiment the splice loss was kept at 1 dB. The results of this test are shown in Figure 7.34 together with the theoretical calculations. As expected, the modal noise penalty depends strongly on the cutoff wavelength. Once again, the measurement results are only in qualitative agreement with the theory. For a splice loss of 0.5 dB the difference between calculated and measured cutoff wavelengths is approximately 40 nm.

It was explained earlier that we should expect some disagreement between theory and experiment. Some of the reasons for this disagreement, caused by theoretical assumptions and experimental limitations, are given below:

- The model assumes that system operating wavelength varies randomly due to mode partitioning.

- In the theoretical calculations a factor from the signal component was omitted for ease of calculations.

Unintentional bends are inevitably incorporated during the measurement. These bends result in attenuation of the LP_{11} mode, and they do not affect the bend loss of the LP_{01} mode. Therefore, the modal interference and subsequently the modal noise of the system will be reduced.

In this work we want to determine the upper minimum on the cutoff wavelength and the lower length required to eliminate modal noise. The above assumptions will all contribute to overestimating the modal noise penalty. The industry expects no penalty due to modal noise. By utilizing the conservative theoretical model developed above, with the appropriate limits, no modal noise penalty will be present in any fiber optics system.

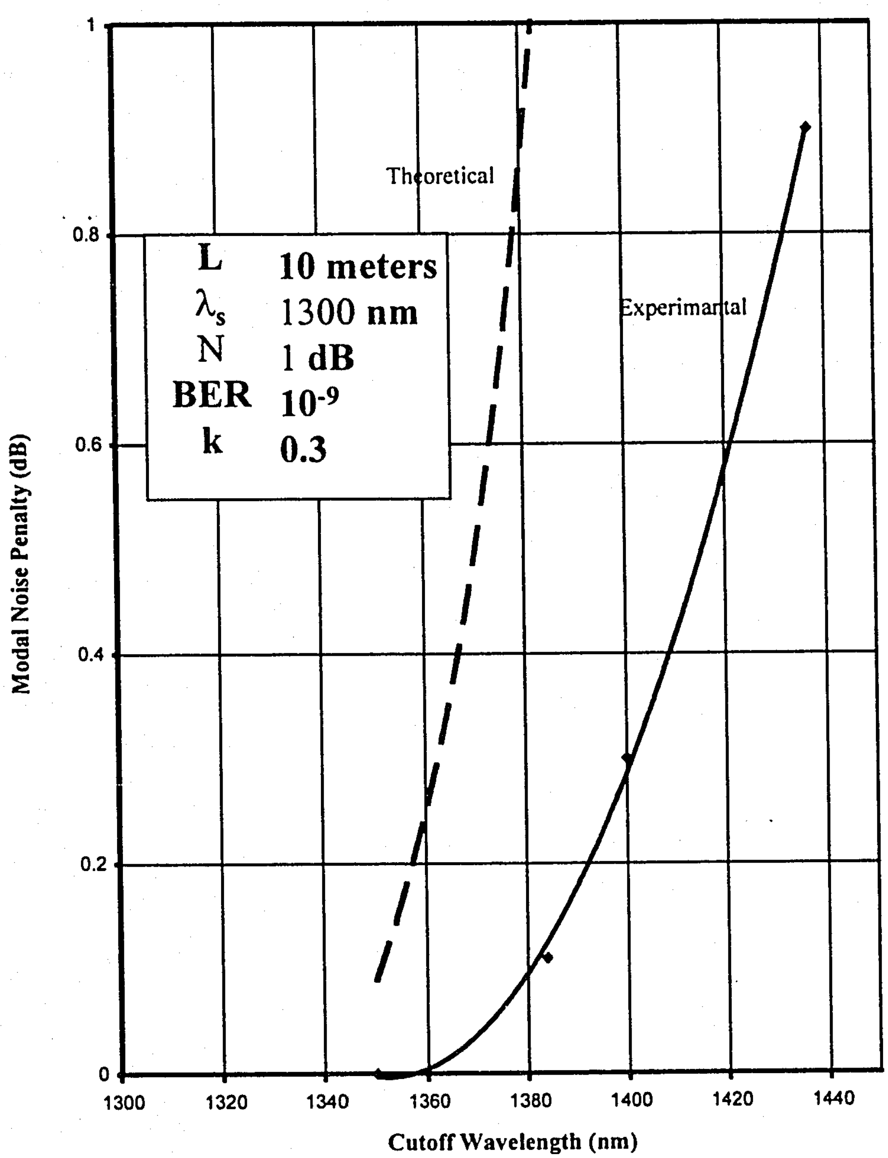

Figure 7.34: Measured and calculated modal noise penalty as a function of cutoff wavelength for a BER of 10^{-9}.

7.8.4 Setting the Modal Noise Limits on Fiber Optics Systems

Now that all the necessary background for the modal noise penalty is in place, it is important to set the lower limits on fiber parameters that are necessary to eliminate any presence of modal noise. These parameters are the upper and lower values of the bend diameter, the lower limit of cutoff wavelength and the minimum fiber length.

The current lower limit of bend diameter is 7.5 cm. As discussed earlier, this limit depends on two parameters: the long-term fiber reliability and the bend loss of the LP_{01} mode. As discussed earlier, a 5-cm bend diameter will exceed both the mechanical and optical requirements of fiber optics systems.

The upper limit of the bend diameter was set to be infinite. It will be shown that the penalty of a straight fiber on the required length is very high. In this work it is recommended that the bend diameter should be at least 7.5 cm.

The currently recommended lower operating wavelength limit is 1260 nm. Even though no operating system specifies operating wavelengths below 1285 nm, standards organizations recommend the lower value in case the cooling mechanism of the laser package should fail, and the operating wavelength shifts to these values due to the higher temperature. These effects cause the energy gap between the conduction and valence bands of the semiconductor to change, affecting the wavelength of the light emitted by the device. This argument is extremely conservative, and introduces severe limitations on the operating system. If a system designed for operation at 1310 nm experiences such a shift in its operating wavelength, it will fail for reasons other than modal noise such as power limitations due to the optical fiber attenuation change of the LP_{01} mode or by the noise generated due to chromatic dispersion degradation. In this work the lower limit of the operating wavelength will coincide with the worst case specification of 1285 nm. The same value is used in the design of fiber optics systems.

The next parameter to be defined is the lower limit of the fiber length. It was explained in Section 7.2 that modal interference changes into modal noise if laser wavelength changes due to mode hopping are smaller than the periodicity of the modal interference pattern. This fiber length, depending on the cutoff wavelength, corresponds to 1.5 meters. In the following calculations, fiber length will be reduced to 0.5 meters. If the system will meet the modal noise criteria for 0.5 meters, it will operate for any fiber length.

The last remaining parameter is the mode partition noise, *k*. For most practical applications this value varies between 0.3 and 0.5. In the following calculations the worst case value of 1 will be used. This value corresponds to a double-moded laser, where the optical power can switch from the one mode to the other arbitrarily.

Table IV summarizes the assumptions made in order to proceed with the calculations of the modal noise penalty. As mentioned, all the assumed values are under the worst-case scenario. This is necessary in order to eliminate any future concerns related to modal noise.

It is also assumed that the worst-case allowable modal noise penalty is 0.5 dB. This value is small compared to other penalties and will not affect the system performance. Finally, the worst-case splice loss is 2 dB. Usually the splice and connectorization loss of fiber optics systems is below 0.5 dB, and most often of the order of 0.1 dB.

Table IV: Worst-case values used to determine modal noise limits

Parameter	*Worst-case Value*	*Unit*
Bend Diameter (upper Limit)	∞	cm
Bend Diameter (Lower Limit)	8	cm
Cutoff Wavelength (Upper Limit)	1285	nm
Fiber Length	0.5	m
Mode-Partitioning Noise	1	
Splice Loss (Upper Limit)	2	dB
Modal Noise Penalty	0.5	dB

7.9 Determining the lower cutoff wavelength limit

7.9.1 The case of unbent fiber

Up to now the lower value of the cutoff wavelength was determined from a very simple statement: the effective cutoff wavelength of a straight fiber at the desired length shall be lower than the "worst case" wavelength of the system's source. Since the lower wavelength limit was set at 1260 nm, the cutoff wavelength for the desired fiber length should be lower than this value. Of course, this value is adjusted by the layout configuration. As mentioned earlier, the fiber layout conditions for the factory measurement require a 2-meter fiber length and a 28-cm diameter bend. For fibers shorter than 2 meters, the cutoff wavelength increases, while for longer fibers, it decreases. By knowing the length and bend dependence of cutoff wavelength and the lower wavelength limit, we can predict the factory-measured cutoff wavelength and set the proper industrial specifications.

In this work the factory-measured cutoff wavelength for a system with operating wavelength of 1285 nm is estimated by using the data in Sections 7.5 and 7.7. This plot is given in Figure 7.35. This figure was made under the assumption that the cutoff wavelength of both fiber types is identical at a length of two meters. As expected, the allowable cutoff wavelength of the fiber increases with the fiber length.

In the above plot we notice that the allowable cutoff wavelength for depressed-cladding fiber is higher than that of matched, for lengths greater than two meters. The opposite is true for lengths shorter than two meters. The explanation is that the cutoff wavelength of the depressed-cladding fiber has a stronger length dependence than does the matched-cladding fiber. This is due to the fact that there is no leakage-loss effect in the matched-cladding fiber, whereas there is in the depressed-cladding fiber.

From the above observations we see that if straight fiber lengths are used in the optical system, the matched-cladding fiber is preferable to depressed-cladding for lengths less than two meters and vice versa for lengths greater than two meters.

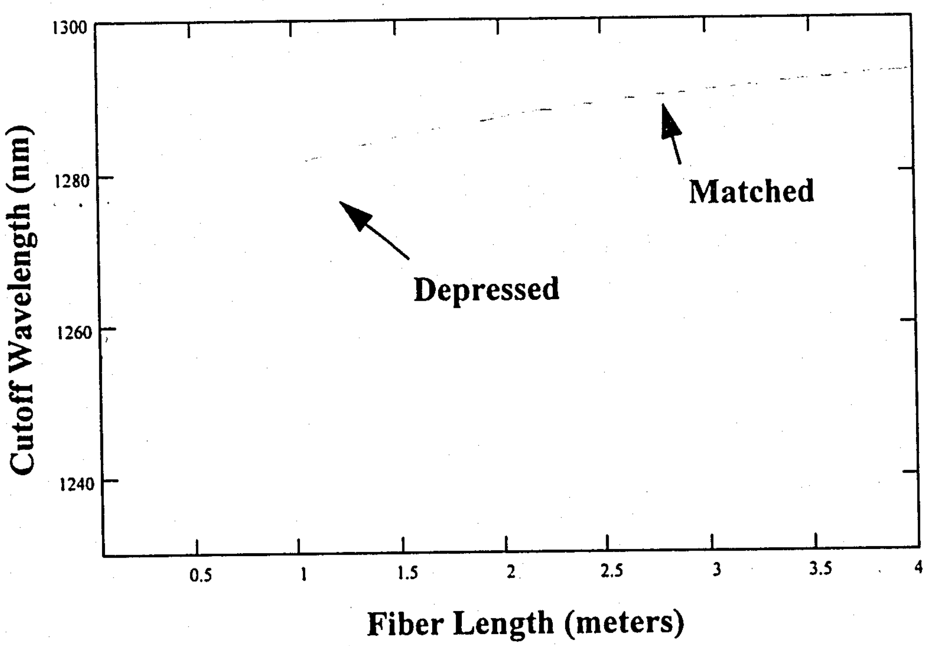

Figure 7.35: Estimated cutoff wavelength as a function of length for matched and depressed-cladding fibers.

Similar observations can be drawn if we use the modal noise penalty approach. By using the equations given in Section 7.8, the maximum allowable cutoff wavelength as a function of splice loss for different levels of modal noise penalty can be calculated. The calculations were made using MathCad, and the complete program is shown in Appendix 5.

The results of these calculations, shown in Figure 7.36, demonstrate that the maximum allowable cutoff wavelength depends not only on the fiber type (matched or depressed) but also on the maximum allowed modal noise penalty, the splice loss and of course the length of the fiber. This model is more complete and, contrary to previous arguments within the fiber optics industry, easily understood.

From this graph we observe that the maximum allowable factory-measured cutoff wavelength increases with the modal noise penalty, the rate of dependence on the modal noise penalty is greater for depressed rather than matched-cladding fibers, and that the depressed-cladding fiber has higher maximum cutoff wavelength values for modal noise penalties greater than 0.6 dB and splice losses less than 0.5 dB if the fiber length is 1 meter. For short fiber lengths the matched-cladding has the advantage for any imposed penalty and splice loss, while for long ones (of about 10 meters) the depressed-cladding fiber can accommodate higher cutoff wavelengths.

Figure 7.37 shows the dependence of the cutoff wavelength on the splice loss for 0.05-, 0.5- and 1-dB modal noise penalties. As seen from this graph, the maximum allowable cutoff wavelength for matched-cladding fiber is higher than that of depressed-cladding for length of one meter. The opposite is true for lengths greater than two meters. Since in our case we are interested for the maximum allowable wavelength in fiber management system configurations, lengths of the order of 1 meter are investigated.

Another important observation is that the maximum allowable cutoff wavelength is approximately 1276 nm for matched and 1266 nm for depressed-cladding, if the splice loss at each point is 2 dB and the modal noise penalty 0.1 dB.

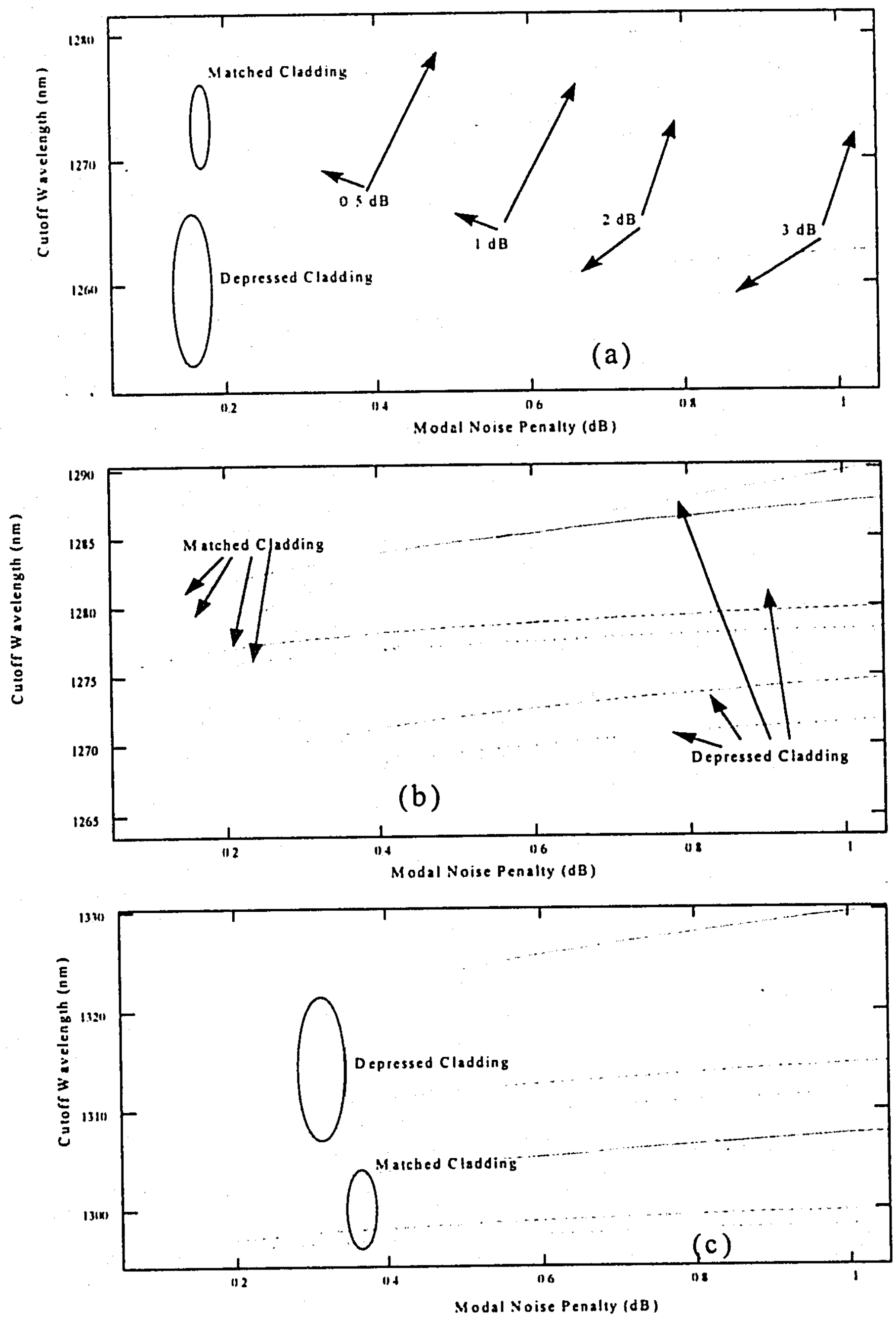

Figure 7.36: Maximum cutoff wavelength of unbent single mode fibers as a function of modal noise penalty for splice losses of 0.5, 1, 2 and 3 dB. The three different plots correspond to fiber lengths of 0.5 meters (a), 1 meter (b) and 10 meters (c).

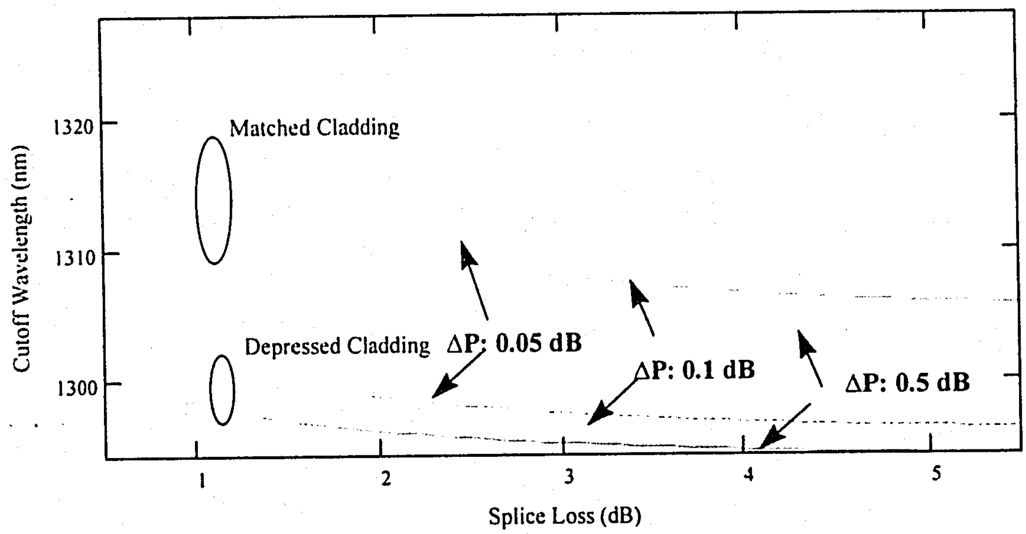

Figure 7.37: Upper limit of cutoff wavelength for matched and depressed-cladding fibers at 10 meters length and 0.05, 0.1 and 0.5 dB modal noise penalty. No bend is applied.

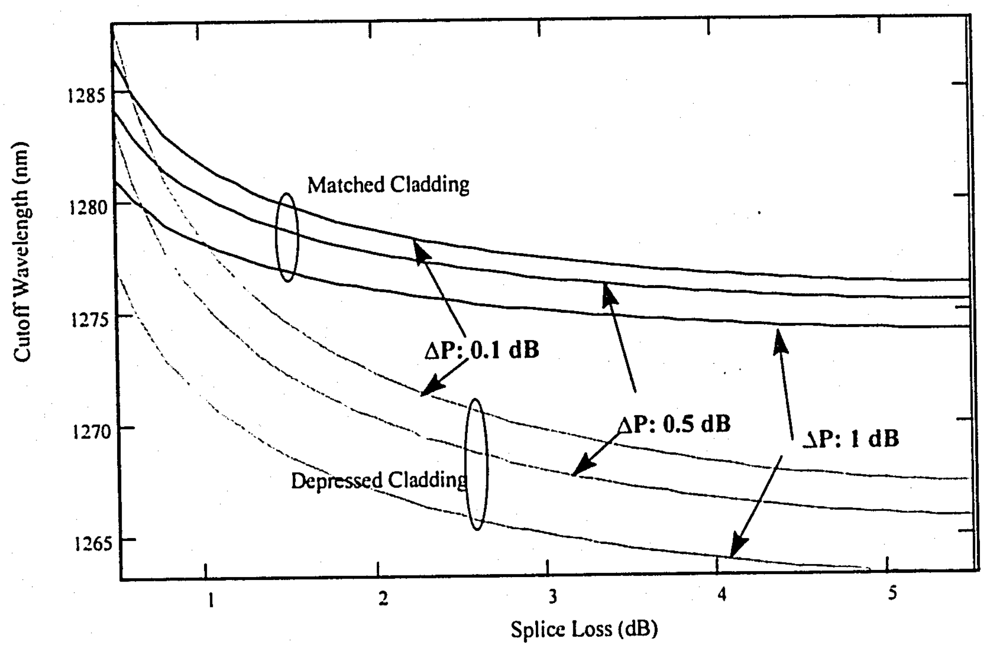

Figure 7.38: Maximum allowable cutoff wavelength as a function of splice loss for modal noise penalties of 0.1, 0.5, and 1 dB. The fiber length is 1 meter.

We also observe that the cutoff wavelength increases as the splice loss at the two splice points decreases. For zero splice loss, the cutoff wavelength reaches infinity. We also see that the cutoff wavelength of depressed-cladding fibers has a stronger dependence on the splice loss than for matched-cladding fibers. As an example, for a modal noise penalty of 1 dB and a change in splice loss between 1 and 2 dB, the maximum cutoff wavelength of a depressed-cladding fiber changes by approximately 10 nm, while that of a matched-cladding fiber changes by 5 nm. The same can be said for the modal noise penalty. For a 2-dB splice loss and a change in modal noise penalty from 0.1 to 1 dB, the maximum cutoff wavelength changes by 5 nm for a matched-cladding fiber and by 15 nm for a depressed-cladding fiber. Due to all the above observations, matched-cladding fiber types are preferable under conditions of unbent deployment and short lengths.

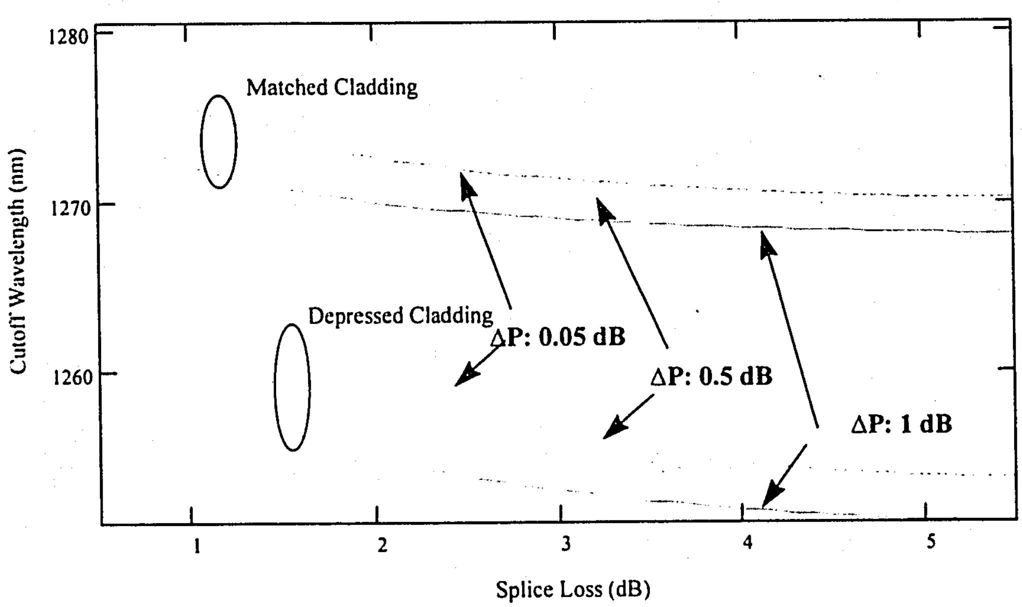

Figure 7.39: Same as Figure 7.37 but with a fiber length of 0.5 meters.

This cutoff wavelength limit reduces even further if the required length becomes 0.5 meters. As shown in Figure 7.39, the required cutoff wavelength becomes approximately

1250 nm for the case of depressed-cladding fiber and 1270 nm for the matched case. In this case the modal noise penalty and the splice loss remain the same.

These cutoff wavelength limits are difficult to achieve and they introduce a significant limitation to the design of single mode fiber since they reduce the design window significantly. An easy way to increase the cutoff wavelength of the fiber is to introduce intentional bends in the fiber. Another scenario is to provide several fiber types having different cutoff wavelengths. This will increase the complexity of the fiber optics transmission systems significantly. Such an approach is not in the best interests of the fiber supplier and end user.

7.9.2 The case of bent fiber

As was determined theoretically and experimentally earlier, a bend in the fiber configuration causes the cutoff wavelength to reduce. Or, in other words, the maximum allowable factory measured cutoff wavelength will be allowed to increase as the bend diameter on the deployed fiber decreases. This effect was utilized to obtain the maximum allowable factory measured cutoff wavelength as a function of the bend diameter. Once again, the experimentally determined values shown in table III were used to obtain the calculated results.

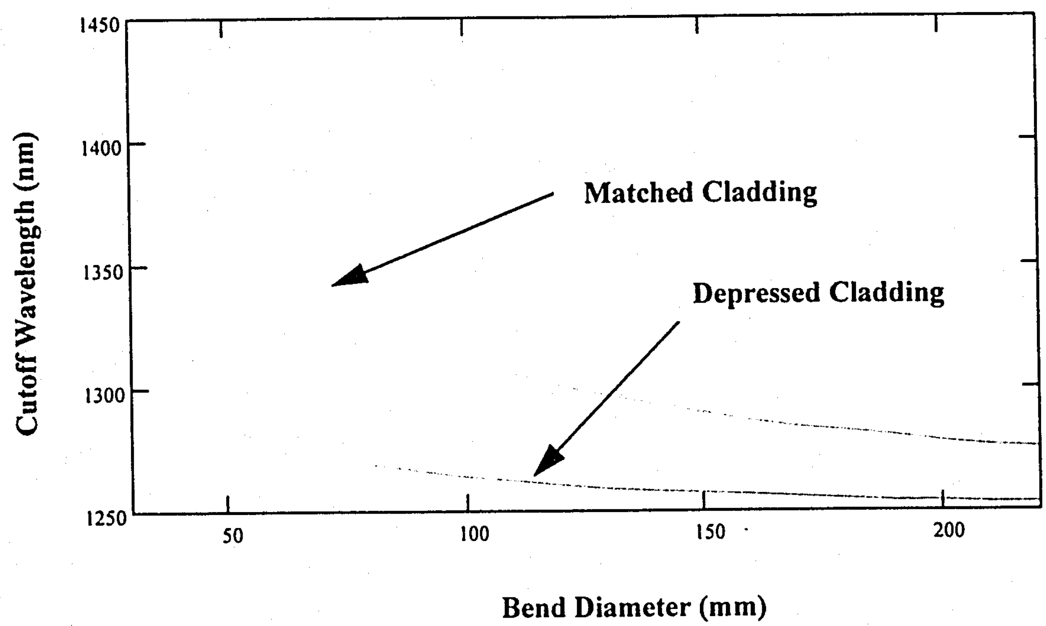

Figure 7.40: Maximum allowable cutoff wavelength as a function of the bend diameter of optical fiber. The fiber length for this fiber is 0.5 meters.

In Figure 7.40, the maximum allowable cutoff wavelength increases significantly as the bend diameter decreases. As expected, the matched-cladding fiber shows a stronger dependence on the imposed bend to the depressed-cladding fiber. This curve was generated by evaluating the change in cutoff wavelength due to the imposed length and bend without considering the effect of modal noise.

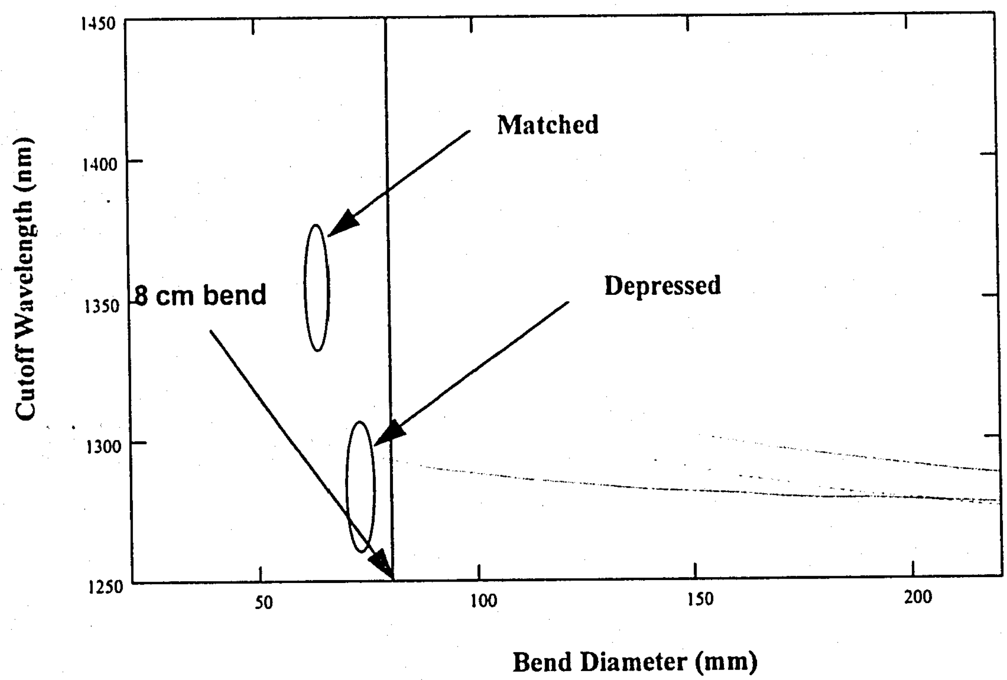

Figure 7.41: Maximum allowable cutoff wavelength as a function of the bend diameter for 0.5, 1 and 2 meters fiber lengths. The modal noise penalty is 0.5 dB and the loss at each splice point is 2 dB.

The higher attenuation of the LP_{11} mode in the matched-cladding fiber, is caused by the larger mode field diameter and the lower difference between theoretical and effective cutoff wavelength, as compared to the depressed-cladding fiber. Matched cladding fibers with lower mode field diameters have lower bend dependence of cutoff wavelength.

Figure 7.41 is a plot of the maximum allowable cutoff wavelength as a function of the bend diameter for fiber lengths of 0.5, 1 and 2 meters. In that case, the modal noise penalty is 0.5 dB and the system operating wavelength is 1285 nm. We observe once again that as the bend diameter decreases the maximum cutoff wavelength increases more rapidly for matched-cladding fiber compared to depressed-cladding fiber. From the cutoff wavelength changes for the three fiber lengths, the depressed-cladding fiber design shows a greater dependence compared to the matched-cladding. Once again this is due to the leakage loss of the LP_{11} mode, as described in the previous chapter.

For a bend diameter of 8 cm, the maximum allowable cutoff wavelength of the depressed-cladding fiber is 1270 nm, while that of the matched is 1330 nm. Since current commercial fibers have a specified maximum cutoff wavelength 1330 nm, any commercially available matched-cladding fiber can be used to lengths of 0.5 meters, if an imposed bend of 8 cm is introduced. The cutoff wavelength of commercially available depressed-cladding fibers should be selected to be below 1270 nm in order to eliminate any concerns of modal noise.

In Figure 7.42, the cutoff wavelength is plotted as a function of splice loss for matched and depressed-cladding fibers. In these plots we observe that the cutoff wavelength limit has a small dependence on the splice loss as compared to other parameters such as the imposed bend or modal noise penalty. We also observe that the fiber length increases the upper cutoff wavelength limit only slightly in matched-cladding fibers but more drastically in depressed-cladding fibers. As an example, in the case of matched-cladding fibers with 2 dB splice loss, the upper limit of cutoff wavelength changes from 1330 nm to 1335 nm and 1355 nm for fiber for fiber lengths of 0.5, 1 and 10 meters. In the case of depressed-cladding fibers, however, the upper cutoff wavelength limit changes from 1270 nm to 1290 nm and 1330 nm for the same fiber lengths

A summary of the results is shown in Figures 7.43 and 7.44. These graphs compare the cutoff wavelength of matched and depressed-cladding fibers for fiber lengths of 0.5, 1 and 10 meters. Figure 7.43 is a plot of the maximum cutoff wavelength as a function of splice loss for fibers in the unbent configuration, while the one in Figure 7.44 is for the bent configuration. We observe that the maximum cutoff wavelength for a 10 meter fiber length, that corresponds to the minimum length used in fiber optics cable repairs, is greater than 1330 nm for the bent configuration of matched and depressed-cladding fibers. However, if the fiber length reduces to 0.5 meters, as is the case of connectorized patchcords, the maximum cutoff wavelength reduces to 1330 nm and 1270 nm for matched and depressed-cladding fibers respectively.

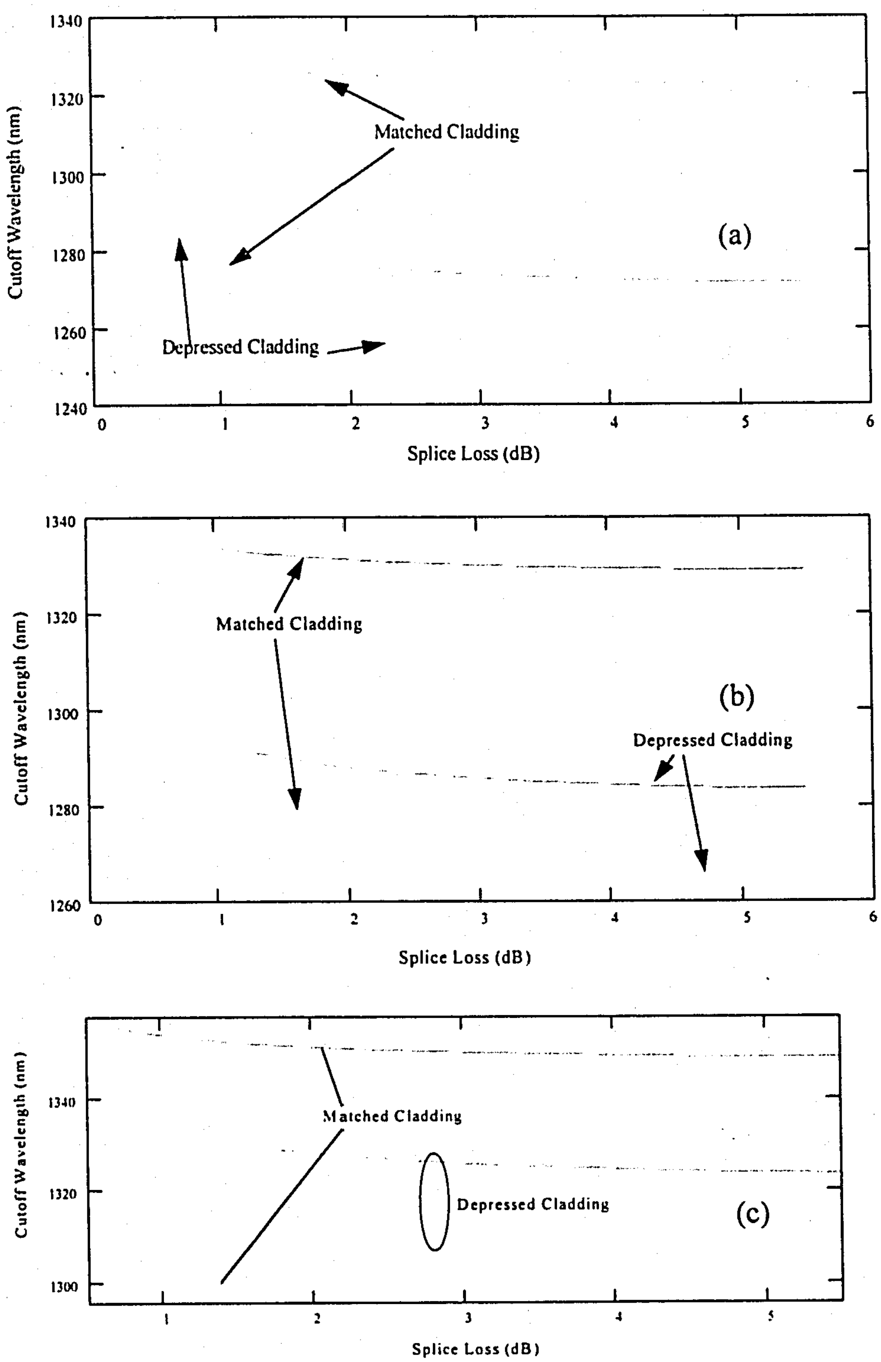

Figure 7.42: Maximum cutoff wavelength as a function of splice loss for bent (solid) and unbent (dashed) matched- and depressed-cladding fibers. The three different plots correspond to lengths of 0.5 meters (a), 1 meter (b), and 10 meters (c).

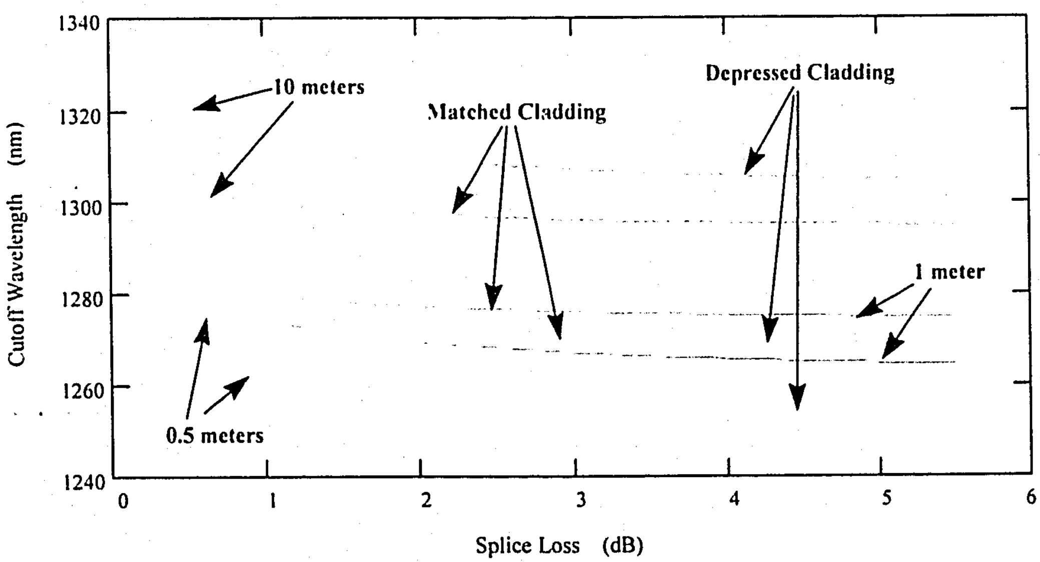

Figure 7.43: Maximum cutoff wavelength as a function of splice loss for 0.5, 1 and 10 meters of fiber length and no applied bend.

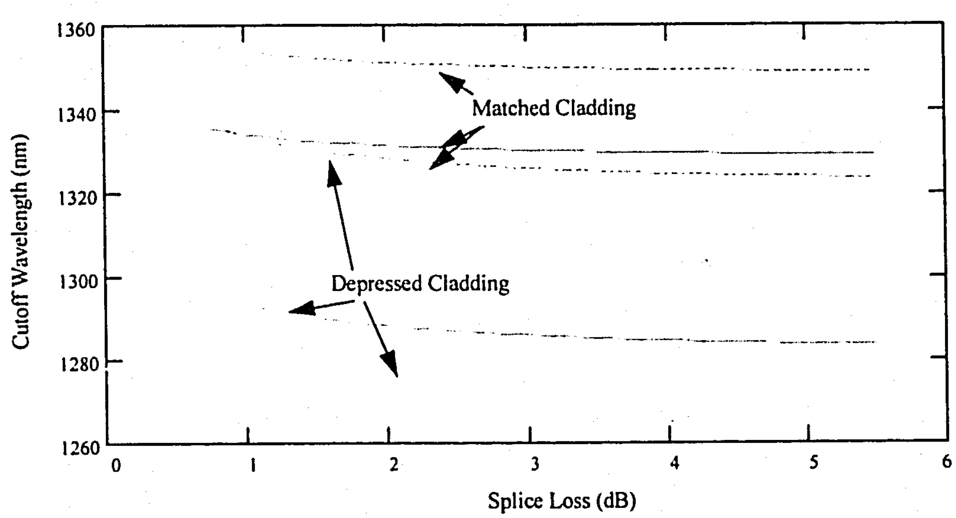

Figure 7.44: Upper limit of cutoff wavelength for minimum fiber length of 0.5, 1 and 10 meters. An 8 cm bend is applied in all configurations.

7.10 Design window completion

There is a great desire within the fiber optics industry to minimize the types of optical fibers used for telecommunications. Currently the two most widely used fiber types are the dispersion-shifted and dispersion-unshifted fibers. Even though there are differences between the designs of different manufacturers, every effort has been made to guarantee their compatibility. It is preferable to use the same fiber design in different applications by modifying the layout configuration of the optical fibers.

The work in this chapter was performed to calculate and establish the cutoff wavelength and the physical layout limits needed for the configuration of short fiber lengths in fiber management frames. The purpose of this work is to reduce the fiber length and the bend diameter requirements and therefore to increase the allowable density of the fiber connections in frames without penalizing the system with another performance degradation. This worked established the upper cutoff wavelength limits of both matched and depressed-cladding fibers. These limits will be used to enclose the design window of these fiber types.

The complete design diagram for matched-cladding fiber is shown in Figure 7.45. The shaded areas are the windows within which the fiber is allowed to operate. Fibers designed within the light colored area can operate at any length limit if they are bent to a diameter of 8 cm. Fibers within the light and dark area can be used in cases where the fiber length is greater than 10 meters. From this figure we can observe that there is very little increase in the design window if the fiber length is raised to 10 meters.

Figure 7.46 shows the design diagram of a depressed-cladding fiber. As described above, fibers with no length limitation are allowed to operate in the light shaded area, while fibers with a 10 meter length limitation can be operated into the dark area.

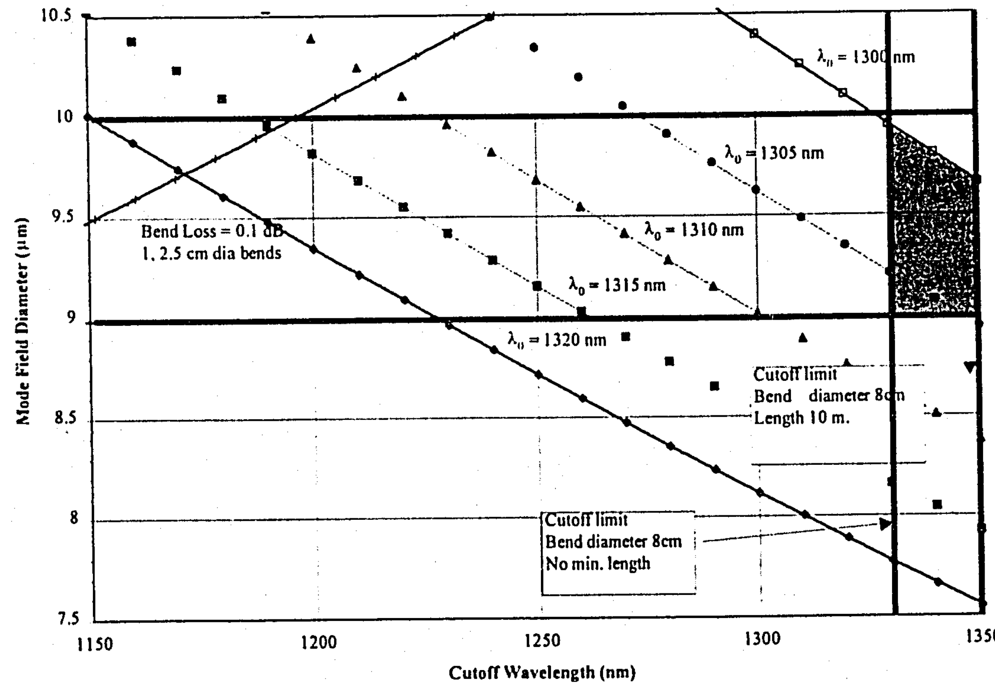

Figure 7.45: Design diagram of matched-cladding fiber

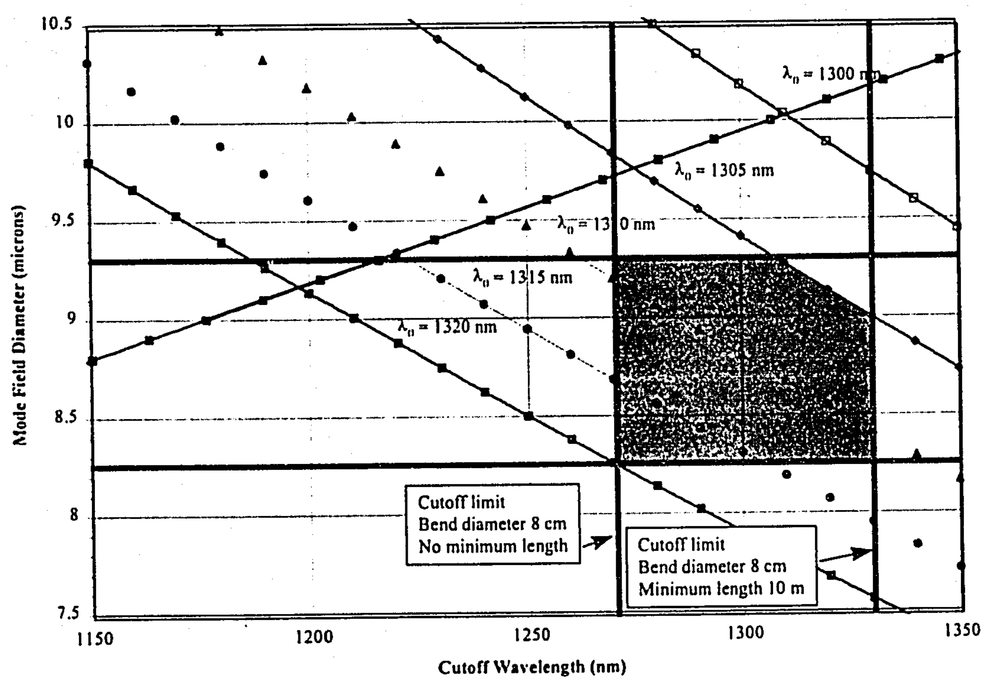

Figure 7.46: Design diagram of a depressed-cladding fiber

From this diagram we can conclude that depressed-cladding fiber should be selected with low cutoff wavelengths in order to be used at any length. Manufacturers are forced to fabricate special fibers with low cutoff wavelength in order to meet the short length needs. The design window of the depressed-cladding fiber increases significantly if the minimum fiber length is raised to 10 meters. Even in that case, the design window remains smaller than the matched-cladding fiber.

The modal noise model developed in this section can increase the system flexibility significantly. Even though it is still conservative, it allows for variations in the operating parameters and in the fiber type being used. The conservative nature of this model was proven experimentally in this section. Even under this conservative scenario, the maximum cutoff wavelength is significantly higher to the one used by the internationally established standards.

The test is performed by measuring the time delay of each pulse at discrete wavelengths. The time delay data are plotted as a function of wavelength, and for dispersion-unshifted fibers they follow a Sellmeier type of equation. These data are differentiated, and the point where the resulting curve crosses the zero axis defines the zero dispersion wavelength. The slope at this point, calculated from the measured data, gives the slope at the zero dispersion wavelength. The dispersion at any other wavelength is found from these two values. The time delay equation between 1200 and 1600 nm is given as:

$$\tau(\lambda) = \tau_0 + S_0 \frac{\lambda^2 - \lambda_0^2}{\lambda^2} \tag{8.1}$$

where λ_O is the zero dispersion wavelength and S_O the slope at this wavelength. The above equation can be differentiated, yielding the chromatic dispersion D as a function of wavelength:

$$D(\lambda) = \frac{S_0}{4}\left[\lambda - \frac{\lambda_0^4}{\lambda^3}\right] \tag{8.2}$$

(b) Fiber spectral attenuation (used to measure the bend loss and cutoff wavelength)

The spectral attenuation test station was used to measure the bend loss and the cutoff wavelength of the fiber. The station is described in detail in Section 5.5.1. A brief description is found in reference [84].

The test station used in this study was capable of achieving an accuracy of 0.01 dB, and dynamic rage of approximately 40 dB over a wide wavelength range. Precise equipment was necessary in order to measure bend losses of the order of 0.01 dB.

(c) Fiber Mode Field Diameter (MFD)

The mode field diameter of the fiber defines the distribution of the field amplitude across the fiber end face, and can provide the user with a means of specifying interfiber compatibility since mode field diameter mismatch can result to high splice and connectorization loss.

The value of the MFD depends on its definition. The industry has established a standard definition in order to achieve compatibility between manufacturers and the users. These are called the "Petermann I" and "Petermann II" definitions, and are given by the expressions[85]:

Petermann I definition (rms width in the near field)

$$w_1^2 = \frac{\int_{-\infty}^{\infty} \psi^2 r^3 dr}{\int_{-\infty}^{\infty} \psi^2 r dr} = \frac{1}{k^2} \frac{\int_{-\infty}^{\infty} \left[\frac{d\Psi}{d\theta}\right]^2 \theta d\theta}{\int_{-\infty}^{\infty} \Psi^2 \theta d\theta} \tag{8.3}$$

Petermann II definition (rms width in the far field)

$$w_1^2 = \frac{\int_{-\infty}^{\infty} \psi^2 r^3 dr}{\int_{-\infty}^{\infty} \left[\frac{d\psi}{dr}\right]^2 r dr} = \frac{1}{k^2} \frac{\int_{-\infty}^{\infty} \Psi^2 \theta d\theta}{\int_{-\infty}^{\infty} \Psi^2 \theta^3 d\theta} \tag{8.4}$$

In the above expressions $\psi^2(r)$ is the near field intensity distribution of the fiber, $\Psi^2(r)$ is the far field intensity distribution, r and θ are the radial and angular coordinates and λ is the vacuum wavenumber. From these relationships it is possible to measure the fiber's mode field diameters from the near or far field intensity pattern.

The methods that are currently in use are divided into two major categories:

- The near-field techniques, where the MFD is calculated from the near-field intensity distribution and where the "Petermann I" definition is mainly used[86].

- The far-field techniques, where the fiber field distribution is measured as a function of angle in the far-field. In these cases, the "Petermann II" definition is used[87].

Even though the two definitions are different from each other, they usually give similar results for fibers with a refractive index approximated by a step-index profile, and at wavelengths of operation close to the cutoff wavelength of the second-order (LP_{11}) mode. In that case the mode-field-diameter of the fiber can be approximated by a Gaussian function, simplifying greatly its definition. For fibers where the mode field diameter is represented exactly by a Gaussian curve, the "Petermann I" and the "Petermann II" definitions are identical[88].

In order to define precisely the design diagram, an accurate measurement of the fiber MFD is essential. In this work, the fiber MFD is measured from data extracted from the far-field intensity distribution of the fiber. The two techniques used were:

- The variable-aperture method
- The far-field-scanning Method

The variable-aperture[89, 90] method is based on a measurement of the optical power as transmitted through a set of circular apertures that are located in the far field. The optical power through the apertures is focused onto a 300-μm diameter InGaAs PIN photodiode with a set of two collimating lenses.

The far-field scanning method[91] measures the far-field power that is emitted from the fiber as a function of angle. For that purpose, a small-area detector is placed on a rotary stage and scans angularly the optical power of the fiber in the far-field. With this method, the power distribution in the far field is obtained directly.

With the above methods the MFD given by the "Petermann II" definition can be evaluated with good accuracy, if conventional fiber is used. For unconventional fiber, such as dispersion-shifted or dispersion-flattened fibers, the variable-aperture technique may be limited due to the maximum angle that it can accept in the far field, which depends on the maximum aperture size and the collection optics used. For these measurements, the far-field scanning technique should be used.

9. CONCLUSIONS

The purpose of this work was to determine of the design diagrams of the two most widely used dispersion unshifted fiber types: the matched and the depressed-cladding fibers. The parameters that determine the design diagram, the chromatic dispersion, the bend loss and the modal noise of the fibers, were analyzed completely.

The first parameters analyzed were the propagation properties of the fiber. For that reason, two models based on finite differences and finite elements were compared. The finite-difference model that was proven to have the greater accuracy of the two was used to calculate numerically the propagation characteristics of the fiber. From the fiber's propagation properties the chromatic dispersion characteristics for both dispersion-unshifted fiber types were determined. The zero dispersion wavelength limits were defined in the design diagram in terms of the MFD and cutoff wavelength of the fiber. The models were used to determine the dependence of the dispersion slope on the zero dispersion wavelength of the fiber. Since the chromatic dispersion depends on both of these parameters, the dispersion slope value can influence the design parameters significantly, especially at high zero dispersion wavelengths where the dispersion slope is smaller.

The same models were utilized to determine the propagation characteristics of a unique dispersion-shifted fiber with low scattering coefficient and low dispersion slope. This model can be used to determine the dispersion properties of dispersion-shifted or even dispersion-compensated fibers. Since this is outside the scope of this work, these fiber types were not studied in depth.

The bend and modal noise properties of the matched and depressed-cladding fibers were also studied in detail. These two parameters, together with the chromatic dispersion, complete the design diagram of dispersion-unshifted single-mode fibers for all standard applications. Even though the applications of these fiber types are exactly the same, completely different mechanisms influence the bend loss and modal noise properties. Therefore, the limits dictated on the design diagram by these two parameters are different.

By using numerical and experimental results, it was found that the fundamental mode of matched-cladding fibers has lower bend sensitivity than depressed-cladding fibers when bends greater than 4 cm diameter are applied. This property makes the matched-cladding fiber less sensitive to losses caused in splice organizers. This fiber type gives greater flexibility to the cable designer, since he can use tighter helixes in the fiber tubes for a loose tube cable design. On the contrary, depressed-cladding fibers perform better when the cable is exposed to microbending caused by low temperatures or low-cost cables.

In this work a lot of effort was placed on studying the effect of modal noise on the system parameters. The modal noise effect is of great importance in the field deployment of fiber. Scientists have studied this phenomenon very little, and standards organizations have dictated limits based on perceptions rather than technical knowledge. These conditions have placed severe limitations on the deployment of fiber optics systems and on their proper management in central or remote offices. In this work we have seen that the fiber length has a small impact on the modal noise penalty, even for depressed-cladding fibers. On the contrary, bends strip the LP_{11} mode quickly and reduce the modal noise penalty significantly. If an 8-cm bend diameter is used in every fiber, the upper limit of cutoff wavelength will increase to 1330 nm for matched-cladding and 1310 nm for depressed-cladding fibers. The fiber length will be reduced to 0.5 meters. This parameter completes the design diagram and defines the window within which the fiber is allowed to operate.

In addition to the above, the minimum bend diameter was set. A reduction of this bend diameter improves the fiber density, design flexibility and user friendliness in the distribution frames and splice organizers. By careful evaluation of the long-term strength reliability and the bend loss of the fundamental mode, this bend diameter limit was reduced from 8 to 5 cm. This limit, together with the design window, completes the deployment operation of dispersion unshifted single-mode fibers and their parameter limitations.

There is always a tendency to compare the two fiber designs. Inevitably, each fiber design has advantages and disadvantages. We can summarize by saying that the matched-cladding fiber is a simpler design and potentially of lower cost. Its simplicity gives it the potential to be a robust design if it is properly fabricated. For that reason all major fiber manufacturers, including AT&T, are switching to this fiber type. In the near future the fiber design will improve further by reducing the mode field diameter of the matched-cladding fiber closer to that of the depressed-cladding type. In that case, the matched-cladding fiber will outperform the depressed-cladding type in all the areas described above. In order to accomplish this, the scattering loss contribution due to the GeO_2 doping should be improved. Simultaneously, the refractive index profile should be closer to a step index in order to improve the chromatic dispersion properties of the fiber. An in-depth study of this topic is necessary in order to improve the properties of the commercially available single-mode fiber.

10. SUGGESTIONS FOR FURTHER STUDY

Several workers believe that the propagation properties of optical fibers have been studied completely. This work demonstrates that deeper understanding of several areas in fiber propagation properties is necessary. Some suggestions for further work are proposed below:

- Theoretical and experimental work is necessary to optimize the design parameters of matched-cladding single-mode fiber. As mentioned above, fibers with MFDs between 8.5 to 9.5 μm will have superior bend and microbend performance. This will be achieved by an in-depth theoretical and experimental study of the Rayleigh scattering and dispersion properties of the fiber.

- The finite-difference model can be used to determine the design limitations of dispersion-shifted fibers. These fiber types have complicated profiles and this model, together with the bend sensitivity evaluation, can define the operating parameters in terms of the mode field diameter and cutoff wavelength.

- The same model can be used to design dispersion-compensated fibers.

- A subject of great interest is the nonlinear properties of optical fibers. Nonlinear characteristics, such as the Kerr effect, etc., the nonlinear properties of dispersion-shifted and dispersion-unshifted fibers can be evaluated.

- A finite-element or finite-difference model can be developed to evaluate the bend sensitivity of the optical fibers. A comparison between this model and the one used in this work may be able to reduce the differences between theory and experiment. This model should include the refractive index properties of the coating material and the reflections that occur in the coating/cladding interface.

This list can be increased even further. The author believes that more work on this subject will improve the properties of optical fibers, their deployment conditions and their user friendliness. A complete understanding of the propagation properties of optical fibers will reduce their manufacturing and deployment costs and will secure their future as the desired telecommunications media of choice for the present and the future. This work will contribute to increase and spread the bandwidth of knowledge of the human race.

REFERENCES

(1) F.D. Kapron, D.B. Keck, and R.D. Maurer, "Radiation losses in glass optical waveguides", Appl. Phys. Lett., 17, pp. 423-425, 1970.

(2) J.E. Midwinter, Optical Fibers for Transmission, Wiley, N.Y., 1979.

(3) D. Gloge and E.A.J. Marcatili, " Multimode theory of graded-core fibers", B.S.T.J., 52, pp. 1563-1578, 1973.

(4) D. Gloge, "Weakly guiding fibers", Appl. Optics, 10, pp. 2252-2288, 1971.

(5) D.N. Payne and W.A. Gambling, "Zero material dispersion in optical fibers", Electr. Lett., 12, pp. 549-550, 1976.

(6) W.A. Gambling, H. Matsumura, and C.M. Ragdale, "Curvature and microbending losses in single mode optocal fibers", Opt. and Quantum Electr., 11, pp. 43-59, 1979.

(7) H. Kanamori, H Yokota, G. Tanaka, M. Watanabi, Y. Ishiburo, I. Yoshida, T. Kakii, S. Itoh, Y Asano, and S Tanaka, "Transmission characteristics and reliability of pure-silica-core single mode fibers", IEEE J. Lightwave Tech., 4, 1144, 1986.

(8) Y. Kobayashi, Y. Hayashi, G. Motosugi, and J. Yoshida, "Optimal design for 1.55 lm 450 Mbit/s high-sensitivity detector", Technical Digest, Optical Fiber Communications, paper WH3, 1986.

(9) L. J. Cimini, L.J. Greenstein, Adel. A.M. Saleh, " Optical equilization to combat the effect of laser chirp and fiber dispersion", Technical Digest, Optical Fiber Communications, paper WC4, 1990.

(10) T.A Lenahan, "Calculation of modes in an optical fiber using the finite element method and EISPACK", B.S.T.J., 62, pp. 2663-2694, 1983.

(11) K. Ikamato and T. Okoshi, "Vectorial wave analysis of inhomogenous optical fibers using FEM", IEEE Trans. MTT, 26, pp. 109-114, 1978.

(12) C. Yeh, K. Ha, S.B. Dong, and W. P. Brown, "Single mode optical waveguides", Appl. Optics, 18, pp. 1490-1504, 1979.

(13) F.D. Kapron, "Chromatic dispersion format for single mode and multimode fibers", Technical Digest, Optical Fiber Communications, paper TU92, 1987.

(14) D. Marcuse, "Influence of curvature on the losses of doubly clad fibers", Appl. Optics, 27, pp. 4208-4213, 1982.

(15) W.A. Reed and D.L. Philen, "Study of algorithms used to fit group delay data for single mode optical fibers", Techical Digest, Symposium on Optical Fiber Measurements, pp. 7-10, 1986.

(16) M.A. Saifi, S.J. Jang, L.G. Cohen, and J. Stone, "Trianguler profile single mode fibers", Opt. Letters, 7, pp.43-45, 1982.

(17) B.J. Ainslie, K.J. Beales, C.L. Day and J.D. Rush, "The design and fabrication of monomode optical fibers", IEEE Trans. MTT, 30,1360-1370, 1982.

(18) B.J. Ainslie and K.R. Day, "A review of single mode fibers with modified dispersion characteristics", IEEE J. Lightwave Tech., 4, 167-176, 1986.

(19) M.A. Saifi, S.J. Jang, L.G. Cohen, and J. Stone, "Triangular-profile single mode fibers", Optics Letters, 7, pp.43-45, 1982.

(20) D.M. Cooper, S.P. Craft, C.R. Day, and B.J. Ainslie, "Multiple-index structure for dispersion shifted single-mode fibers", Technical Digest, Optical fiber communications, paper MF5, 1985.

(21) T.D. Craft and J.E. Ritter, "Low loss dispersion shifted single-mode fiber manufactured by the OVD process", Technical Digest, Optical Fiber Communications, paper WD2, 1985.

(22) L.G. Cohen, W.L. Mammel and S.J. Jang, "Low-loss quadruple-clad single-mode lightguides with dispersion below 2ps/km-nm over 1.28 μm to 1.65 μm wavelength range", Electronics letters, 18, pp. 1023-1024, 1982.

(23) P. Geittner and H. Lydtin, "Dispersion-modified single-mode fibers", Technical Digest, Optical Fiber Communications, paper WI1, 1988.

(24) J.A. Dixon, M.S. Giroux, A.R. Isser and R.V. Vandewoestine, "Bending and microbending performance of single-mode optical fibers", Technical Digest, Optical Fiber Communications, paper TUA2, 1987.

(25) H. Murata, "Recent developments in vapour phase axial deposition", IEEE J. Lightwave Tech., 4, 1026, 1986

(26) S. Kawakami and S. Nishida,"Characteristics of a doubly clad optical fiber with a low-index inner cladding", IEEE Trans. on Quantum Electronics, QE-11, pp. 879-887, 1974.

(27) S.J. Jang, L.G. Cohen, W.L. Mammel, and M.A Saifi, "Experimental verification of ultra-wide bandwidth spectra in doubly-clad single mode fibers", B.S.T.J., 61, pp. 385-390, 1982.

(28) M.J. Adams, An introduction to optical waveguides. New York: Wiley, 1981.

(29) D. Gloge, "Optical waveguide transmission", Proc. IEEE, 58, pp. 1513-1522, 1970.

(30) D.N. Payne, A.J. Barlow, J.T. Ramskov Hansen, “Development of low- and high-birefringences of optical fibers”, IEEE J. Quantum Elec., 18, pp. 477-488, 1982.

(31) Y. Sasaki, K. Okamoto, T. Hosake, and N Shibata, "Polarization maintaining and absorption-reducing fibers"; Technical Digest, Optical Fiber Communications, paper THCC6, 1982.

(32) T. Okoshi, “Single -polarization single-mode optical fibers”, IEEE J. Quantum Electronics, 17, pp. 879-884, 1981.

(33) D. Marcuse, "Loss analysis of single-mode optical fibers", Bell Syst. Tech. J., 56, pp., 703-718, 1977.

(34) K. Petermann and R. Kuhne, "Upper and lower limits for the microbending loss in arbitrary single mode fibers", IEEE J. Lightwave Tech., 4, pp. 2-7, 1986.

(35) K. Petermann, "Theory of microbending loss in monomode fibers with arbitrary refractive index profile", Arch. Elektron. Ubertr., 30, 337-342, 1976.

(36) K. Petermann, "Fundamental mode microbending loss in graded index and W-fibers", Opt. and Quant. Electron., 9, pp. 167-175, 1977.

(37) K. Ikamoto and T. Okoshi, "Vectorial wave analysis of inhomogenous optical fibers using finite element method", IEEE Trans. MTT, 26, pp. 109-114, 1978.

(38) C. Yeh, K. Ha, S.B. Dong, and W.P. Brown, " Single mode optical waveguides", Appl. Opt., 18, pp. 1490-1504, 1979.

(39) M. Abramowitz and I.A. Stegun, "Handbook of mathematical functions", Dover, New York, 1972.

(40) W.L. Mammel and L.G. Cohen, "Numerical prediction of fiber transmission characteristics for arbitrary refractive index profiles", Appl. Optics, 21, 699, 1982.

(41) P.C. Schultz, "Ultraviolet absorption of titanium and germanium in fused silica", Proc. Int. Congr. Glass, 3, p. 155, 1977.

(42) K. Rau, A. Muhlich, N. Treber, "Progress in silica fibers with fluorine dopant", Top. Meet. Opt. Trans., TUC4, 1977.

(43) I.H. Malitson, "Interspecimen comparison of refractive index of pure silica", J. Opt. Soc. Amer., 55, pp. 1205-1209, 1965.

(44) J.W. Fleming, "Material dispersion in lightguide glasses", Electr. Lett., 14, 326-328, 1978.

(45) J.W. Fleming, "Dispersion in GeO_2-SiO_2 glasses", Appl. Opt., 23, pp. 4486-4493, 1984.

(46) Telecommunication industry association (TIA) fiber optics test procedures (FOTP) 168 and 169,.Measurement of chromatic dispersion of single mode fiber.

(47) L.E. Sutton and O.N. Stavroudis, "Fitting refractive index data by least squares", J. Opt. Soc. Am., 51, pp. 901-905, 1961.

(48) L.G. Cohen, D. Marcuse, and W.L. Mammel, "Radiating leaky-mode losses in single-mode lightguides with depressed-index claddings" Technical Digest, Optical Fiber Communications, THCC1, 1982.

(49) A. Tomita and L.G. Cohen, "Leaky-mode loss of the second propagaing mode in single-mode fibers with index well profiles", Appl. Optics, 24, pp. 1704-1707, 1985.

(50) S. Kawakami and S. Nishida, "Perturbation theory of a doubly clad optical fiber with a low-index inner cladding", IEEE J. Quant. Electr., 11, pp. 130-135, 1975.

(51) M. Monerie, "Propagation in doubly-clad single-mode fibers", IEEE Trans. Quant. Electr., pp. 535-542, 1982.

(52) P.R. Bark and N. Oestreich, "Stress-strain behavior of optical fiber cables", 27 Proc. Int. Wire & Cable Symb., 1978.

(53) D. Marcuse, "Curvature loss formula for optical fibers", J. Opt. Soc. Am., 66, 216-224, 1976.

(54) D. Marcuse, "Field deformation and loss caused by curvature of optical fibers", J. Opt. Soc. Amer., 66, 311-320, 1976.

(55) A.W. Snyder, I.A. White and D.J. Mitchell, "Radiation from bend optical waveguides", Electr. Lett., 11, pp. 332-333, 1975.

(56) W.A. Gambling, H. Matsumura and C.M. Ragdale, "Curvature and microbending losses in single-mode optical fibers", Opt. Quant. Electr., 11, 43-59, 1979.

(57) D. Marcuse, "Influence of curvature on the losses of doubly-clad single mode fibers", Appl. Opt., 21, pp. 4208-4216, 1982.

(58) W.A Gambling and H. Matsumura, "Propagation characteristics of curved fibers", Trans. IECE Japan, E61, 196, 1978.

(59) K. Nagano, "Change of the refractive index in an optical fiber due to external forces", Appl. Opt., 17, pp. 2080-2087, 1978.

(60) Telecommunication industry association (TIA) fiber optics test procedures (FOTP) 80 "Cutoff wavelength of uncabled single mode fiber by the transmission method"

(61) G. A. Heckmann, "Modal noise in single-mode fibers operated slightly above cutoff", Electronics Letters, 17, 499, 1981

(62) L. Wei, C. Saravanos and R.S. Lowe, "Practical upper limits to cutoff wavelength for different single-mode fiber designs", IEEE Journal of Lightwave Technology, 5, 1147-1151, 1987

(63) K. Abe, Y. Lacroix, L. Bonnell, Z. Jakubczyk, "Modal interference in a short fiber section: Fiber length, splice loss, cutoff, and wavelength dependencies", IEEE Journal of Lightwave Technology, 10, 401-406, 1992

(64) K. Ogawa, "Analysis of moda partition noise in laser transmission systems", IEEE Journal of Quantum Electronics, 18, 849-855, 1981

(65) Y. Okano, K. Nakagawa, T. Ito, "Laser mode partition noise evaluation for optical fiber transmission", IEEE Trans. Commun., 28, 238-243, 1980

(66) K. Ogawa and R. S. Vodhanel, "Measurement of mode partition noise of laser diodes", IEEE Journal of Quantum Electronics, 18, 1090-1093, 1981

(67) P. Liu and K. Ogawa, "Statistical measurements as a way to study mode partition in injection lasers", Journal of Lightwave Technology, 2, 22-28, 1984

(68) K. Petermann and G. Arnold, "Noise and distortion characteristics of semiconductor lasers in optical fibers communications systems", IEEE Transactions on Microwave Theory and Techniques, 30, 389-401, 1982

(69) N. Shinoni, K. Aiki, I Ito, Applied Physics Letters, 33, 990-993, 1978

(70) W. Steifer, R. D. Burnham, D. R. Scifres, "Effects of external reflectors on longitudinal modes of distributed feedback lasers", IEEE Journal of Quantum Electronics, 11, 144, 1975

(71) M. Yamada and Y. Suematsu, "A condition of signle logitudiadal operation in injection lasers with index-guiding structure", IEEE Journal of Quantum Electronics, 15, 743-749, 1979

(72) I. Garrett and C. J. Todd, "Review: Components and systems for long-wavelength monomode fiber transmission", Journal of Lightwave Technology, 1, 131-138, 1983

(73) J. C. Goodwin and P. J. Vella, "Modal noise in short fiber sections", IEEE Journal of Lightwave Theory, 8, 151-160, 1990

(74) A. W. Snyder and J. D. Love, "Optical waveguide theory", Chapman and Hall, 1983

(75) D. Marcuse, "Influence of curvature on the losses of doubly clad fibers", Applied Optics, 21, 4208, 1982

(76) W. Anderson and T. Lenahan, "Length dependence of the effective cutoff wavelength in single-mode fibers", IEEE Journal of Lightwave Technology, 2, 238-242, 1984

(77) F. M. Sears, I.A. White, S.P. Gentry, "Cable cutoff wavelength and attenuation of the LP_{11} mode", Technical Digest, Optical Fiber Communications, paper TUL19, 1986

(78) M.J. Matthewson, C.R. Kurrkjian, S. Gulati, "Strength measurement of optical glass fibers by bending", Journal of American Ceramic Society, 69, 815-821, 1986

(79) Telecommunication industry association (TIA) fiber optics test procedures (FOTP) 97, Procedure for measuring the static fatigue of optical fiber in two-point bending, 1992

(80) S. Nagel, "Reliability issues in optical fibers", AT&T Bell Laboratories Technical Journal, 1986

(81) D. G. Duff and F.T. Stone, "Measurements of modal noise in single mode lightwave systems", Technical Digest, Optical Fiber Communications, paper WC4, 1985.

(82) R.A. Linke, "Modulation induced transient chirping in single-frequency lasers", IEEE J. Quant. Electr., 21, pp.593-597, 1985.

(83) L.G. Cohen and C. Lin, "A universal fiber-optic (UFO) measuring system based on a near-IR fiber Raman laser", IEEE J. Quant. Electr., 14, pp. 855-862, 1978.

(84) Telecommunication industry association (TIA) fiber optics test procedures (FOTP) 78, "Spectral attenuation cutback measurement of single-mode optical fibers", 1994

(85) K. Petermann, "Microbending loss in monomode fibers", Electr. Lett., 20, pp. 107-109, 1976.

(86) S.C. Fleming, "Preferred appproaches to the determination of optical fibre mode field diameter", Electr. Lett., 23, pp. 338-339, 1987.

(87) C. Saravanos and R.S. Lowe, "New approach for determining the non-Gaussian mode field of single-mode fiber from measurement in the far-field", Electr. Lett., 21, pp. 898-899, 1985.

(88) G. Coppa, P. Di Vitta and U. Rossi, "Parametri dimensionali nella caratterizazione delle fibre ottiche monomode", Atti della conf., pp. 323-326, 1984.

(89) E. Nicolaisen and P. Danielsen, "Calculated and measured spot size of equivalent gaussian field in single-mode optical fibers", Electr. Lett., 19, pp. 27-28, 1983.

(90) C. Saravanos and R.S. Lowe, “The measurement of non-Gaussian mode fields by the far-field axial scanning technique”, IEEE Journal of Lightwave Technology, 5, 1563-1566, 1985.

(91) K. Hotate and T. Okoshi, "Measurement of refractive index profile and transmission characteristics of single-mode optical fiber from its exit rradiation pattern", Appl. Opt., 18, pp. 3265-3271, 1979.

(92) D. Marcuse, “Loss analysis of single-mode fiber splices”, Bell Sust. Tech. J., 56, 703-718, 1977.

(93) W. L. Mammel and L.G. Cohen, “Numerical prediction of fiber transmission characteristics for arbitrary refractive index profiles”,Appllied Optics, 21, pp 699-703, 1982.

APPENDIX 1

A Finite Element Method Program to calculate the Propagation Properties of Optical Fibers

```
      dimension a(27,27),t(27,27),eival(27),eivec(27,27),tl(27)
      dimension vn(27),nv1(27),nv2(27),iv(27,2),r(28)
      dimension aa(2,2),st(2,2)
c      data vn/.9954,.8117,.5293,.2595,.0583,.0099,.1029,
c     & .2724,.42,.5596,.7124,.8603/
      data vn/.9954,.940,.8117,.6778,.5293,.3759,.2594,.1476,
     & .0583,.0151,.0099,.0414,.1029,.1883,.2723,.3469,.42,
     & .4912,.5596,.6340,.7124,.7871,.8602,.9334,.9849/
c     nsco = 25 seg in core, nscl = 2 seg in cladding
c     vn contains n(r) info
      data r/12.5,0.,0.04,0.08,0.12,0.16,0.2,0.24,0.28,0.32,
     & 0.36,0.40,0.44,0.48,0.52,0.56,0.60,0.64,0.68,0.72,0.76,
     & 0.80,0.84,0.88,0.92,0.96,1.,2./
      data nv1/2,3,4,5,6,7,8,9,10,11,12,13,14,15,16,17,18,19,
     & 20,21,22,23,24,25,26,27,28/
      data nv2/3,4,5,6,7,8,9,10,11,12,13,14,15,16,17,18,19,20,
     & 21,22,23,24,25,26,27,28,1/
      open(6,file='costa.out',status='new')
      ndir=1
      nsco=25
      noptl=28
      nos=noptl-1
c      do 300 i=1,nsco
c300  vn(i)=0.
c     the above puts values for n(r) in the core
      nscl=nos-nsco
      do 301 i=1,nscl
      k=nsco+i
301   vn(k)=1.
c
      vval=1.5
      vvali=vval
      do 1000 ll=1,21
      vval=vvali+(ll-1.)*.1
c     vval = value of v from graph
      v2=vval**2
      write(6,fmt=201)noptl,nos,nsco,vval
201   format(' no of nodes',i3,' elements',i3,' nscore',i3,' v = '
```

```
     & ,e17.7/)
c     v2 is v**2 in the eqn
      nn=noptl-ndir
      nn3=nn-4
      do 602 i=1,nos
      iv(i,1)=nv1(i)
602   iv(i,2)=nv2(i)
      do 6 i=1,nn
      tl(i)=0.
      do 6 j=1,nn
      t(i,j)=0.
6     a(i,j)=0.
      do 16 is=1,nos
      i1=iv(is,1)
      i2=iv(is,2)
      r2=r(i2)
      r1=r(i1)
      vl=abs(r2-r1)
      vl2=vl*vl
      rpr=r1+r2
      rr2=(r2*r2-r1*r1)/(2.*vl2)
      rr3=(r2*r2*r2-r1*r1*r1)/(3.*vl2)
      rr4=(r2*r2*r2*r2-r1*r1*r1*r1)/(4.*vl2)
c     write(6,fmt=202)is,r1,r2,vl
202   format(' seg',i3,' start',e17.7,' end',e17.7,e17.7)
      do 23 i=1,2
      l=iv(is,i)-ndir
      if(iv(is,i).le.ndir) go to 23
      aa(1,1)=(r1+r2)/(2.*vl)
      aa(1,2)=-aa(1,1)
      aa(2,1)=aa(1,2)
      aa(2,2)=aa(1,1)
      st(1,1)=r2*r2*rr2+rr4-2.*r2*rr3
      st(2,2)=r1*r1*rr2+rr4-2.*r1*rr3
      st(1,2)=rpr*rr3-rr4-r1*r2*rr2
      st(2,1)=st(1,2)
      do 14 k=1,2
      if(iv(is,k).le.ndir) go to 15
      lc=iv(is,k)-ndir
      t(l,lc)=t(l,lc)+st(i,k)*v2
      a(l,lc)=a(l,lc)+aa(i,k)+vn(is)*st(i,k)*v2
      go to 14
15    tl(i)=tl(i)
14    continue
23    continue
```

```
16   continue
     mm=nn**2
     call nroot(nn,mm,a,t,eival,eivec)
     do 303 i=1,nn
303  eival(i)=sqrt(eival(i))
     print 2,(eival(i),i=nn3,nn)
     write(6,fmt=2)(eival(i),i=nn3,nn)
2    format(' eigen',e17.7/)
1000 continue
     stop
     end
     subroutine nroot(m,mm,a,b,xl,x)
     dimension a(mm),b(mm),xl(m),x(mm)
c     double precision a,b,xl,x,sumv,dabs,dsqrt
     k=1
     do 10 j=2,m
     l=m*(j-1)
     do 10 i=1,j
     l=l+1
     k=k+1
10   b(k)=b(l)
     mv=0
     call eigen(b,x,m,mm,mv)
     l=0
     do 20 j=1,m
     l=l+j
20   xl(j)=1./sqrt(abs(b(l)))
c20  xl(j)=1.0d0/dsqrt(dabs(b(l)))
     k=0
     do 30 j=1,m
     do 30 i=1,m
     k=k+1
30   b(k)=x(k)*xl(j)
     do 40 i=1,m
     n2=0
     do 40 j=1,m
     n1=m*(i-1)
     l=m*(j-1)+i
c     x(l)=0.0d0
     x(l)=0.0
     do 40 k=1,m
     n1=n1+1
     n2=n2+1
40   x(l)=x(l)+b(n1)*a(n2)
     l=0
```

```
      do 50 j=1,m
      do 50 i=1,j
      n1=i-m
      n2=m*(j-1)
      l=l+1
      a(l)=0.0
      do 50 k=1,m
      n1=n1+m
      n2=n2+1
50    a(l)=a(l)+x(n1)*b(n2)
      call eigen(a,x,m,mm,mv)
      l=0
      do 60 i=1,m
      l=l+i
60    xl(i)=a(l)
      do 70 i=1,m
      n2=0
      do 70 j=1,m
      n1=i-m
      l=m*(j-1)+i
c     a(l)=0.0d0
      a(l)=0.0
      do 70 k=1,m
      n1=n1+m
      n2=n2+1
70    a(l)=a(l)+b(n1)*x(n2)
      l=0
      k=0
      do 100 j=1,m
c     sumv=0.0d0
      sumv=0.0
      do 80 i=1,m
      l=l+1
80    sumv=sumv+a(l)*a(l)
c90   sumv=dsqrt(sumv)
90    sumv=sqrt(sumv)
      do 100 i=1,m
      k=k+1
100   x(k)=a(k)/sumv
      return
      end
      subroutine eigen(a,r,n,nn,mv)
      dimension a(nn),r(nn)
c     double precision a,r,anorm,anrmx,thr,x,y,sinx,sinx2,cosx,
c    &cosx2,sincs,range,dabs,dsqrt
```

```
c10   range=1.d-12
10   range=1.e-12
     if(mv-1) 20,50,20
20   iq=-n
     do 40 j=1,n
     iq=iq+n
     do 40 i=1,n
     ij=iq+i
c    r(ij)=0.0d0
     r(ij)=0.
     if(i-j) 40,30,40
c30  r(ij)=1.0d0
30   r(ij)=1.
40   continue
c50  anorm=0.0d0
50   anorm=0.
     do 70 i=1,n
     do 70 j=i,n
     if(i-j) 60,70,60
60   ia=i+(j*j-j)/2
     anorm=anorm+a(ia)*a(ia)
70   continue
     if(anorm) 360,360,80
c80  anorm=1.414d0*dsqrt(anorm)
80   anorm=1.414*sqrt(anorm)
     anrmx=anorm*range/float(n)
     ind=0
     thr=anorm
90   thr=thr/float(n)
100  l=1
110  m=l+1
120  mq=(m*m-m)/2
     lq=(l*l-l)/2
     lm=l+mq
c130 if(dabs(a(lm))-thr) 290,140,140
130  if(abs(a(lm))-thr) 290,140,140
140  ind=1
     ll=l+lq
     mm=m+mq
     x=0.5*(a(ll)-a(mm))
c    x=0.5d0*(a(ll)-a(mm))
150  y=-a(lm)/sqrt(a(lm)*a(lm)+x*x)
c150 y=-a(lm)/dsqrt(a(lm)*a(lm)+x*x)
     if(x) 160,170,170
160  y=-y
```

```
170   sinx=y/sqrt(2.*(1.+(sqrt(1.-y*y))))
c170   sinx=y/dsqrt(2.d0*(1.d0+(dsqrt(1.d0-y*y))))
      sinx2=sinx*sinx
c180   cosx=dsqrt(1.0d0-sinx2)
180   cosx=sqrt(1.0-sinx2)
      cosx2=cosx*cosx
      sincs=sinx*cosx
      ilq= n*(l-1)
      imq= n*(m-1)
      do 280 i=1,n
      iq=(i*i-i)/2
      if(i-l) 190,260,190
190   if(i-m) 200,260,210
200   im=i+mq
      go to 220
210   im=m+iq
220   if(i-l) 230,240,240
230   il=i+lq
      go to 250
240   il=l+iq
250   x=a(il)*cosx-a(im)*sinx
      a(im)=a(il)*sinx+a(im)*cosx
      a(il)=x
260   if(mv-1) 270,280,270
270   ilr=ilq+i
      imr=imq+i
      x=r(ilr)*cosx-r(imr)*sinx
      r(imr)=r(ilr)*sinx+r(imr)*cosx
      r(ilr)=x
280 continue
      do 400 j=i,n
      jq= jq+n
      mm=j+(j*j-j)/2
      if(a(ll)-a(mm)) 370,400,400
370   x=a(ll)
      a(ll)=a(mm)
      a(mm)=x
      if(mv-1) 380,400,380
380   do 390 k=1,n
      ilr=iq+k
      imr=jq+k
      x=r(ilr)
      r(ilr)=r(imr)
390   r(imr)=x
400   continue
```

```
return
end
```

APPENDIX 2

A Finite Difference Method Program to calculate the Propagation Properties and Chromatic Dispersion of Optical Fibers

```
/*

Notation:

V: normalized freauency.
B: normalized propagation constant.
S: number of the elements used.
h: length of each element.
E: scalar field.
K: Bessel function K.
wl: wavelength.
Ge: GeO2 concetration.
F: Florin concentration.
t: group delay.

*/



#include <stdio.h>
#include <conio.h>
#include <ctype.h>
#include <math.h>
#include <stdlib.h>



double U,Vc,E_core[800], N[800];
float  h,s,S;

void step_profile(void);
void power_profile(void);
void numerical_profile(void);

double eigen(double V);
double cutoff(double V);

double Core(int m, double V, double B);
double Clad(int m, double V, double B);

double BesselK(int n, double x);
long double factorial(int m);
long double phi(int m);
```

```
double Ge_core_concentration(double NA0,double wl,double Ge_clad, double F_clad);
double zero_dispersion(double Ge_core, double Ge_clad, double F_clad, double wlc);
void cal_dispersion(double Ge_core, double Ge_clad, double F_clad, double wlc);
double fiber_param(double wl0, double wlc, double Ge_clad, double F_clad);

double n(double Ge, double F, double wl);
double dn(double Ge, double F, double wl);
double calc_R(void);
double group_delay(double wl, double Ge_core, double Ge_clad, double F_clad, double R, double B);



int main()
{
 char cmd, name[30];
 char inbuf [130];
 double V,B,R,NA0,NA,NAc,n_core,n_clad;
 double t,wl,wlc,wlcs,wlce,wlcst,wl0,wl0s,wl0e,wl0st,Ge_core,Ge_clad,F_clad,MFD,a;
 FILE *file_prt;


 prof_type: /* select type of refractive index profile */
 do {
        clrscr();
        printf("\n");
        printf("Select the type of index profile:");
        printf("\n 1. Step profile.");
        printf("\n 2. Power law  profile.");
        printf("\n 3. Numerical data from a file.");
        printf("\nPress number of the type you want or press Q to quit the program...");
        cmd=toupper(getch());
        printf("\n");

    switch(cmd)
        {
        case '1': step_profile(); goto start;
        case '2': power_profile(); goto start;
        case '3': numerical_profile(); goto start;
        default : printf("Invalid choice! Try again...\n");
        }
    } while(cmd != 'Q');
  return 0;


  start: /* Start calculations */
  do {
     printf("\n");
         printf("Operation desired:");
         printf("\n1. Find the eigen value for a given V value.");
         printf("\n2. Find the cutoff wavelength of the LP11 mode.");
         printf("\n3. Calculate the chromatic dispersion.");
         printf("\n4. Goto the previous menu.");
         printf("\nPress the number of the operation you want or press Q to quit the program...");
```

```
cmd=toupper(getch());

printf("\n");

switch(cmd)
        {
        case '1':
                                printf("Input the V value: ");
                                gets(inbuf);
                                sscanf(inbuf,"%lf", &V);
                                B=eigen(V);
                                printf("B = %f\n",B);
                                break;
        case '2': printf("Input the initial value of V: ");
                                gets(inbuf);
                                sscanf(inbuf, "%lf", &V);
                                Vc=cutoff(V);
                                printf("V_cutoff = %f\n",Vc);
                                break;
        case '3': Vc=cutoff(2.405);
                                printf("Input Ge concentration in the cladding:  ");
        gets(inbuf);
                                sscanf(inbuf, "%lf", &Ge_clad);
            printf("Input F concentration in the cladding:  ");
            gets(inbuf);
                                sscanf(inbuf, "%lf", &F_clad);
                                do {
                                printf("\n");
                                        printf("Operation desired:\n");
                                        printf("1. Given fiber parameters, calculate the group delay.\n");
                                        printf("2. Given fiber parameters, find the zero dispersion
wavelength.\n");
                                        printf("3. Given fiber parameters, calculate the dispersion.\n");
                                        printf("4. Generate the data of MFD-cutoff curves for different\n");
                                        printf("   zero dispersion wavelengths.\n");
                                        printf("5. Goto the previous menu.\n");
                                        printf("Press the number of the operation you want or press Q to quit
the program...");
                                cmd=toupper(getch());

                                printf("\n");

                                switch(cmd)
                                        {   case '1':do {
                                                printf("\n");
                                                printf("\nData to input:");
                                                printf("\n1. NA and cutoff wavelength.");
                                                printf("\n2. MFD and cutoff wavelength.");
                                                printf("\n3. Goto the previous menu.");
                                                printf("\nPress the number of the operation you want... ");
                                                cmd=toupper(getch());
                                                printf("\n");

                                                switch(cmd)
```

```
{
case '1': printf("Input the NA:  ");
gets(inbuf);
sscanf(inbuf, "%lf", &NA0);
printf("Input the cutoff wavelength en nm:  ");
gets(inbuf);
sscanf(inbuf, "%lf", &wlc);
wl=1310;

Ge_core=Ge_core_concentration(NA0,wl,Ge_clad,F_clad);

n_clad=n(Ge_clad,F_clad,wlc);

n_core=n(Ge_core,0,wlc);

NAc=sqrt(n_core*n_core-n_clad*n_clad);

for(wl=1290;wl<=1330;wl=wl+2)
{

NA=sqrt(pow(n(Ge_core,0,wl),2)-pow(n(Ge_clad,F_clad,wl),2));

V=Vc*wlc/wl*(NA/NAc);

B=eigen(V);

R=calc_R();

t=group_delay(wl,Ge_core,Ge_clad,F_clad,R,B);

printf("Wavelength = %.5f,  Group delay = %.10f\n",wl,t);
}
break;
case '2': printf("Input the MFD en micron:  ");
gets(inbuf);
sscanf(inbuf, "%lf", &MFD);
printf("Input the cutoff wavelength en nm:  ");
gets(inbuf);
sscanf(inbuf, "%lf", &wlc);

a=1000*MFD/2/(0.65+0.434*pow(1310/wlc,1.5)+0.0149*pow(1310/wlc,6));

NA0=Vc*wlc/(2*3.14*a);

Ge_core=Ge_core_concentration(NA0,wlc,Ge_clad,F_clad);

n_clad=n(Ge_clad,F_clad,wlc);

n_core=n(Ge_core,0,wlc);

NAc=sqrt(n_core*n_core-n_clad*n_clad);

for(wl=1290;wl<=1330;wl=wl+4)
```

```
{

NA=sqrt(pow(n(Ge_core,0,wl),2)-pow(n(Ge_clad,F_clad,wl),2));

V=Vc*wlc/wl*(NA/NAc);

B=eigen(V);

R=calc_R();

t=group_delay(wl,Ge_core,Ge_clad,F_clad,R,B);

printf("Wavelength = %.5f,  Group delay = %.10fn",wl,t);
}
break;
fault : printf("Invalid choice! Try again...\n");
break;
}
} while(cmd != '3');
break;
case '2':do {
printf("\n");
printf("\nData to input:");
printf("\n1. NA and cutoff wavelength.");
printf("\n2. MFD and cutoff wavelength.");
printf("\n3. Goto the previous menu.");
printf("\nPress the number of the operation you want... ");
cmd=toupper(getch());
printf("\n");

switch(cmd)
{
case '1': printf("Input the NA:  ");
gets(inbuf);
sscanf(inbuf, "%lf", &NA0);
printf("Input the cutoff wavelength en nm:  ");
gets(inbuf);
sscanf(inbuf, "%lf", &wlc);
wl=1310;

Ge_core=Ge_core_concentration(NA0,wl,Ge_clad,F_clad);

wl0=zero_dispersion(Ge_core,Ge_clad,F_clad,wlc);
break;
case '2': printf("Input the MFD en micron:  ");
gets(inbuf);
sscanf(inbuf, "%lf", &MFD);
printf("Input the cutoff wavelength en nm:  ");
gets(inbuf);
sscanf(inbuf, "%lf", &wlc);

a=1000*MFD/2/(0.65+0.434*pow(1310/wlc,1.5)+0.0149*pow(1310/wlc,6));
```

```
NA0=Vc*wlc/(2*3.14*a);

Ge_core=Ge_core_concentration(NA0,wlc,Ge_clad,F_clad);

wl0=zero_dispersion(Ge_core,Ge_clad,F_clad,wlc);
                    break;
                    default : printf("Invalid choice! Try again...\n");
                                        break;
                              }
                              } while(cmd != '3');
                              break;
                    case '3': do {
                    printf("\n");
                    printf("\nData to input:");
                    printf("\n1. NA and cutoff wavelength.");
                    printf("\n2. MFD and cutoff wavelength.");
                    printf("\n3. Goto the previous menu.");
                    printf("\nPress the number of the operation you want... ");
                    cmd=toupper(getch());
                    printf("\n");

                    switch(cmd)
                                   {
                    case '1': printf("Input the NA:  ");
                         gets(inbuf);
                         sscanf(inbuf, "%lf", &NA0);
                         printf("Input the cutoff wavelength en nm:  ");
                         gets(inbuf);
                         sscanf(inbuf, "%lf", &wlc);
                         wl=1310;

Ge_core=Ge_core_concentration(NA0,wl,Ge_clad,F_clad);

cal_dispersion(Ge_core,Ge_clad,F_clad,wlc);
                                        break;
                    case '2': printf("Input the MFD en micron:  ");
                         gets(inbuf);
                         sscanf(inbuf, "%lf", &MFD);
                         printf("Input the cutoff wavelength en nm:  ");
                         gets(inbuf);
                         sscanf(inbuf, "%lf", &wlc);

a=1000*MFD/2/(0.65+0.434*pow(1310/wlc,1.5)+0.0149*pow(1310/wlc,6));

NA0=Vc*wlc/(2*3.14*a);

Ge_core=Ge_core_concentration(NA0,wlc,Ge_clad,F_clad);

cal_dispersion(Ge_core,Ge_clad,F_clad,wlc);
                         break;
                         default : printf("Invalid choice! Try again...\n");
                         break;
                         }
```

```
                        } while(cmd != '3');
                        break;
            case '4': printf("Input the start zero dispersion wavelength en nm:  ");
    gets(inbuf);
                    sscanf(inbuf, "%lf", &wl0s);
    printf("Input the end zero dispersion wavelength en nm:  ");
    gets(inbuf);
                    sscanf(inbuf, "%lf", &wl0e);
    printf("Input the step of zero dispersion wavelength en nm:  ");
    gets(inbuf);
                    sscanf(inbuf, "%lf", &wl0st);
    printf("Input the start cutoff wavelength en nm:  ");
    gets(inbuf);
                    sscanf(inbuf, "%lf", &wlcs);
    printf("Input the end cutoff wavelength en nm:  ");
    gets(inbuf);
                    sscanf(inbuf, "%lf", &wlce);
    printf("Input the step of cutoff wavelength en nm:  ");
    gets(inbuf);
                    sscanf(inbuf, "%lf", &wlcst);
    printf("Input the file name: ");
                    gets(inbuf);
                    sscanf(inbuf,"%s", &name);
                    file_prt=fopen(name,"wt");
                    fprintf(file_prt,"zero disp. wavelength (nm)      MFD (micron)
cutoff wavelength (nm) \n");
                    for(wl0=wl0s;wl0<=wl0e;wl0=wl0+wl0st)

{for(wlc=wlcs;wlc<=wlce;wlc=wlc+wlcst)

{MFD=fiber_param(wl0,wlc,Ge_clad,F_clad);
                fprintf(file_prt, "    %.4f                    %.4f
%.4f\n",wl0,wlc,MFD);
                printf("Zero dispersion wavelength =.%.2f,    Cutoff wavelength =
%.2f\n", wl0,wlc);
                                    }
        }
                fclose(file_prt);
                            break;
                    case '5': goto start;
                    case 'Q': break;
                    default : printf("invalid choice. Try again\n");
                }
                } while(cmd != 'Q');
            return 0;
        case '4': goto prof_type;
        case 'Q': break;
        default : printf("Invalid choice. Try again\n...");
        }
    } while(cmd != 'Q');
    return 0;
}
```

```
void step_profile(void)               /* Gives the step profile in the core */
{
 S=200.;
 h=1.0/S;
 for (s=1; s<=S+1; s++) {N[s]=0;}
}


void power_profile(void)     /* Gives the power-law profile in the core */
{
 char inbuf [130];
 double g;

 printf("Input the power number g: ");
 gets(inbuf);
 sscanf(inbuf,"%lf", &g);
 S=200.;
 h=1.0/S;
 for (s=1; s<=S+1; s++) {N[s]=pow((s-1)*h,g);}
}



void numerical_profile(void)          /* Get the profile data from a file in a disk */
{
 char inbuf [130];
 char name[30];
 FILE *file_prt;
 float i,j;
 float tempo,nmax,Ntempo[800];

 printf("Input the file name: ");
 gets(inbuf);
 sscanf(inbuf,"%s", &name);
 file_prt=fopen(name,"rt");
 i=0. ;
 do{
        fgets(inbuf,130,file_prt);
        sscanf(inbuf,"%f", &tempo);
        i=i+1.;
        Ntempo[i]=tempo;
  }
  while (feof(file_prt)==0);
  fclose(file_prt);
  /*for (j=1;j<=i;j++) {printf("%lf\n",Ntempo[j]);}*/
  s=1;
  do{
        Ntempo[s]=(Ntempo[s]+Ntempo[i-s+1])/2;
        s=s+1;
   }
  while (s<=i-s+1);
```

```
for (i=1;i<=s-1;i++) {N[i]=Ntempo[s-i];}
/*for (i=1;i<=s-1;i++) {printf("%lf\n",N[i]);}*/
for (i=1;i<=s-1;i++) {N[i]=1.4465+N[i]-N[s-1];}
for (i=1;i<=s-1;i++) {printf("%lf\n",N[i]);}
nmax=0;
for (i=1;i<=s-1;i++) {nmax=max(nmax,N[i]);}
printf("nmax = %lf\n",nmax);
for (i=1;i<=s-1;i++) {N[i]=(nmax*nmax-N[i]*N[i])/(nmax*nmax-1.4465*1.4465);}
/*for (i=1;i<=s-1;i++) {printf("%lf\n",N[i]);}*/
S=s-1.;
h=1.0/S;
}


double eigen(double V)          /* Find the eigen value for a given V value */
{
 char inbuf [130];
 float m,i;
 double deltaV, B, deltaB, f, fp;

 /*B_input:
 printf("Input the initial value of B: ");
 gets(inbuf);
 sscanf(inbuf, "%lf", &B);*/

 if(V<2.405)
        {B=0.99;}
 else
        {B=0.6;}
 m=0;                  /* m=0 for the LP01 mode, m=1 for the LP11 mode */
 deltaB=1.e-12;

 f=Core(m,V,B)-Clad(m,V,B);
 if(fabs(f)<=1.e-12)
   {return(B);}

 i=0;

 do{                   /* Using Newton method to find the root */
   /*if(1<B*B)
          {printf("\nThe initial value is improper!");
          printf("\n");
          printf("\n");
          goto B_input;}*/
   fp=(Core(m,V,B+deltaB)-Clad(m,V,B+deltaB)-Core(m,V,B-deltaB)+Clad(m,V,B-deltaB))/deltaB/2.0;
   B=B-f/fp;
   f=Core(m,V,B)-Clad(m,V,B);
   i=i+1;
   }
 while(fabs(f)>1.e-12 && i<50);

 return(B);
 }
```

```
double cutoff(double V)                /* Find the cutoff V value of the LP11 mode */
{
 char inbuf [130];
 float m;
 double deltaV,B,f,fp;

 m=1;
 B=1;
 deltaV=1.e-12;

 do{                    /* Using Newton method to find the root */
   f=Core(m,V,B)+1.0;
   fp=(Core(m,V+deltaV,B)-Core(m,V-deltaV,B))/deltaV/2.0;
   V=V-f/fp;
  }
 while(fabs(f)>1.e-12 );

 return(V);
}

double Ge_core_concentration(double NA0,double wl,double Ge_clad,double F_clad)
/* Calculate Ge concentration in the core for a given NA */
{
 double Ge_core,deltaGe,n_clad,n_core,f1,f2,f,fp;
 float i;

 Ge_core=3.0;
 deltaGe=1.e-12;
 i=0;

 do{
          n_clad=n(Ge_clad,F_clad,wl);
          n_core=n(Ge_core,0,wl);
          f=sqrt(n_core*n_core-n_clad*n_clad)-NA0;
          n_core=n(Ge_core-deltaGe,0,wl);
          f1=sqrt(n_core*n_core-n_clad*n_clad)-NA0;
          n_core=n(Ge_core+deltaGe,0,wl);
          f2=sqrt(n_core*n_core-n_clad*n_clad)-NA0;
          fp=(f2-f1)/2/deltaGe;
          Ge_core=Ge_core-f/fp;
          i=i+1;
          }
          while(fabs(f)>1.e-12 && i<50);

  return(Ge_core);
 }


double zero_dispersion(double Ge_core,double Ge_clad,double F_clad,double wlc)
/* Calculate zero-dispersion wavelength */
{
 char inbuf[130];
```

```
float i;
double wl,deltawl,V,B,R,n_core,n_clad,NA,NAc,dn;
double t,t1,t2,tp,tpp;

wl=1310;
deltawl=0.1;
n_clad=n(Ge_clad,F_clad,wlc);
n_core=n(Ge_core,0,wlc);
NAc=sqrt(n_core*n_core-n_clad*n_clad);
i=0;

do{
        NA=sqrt(pow(n(Ge_core,0,wl),2)-pow(n(Ge_clad,F_clad,wl),2));
        V=Vc*wlc/wl*(NA/NAc);
        B=eigen(V);
        R=calc_R();
        t=group_delay(wl,Ge_core,Ge_clad,F_clad,R,B);
        NA=sqrt(pow(n(Ge_core,0,wl-deltawl),2)-pow(n(Ge_clad,F_clad,wl-deltawl),2));
        V=Vc*wlc/(wl-deltawl)*(NA/NAc);
        B=eigen(V);
        R=calc_R();
        t1=group_delay(wl-deltawl,Ge_core,Ge_clad,F_clad,R,B);
        NA=sqrt(pow(n(Ge_core,0,wl+deltawl),2)-pow(n(Ge_clad,F_clad,wl+deltawl),2));
        V=Vc*wlc/(wl+deltawl)*(NA/NAc);
        B=eigen(V);
        R=calc_R();
        t2=group_delay(wl+deltawl,Ge_core,Ge_clad,F_clad,R,B);
        tp=(t2-t1)/deltawl/2;
        tpp=(t2-2*t+t1)/deltawl/deltawl;
        printf("Wavelength = %.5f,  Dispersion = %.10f,  Slope = %.10f\n",wl,tp,tpp);
        wl=wl-tp/tpp;
   i=i+1;
  }
 while(fabs(tp)>1.e-6 && i<10);

 printf("Zero dispersion wavelength = %f\n",wl);

 return(wl);

 }


 void cal_dispersion(double Ge_core,double Ge_clad,double F_clad,double wlc)
 /* Claculate dispersion in a wavelength range */
 {
  char inbuf[130],cmd;
  float i;
  double wl,deltawl,V,B,R,n_core,n_clad,NA,NAc,dn;
  double t,t1,t2,tp,tpp;


  wl=1250;
  deltawl=0.1;
  n_clad=n(Ge_clad,F_clad,wlc);
```

```
n_core=n(Ge_core,0,wlc);
NAc=sqrt(n_core*n_core-n_clad*n_clad);

for (i=0;i<=1;i++)
        {
        wl=wl+i*10;
        NA=sqrt(pow(n(Ge_core,0,wl-deltawl),2)-pow(n(Ge_clad,F_clad,wl-deltawl),2));
        V=Vc*wlc/(wl-deltawl)*(NA/NAc);
        B=eigen(V);
        R=calc_R();
        t1=group_delay(wl-deltawl,Ge_core,Ge_clad,F_clad,R,B);
        NA=sqrt(pow(n(Ge_core,0,wl+deltawl),2)-pow(n(Ge_clad,F_clad,wl+deltawl),2));
        V=Vc*wlc/(wl+deltawl)*(NA/NAc);
        B=eigen(V);
        R=calc_R();
        t2=group_delay(wl+deltawl,Ge_core,Ge_clad,F_clad,R,B);
```

APPENDIX 3

A program to calculate the Bend Loss of a Depressed-Cladding Single-Mode Fiber

```
DECLARE SUB Bessel (B!, y!, x!)
N = 1.447           'Refractive index of pure silica at 1310 nm
z7 = 1
CLS
PRINT "Enter the b/a ratio",
INPUT s
PRINT "Enter the fraction of depression",
INPUT x
CONST PI = 3.141592
REM Lc:  Cutoff Wavelength
CONST L = 1.55  'Operating Wavelength
CONST SC = .83  'Stress Correction Constant
CONST Ror = 2.5 'Bend Radius
V = 2.405 * Lc / L     'Normalized Frequency
DIM A(6, 16), k(101), c2(181), S2(181), U(181), i2(181), MFD(16), A2(6, 16)
DIM Lc(6)
REM Parameter Definition
REM A : Bend Loss
REM k : Bend Radius
REM c2 : Waveguide parameter of the Core
REM s2 : Waveguide parameter of inner cladding
REM U :
REM i2 :
REM MFD : Fiber mode field diameter
REM A1 : fiber core
o = 1
FOR Lc1 = 1.1 TO 1.35 STEP .05
A = 0
p = 1
Lc(o) = Lc1
FOR mfd1 = 4 TO 5.5 STEP .1
     MFD(p) = mfd1
     A1 = mfd1 / (.65 + .434 * (1.3 / 1.25) ^ 1.5 + .0149 * (1.3 / 1.25) ^ 6)
     NA = 2.405 * Lc1 / (2 * PI * A1)
     D = NA ^ 2 / (2 * N ^ 2)
     i = 1
     K2 = 0
     REM Normalized Frequency
     V = 2 * PI / L * A1 * N * (2 * D) ^ .5
     REM Normalized Propagation Costant
     U = -.0116 * V ^ 4 + .1493 * V ^ 3 - .7598 * V ^ 2 + 1.9568 * V - .3546
     B = U / V
     REM Parameter of Inner Cladding
     W = (V ^ 2 - U ^ 2) ^ .5
     C1 = W / A1
     REM Square of parameter of outer cladding
```

```
S1 = (V / A1) ^ 2 * (B ^ 2 - (1 - x))
REM Parameter of core
K4 = U / A1
REM Propagation Constant
B1 = N * (2 * PI / L) * (1 - 2 * B ^ 2 * D) ^ .5
REM Inner Cladding Radius
B2 = s * A1

R1 = Ror * SC
    k5 = 0
    R = R1 * 10 ^ 4
    i2 = 0
    R2 = 2 * (1 - D) ^ 2 * N ^ 2 * (2 * PI / L) ^ 2
    R2 = R2 * B2 / C1 ^ 2
    j2 = R * C1 ^ 2
    j2 = j2 / ((2 * PI / L * N * (1 - D)) ^ 2 * 2 * B2)
    j3 = -R * S1 / (2 * B2 * (2 * PI / L * N) ^ 2)

    IF j2 <= 1 THEN
        j2 = j2
    ELSE
        j2 = 1
    END IF

    IF j3 <= 1 THEN
        j3 = j3
    ELSE
        j3 = 1
    END IF

    REM Calculate the starting angle
    j22 = SQR(1 - j2 ^ 2) / j2
    phi2 = INT(ATN(j22) * 180 / PI + 1)

    REM calculate the finishing angle
    j33 = SQR(1 - j3 ^ 2) / j3
    phi3 = INT(ATN(j33) * 180 / PI - 1)
    IF phi3 < 0 THEN 10

    j = 0

    FOR j5 = phi2 TO phi3
        j1 = COS(j5 * PI / 180)
        c2(j + 1) = (C1 ^ 2 - N ^ 2 * (1 - D) ^ 2 * 2 * B2 * j1 / R * (2 * PI / L) ^ 2) ^ .5
        S2(j + 1) = (S1 + N ^ 2 * 2 * B2 * j1 / R * (2 * PI / L) ^ 2) ^ .5

        IF j = 90 THEN
            U(91) = C1 * s * A1
        ELSE
            U(j + 1) = R * (C1 ^ 3 - c2(j + 1) ^ 3)
            U(j + 1) = U(j + 1) / (3 * (1 - D) ^ 2)
            U(j + 1) = U(j + 1) / (N ^ 2 * j1 * (2 * PI / L) ^ 2)
        END IF
```

```
            i2(j + 1) = S2(j + 1) * c2(j + 1) ^ 2 * EXP(-2 * U(j + 1))
            f2 = (U(j + 1) * (V ^ 2 * x * (1 + 2 * B2 * j1 / R) / A1 ^ 2))
            i2(j + 1) = i2(j + 1) / f2
            j = j + 1

        NEXT j5

        REM Perform numerical Integration
        i3 = 0
        j = 1
        FOR j5 = phi2 TO phi3
            i3 = i3 + i2(j)
            j = j + 1
        NEXT j5

        REM Calculate loss
        A(o, p) = i3 * 4 * B2 * K4 ^ 2 / (B1 * V ^ 2)
        CALL Bessel(K1, y, C1 * A1)
        A(o, p) = A(o, p) / K1 ^ 2
        A(o, p) = A(o, p) * 2 * 10 ^ 7

10      S3 = -S1
        A3 = (PI / (S3 ^ 1.5 * R)) ^ .5 * .5 * 10 ^ 7
        CALL Bessel(K1, y, S3 ^ .5 * A1)
        A3 = A3 * (K4 / (V * K1)) ^ 2
        j33 = ATN((1 - j3 ^ 2) ^ .5 / j3)
        A3 = A3 * (PI - j33) * EXP(-2 / 3 * S3 ^ 1.5 * R / B1 ^ 2) / PI
        A(o, p) = A(o, p) + A3

        CALL Bessel(K1, y, C1 * A1)
        A3 = (PI / (C1 ^ 3 * R)) ^ .5 * (K4 / (V * K1)) ^ 2 * .5 * 10 ^ -7
        j22 = ATN(SQR(1 - j2 ^ 2) / j2)
        A3 = A3 * j22 * EXP(-2 / 3 * C1 ^ 3 * R / B1 ^ 2) / PI
        A(o, p) = A(o, p) + A3
        GOTO 20

        CALL Bessel(K1, y, C1 * A1)
        A(o, p) = (PI / (C1 ^ 3 * R)) ^ .5 * (K4 / (V * K1)) ^ 2 * .5 * 10 ^ 7
        A(o, p) = A(o, p) * EXP(-2 / 3 * C1 ^ 3 * R / B1 ^ 2)
        PRINT A(o, p)
20      i = i + 1


50   p = p + 1
NEXT mfd1
    o = o + 1
NEXT Lc1

REM Store data in file
PRINT "what is the filename that you want to store the data";
INPUT A$
OPEN A$ FOR OUTPUT AS #1
FOR p = 1 TO 6
FOR i = 1 TO 15
```

```
PRINT #1, A(p, i), Lc(p), MFD(i)
NEXT i
NEXT p

CLOSE

END

SUB Bessel (B, y, x)
CONST PI = 3.141592
IF x < 12.45 THEN
     l1 = x / 2
     l2 = .5
     l3 = x / 4
     l0 = LOG(x * .5) + .577215664902#
     l4 = l1
     j1 = 1
     j2 = 50
     FOR j = j1 TO j2
          l1 = l1 * x ^ 2 / (4 * j * (j + 1))
          l2 = l2 + .5 / j + .5 / (j + 1)
          l3 = l1 * l2 + l3
          l4 = l4 + l1
     NEXT j
     B = l4 * l0 - l3 + 1 / x
     y = l4
ELSE
     B = (PI / (2 * x)) ^ .5 * EXP(-x) * (1 + 3 / (8 * x))
     y = EXP(x) / (2 * PI * x) ^ .5 * (1 - 3 / (8 * x))
END IF
END SUB
```

APPENDIX 4

A Mathematica Program that calculates the Bend Loss of the LP_{11} Mode

```
(*^

a=4
lamda=1.25
k=2*3.1416/lamda
TableForm[
Table[{V,
x=x /.
FindRoot[
        x*BesselJ[2,x]/BesselJ[1,x]-
        Sqrt[V^2-x^2]*BesselK[2,Sqrt[V^2-x^2]]
        /BesselK[1,Sqrt[V^2-x^2]]==0
        ,{x,2.4}
],

W=Sqrt[V^2-x^2],

NA=V/(k*a),
chi=x/a,

gama=W/a,

index=(NA^2+1.447^2)^.5,

b=((k*index)^2-chi^2)^.5,

R=2.5*10^4,

loss=(3.1416)^.5*chi^2*
        Exp[-2/3*(gama^3/b^2)*R]/
        (gama^1.5*V^2*Sqrt[R]*BesselK[0,W]*BesselK[2,W])*
        2*3.1416*R,
}

{V,2.405,2.605,.005}
]
]

^*)
```